$$\frac{1}{R}\frac{d}{dt}\left[\sigma\frac{\partial\phi}{\partial\sigma}\right]+\frac{RT}{C_pP}\left[P_s\dot{\sigma}+\sigma\dot{P}_s\right]=-Q$$

$$\frac{\partial\phi}{\partial\sigma}=-\frac{RT}{\sigma}$$

$$\frac{d\vec{V}}{dt}+f\hat{k}\times\vec{V}=-\nabla\phi+\frac{\sigma}{P_s}\frac{\partial\phi}{\partial\sigma}\nabla P_s+\vec{F}$$

$$\frac{\partial P_s}{\partial t}=-\int_0^1\nabla.\left[P_s\,\vec{V}\right]d\sigma$$

$$\frac{\partial}{\partial t}[P_s\,q]+\nabla.\left[P_s\,q\vec{V}\right]+\frac{\partial}{\partial\sigma}[P_s\,q\dot{\sigma}]=P_s\,S$$

$$\nabla.(P_s\vec{V})+\frac{\partial}{\partial\sigma}(P_s\dot{\sigma})+\frac{\partial P_s}{\partial t}=0$$

Climate Change Science & Modeling

Edited by

S.K.Dash and Akhilesh Gupta

सत्यमेव जयते

Government of India
Ministry of Science & Technology
Departmant of Science & Technology
Strategic Programme, Large Initiatives and Coordinated Action Enabler (SPLICE) Division
Climate Change Programme
October 2018

Climate Change Science & Modeling

Edited by

S.K.Dash & Akhilesh Gupta

Government of India
Ministry of Science & Technology
Department of Science & Technology
Strategic Programme, Large Initiatives and
Coordinated Action Enabler (SPLICE) Division
Climate Change Programme
October, 2018

सचिव
भारत सरकार
विज्ञान और प्रौद्योगिकी मंत्रालय
विज्ञान और प्रौद्योगिकी विभाग
टेक्नोलॉजी भवन, न्यू महरौली रोड, नई दिल्ली - 110016

Secretary
Government of India
Ministry of Science and Technology
Department of Science and Technology
Technology Bhavan, New Mehrauli Road, New Delhi - 110016

सत्यमेव जयते

प्रो. आशुतोष शर्मा
Prof. Ashutosh Sharma

FOREWORD

Climate change has emerged as one of the defining global environmental problems of this century, requiring an unprecedented global response supported by substantive and coordinated national efforts by every nation. The 5th Assessment report of Inter-governmental Panel on Climate Change (IPCC) has brought out new results on climate change impacts on different socio-economic sectors besides its impact on physical environment such as melting of icecaps, rising sea levels, heat-waves, storms ,etc. In the year 2016 India formulated its Intended Nationally Determined Contributions (INDCs) and subsequently ratified the Paris Agreement on climate change, which signifies its commitment to the "global cause of environmental protection and climate justice". India had launched an ambitious and sustained response to global CC challenge by launching the National Action Plan on Climate Change (NAPCC) in the year 2008 along with eight national missions addressing some key adaptation and mitigation sectors. The Department of Science & Technology was entrusted with the responsibility of implementing two out of these eight national missions on climate change launched under the aegis of NAPCC. One of them is the National Mission on Strategic Knowledge for Climate Change (NMSKCC) with broad objectives of building human and institutional capacities in the relevant areas of climate change; mapping of the knowledge and data resources relevant to climate change; building strategic knowledge among the various arms of the Government, networking of knowledge institutions, creation of new dedicated centres, etc.

One of the key deliverables of NMSKCC was to promote research in the area of Climate modeling through dedicated centres and network programme. The climate modeling greatly helped assessing current state of climate and its projection on a longer scale of time from a decade to a century. Some of the important issues related to climate modeling studies include, the uncertainties in model projections, downscaling of climate products to the local level, understanding the role of aerosols in climate change and examining the extreme weather phenomena in the warming atmosphere.

Realizing the need for studying the different facets of climate modeling issues, DST as part of NMSKCC initiated a couple of Centres of Excellence, Major R&D Projects and two phases of National Knowledge Network programme on Climate Modeling. The present report is a compilation of results that have come out of projects supported during 2012-16 under a Centre of Excellence at IIT Bombay and 2 Major R&D programmes, one each at IIT Delhi and Allahabad University in the area of climate modeling.

I am pleased to learn that the Climate Change Programme (CCP), SPLICE Division, DST is bringing out a report entitled ***"Climate Change Science & Modeling"*** edited by **Prof S.K.Dash** of IIT Delhi and **Dr Akhilesh Gupta**, Adviser & Head, SPLICE, DST. I am confident the report will be of great use to students, researchers and policy makers. I wish to compliment the contributors and the editors for their great efforts.

(Ashutosh Sharma)

Tel: 00 91 11 26511439 / 26510068 • Fax: 00 91 11 26863847 • E-mail: dstsec@nic.in • website: www.dst.gov.in

PREFACE

Climate change encompasses several areas of science and its impacts are over almost all socio-economic sectors, in particular water, agriculture and health. The quantification of impacts of climate change is very difficult because of large uncertainties in projecting the future climate at different temporal and spatial scales. Future climate is simulated using coupled Atmosphere-Ocean General Circulation Models (AOGCMs) for scenarios that encompass a range of emissions. These models have been developed over the last few decades. The variations between models in their representation of physics and dynamics result in differences in the simulated climate and represent the uncertainty in our state of knowledge. The need for high spatial resolution model simulations in order to carry out regional analysis adds another layer of complexity. The Global coupled models that are available today are too coarse for this purpose. One way of getting closer to the desired resolution is through a downscaling procedure both dynamical and statistical that produces the desired resolution. However, by doing so additional errors are introduced which add to the uncertainty. Despite so much uncertainty in projecting future climate, the climate modeling continues to be the most important scientific tool to initiate all climate actions- both adatation and mitigation.

The Government of India launched eight National Missions as part of National Action Plan on Climate Change (NAPCC). The Department of Science & Technology was entrusted with the responsibility of coordinating two out of these eight national missions. National Mission on Strategic Knowledge for Climate Change (NMSKCC) is one of them which has broad objectives of building human and institutional capacities in the relevant areas of climate change; mapping of the knowledge and data resources relevant to climate change; building strategic knowledge among the various arms of the Government, Identification of knowledge gaps, Networking of knowledge institutions, creation of new dedicated centres, building international cooperation on S&T for climate change research, etc. As part of NMSKCC, DST has supported 11 Centres of Excellence at various national/international institutions and universties; 23 Major R&D Programmes/projects; 7 Human Capacity Building Programmes in CC adaptation and mitigation spearheaded by 6 lead institutions; 8 Global Technology Watch Groups (GTWGs) in 8 adapation and mitigation technology sectors; State Climate Change Cells in 11 non-himalayan States/Union Territories; 7 National Network programmes in the areas of climate modeling, climate change & human health, aerosols, coastal vulnerability and urgan climate; and an Indo-US Fulbright-Kalam Doctoral and Post-Doctoral Fellowship programme in Climate Change.

The present report is a compilation of results that have come out of projects supported during 2012-16 under a Centre of Excellence at IIT Bombay and 2 Major R&D programmes one each at IIT Delhi and Allahabad University in the area of climate modeling.

One of the editors (AG) is grateful to **Prof Ashutosh Sharma**, Secretary, DST for encouragement and motivation. Thanks are due to **Dr Nisha Mendiratta**, Scientist-G & Associate Head; **Dr Susheela Negi**, Scientist-E and **Dr Rabindra Panigrahy**, Scientist-C of Climate Change Programme, SPLICE Division of DST for their support. The authors are also grateful to members of Expert Committee of CCP, DST especially **Prof S.K.Dube**, Chairman, **Dr Mangala Rai,** Co-Chairman for the encouragement. We are thankful to all contributors of the report for their valuable inputs in the preparation of the report.

We sincerely hope that the publication will be of great use to scientists, researchers and policy makers engaged in the field of climate modeling.

Prof S.K.Dash
Centre for Atmospheric Sciences
IIT Delhi, New Delhi-110 016

Dr Akhilesh Gupta
Adviser & Head
Climate Change Programmed, SPLICE Division
Department of Science & Technology
New Delhi-110 016

List of Contributors

No	Name	Affiliation
1	Prof. S.K.Dash	Centre for Atmospheric Sciences,IIT Delhi
2	Prof.U.C.Mohanty	School of Earth Ocean & Climate Sciences, IIT Bhubaneswar
3	Dr. Krishna Mirle Achutarao	Centre for Atmospheric Sciences, IIT Delhi
4	Dr. Sagnik Dey	Centre for Atmospheric Sciences, IIT Delhi
5	Prof. Chandra Venkataraman	DST CoE in Climate Studie, IIT Bombay
6	Dr. Subimal Ghosh	DST CoE in Climate Studies, IIT Bombay
7	Dr. Kaustubh Salvi	DST CoE in Climate Studies, IIT Bombay
8	Dr. Ribu Cherian	DST CoE in Climate Studies, IIT Bombay
9	Prof. Suneet Dwivedi	K.B.Centre of Atmos & Ocean Studies, University of Allahabad
10	Prof. Avinash C. Pandey	K.B.Centre of Atmos & Ocean Studies, University of Allahabad

Table of Contents

Executive Summary

This report is based on the findings of three Major R&D projects supported by Climate Change Programmed of DST. These are: (1) "Modelling Regional Climate Change: Addressing Scientific Uncertainties and Capacity Building Needs" sponsored to the Centre for Atmospheric Sciences at IIT Delhi, (2) "DST Centre for Excellence in Climate Studies" at Indian Institute of Technology Bombay, and (3) "Study of Extreme Rainfall Events Over India in the Context of Climate Change" operational at K. Banerjee Centre of Atmospheric and Ocean Studies, University of Allahabad. Now-a-days, in addition to the use of Global Climate Models (GCMs), high resolution Regional Climate Models (RCMs) are increasingly used to examine climate related phenomena. Therefore, this report focuses on both the types of models.

Today, the important issues concerning the climate change include the uncertainties in model projections, downscaling of climate products to the local level, understanding the role of aerosols in climate change and examining the extreme weather phenomena in the warming atmosphere. The present report throws light on the important findings in each of the above issues.

i) Modelling Regional Climate Change

Exploring the uncertainty in model projections

The future changes in temperature and precipitation over India as simulated by Coupled Global Climate Models under different scenarios (RCP4.5 and RCP8.5) have been investigated in order to understand the uncertainties in these projections. In this study, the uncertainties in the changes have been examined in order to help policymakers make informed decisions. Changes in temperature and precipitation for future time periods are calculated at each grid point and spatially averaged over the Indian land region (6.5N-38.5N, 66.5E-100.5E). Annual, JJA and DJF changes are calculated separately.

The uncertainties in the regional climate model simulations have also been examined in case of RegCM4 climate simulations for the South Asia CORDEX domain. The regional model performance in simulating the Indian summer monsoon circulation and rainfall has been first validated over the reference period 1975-2004 using observed rainfall from different sources, including GPCP and IMD0.5 gridded precipitation data and wind data from the NCEP/NCAR reanalysis. Regional Climate Model Version4 (RegCM4) is found to satisfactorily simulate the main characteristics of the Indian summer monsoon rainfall distribution over the region. More importantly, the model captures various features of the observed changes in rainfall during the last decades. Comparison between the global forcing fields and the downscaled fields shows that RegCM4 is able to resolve regional circulation and rainfall features and their future changes more consistently with observations than with the global model. The future projections for both RCP4.5 and 8.5 scenarios reveal a systematic change over most of the Indian sub-continent which increases with time, consisting of a weakening of monsoon precipitation over central India and the northern and equatorial Indian Ocean. On the other hand, increased precipitation is projected over the Arabian Sea, and the northern Bay of Bengal. The changes are in the range of 4-8 mm/day, which are about 30% of their mean present day values.

Downscaling approaches

Temperature and rainfall are projected for CMIP3 Scenarios at high resolution over the Indian landmass. The present study encompasses a quantile based bias correction methodology for future projection of temperature and statistical downscaling technique employed for future projections for Indian monsoon rainfall at a very fine resolution for 20C3M, A1B, A2 and B1 scenarios. The future projections are done for time slices 2020s, 2050, and 2080.The projections are restricted to the land portion of India and done for some of the future scenarios prescribed by IPCC AR4. The temperature variable is well simulated by the General Circulation Model and just by applying bias correction technique, the future projections are obtained. The projections show gradual rise in temperature with time. The conventional statistical downscaling techniques fails to capture the correlation between multiple sites. This problem is answered through representation of the pattern of multi-site rainfall using rainfall state at for each meteorologically homogeneous zone of India. A model based on K-means clustering technique coupled with a supervised data classification technique, namely Classification And Regression Tree (CART), is used for generation of rainfall states from large-scale atmospheric variables selected for a particular zone. The CART model is then trained to establish relationship between the daily rainfall state of the zone and General Circulation Model (GCM)-simulated, standardized, bias free large-scale climate variables for prediction of rainfall states in future. Unlike temperature, the projected rainfall show increase as well as decrease for the various parts on India. The projection pattern is remaining the same for all the time slices but intensity is changing.

In addition to the above study based on GCM products, the RegCM3 has been used to dynamically downscale the NCMRWF T80 model products. The downscaling experiment over northwest India has been conducted by nesting RegCM with the NCMRWF global spectral model for a period of 28 years (1982–2010) at a horizontal resolution of 30 km. The winter season climate is first compared with observations to study the RegCM's downscaling skill over the northwest India. The results indicate that the wintertime climatology of precipitation, upper airfields at different pressure levels, and the interannual variability are more accurately simulated by the T80 driven RegCM than the T80 itself. Composite analysis for extreme precipitation years suggests that the precipitation and circulation features simulated by the T80 driven RegCM shows better skill compare to T80. A complete and statistically robust study also suggests that downscaling provides a credible means to improve GCM climate simulations. There is significant correlation skill of T80 driven RegCM with less RMSE as compared to T80 model itself. It is found that in all thresholds Equitable Threat Score (ETS) of T80_RegCM are higher than T80. Overall simulation of precipitation is better in the T80 driven RegCM experiment compared to T80 model itself due to better representation of vertical velocity and convective heating rates.

Treatment of aerosols in Regional Climate Models

In the present study anthropogenic aerosol induced changes in present-day aerosol loading and their climatic effects were examined with a focus on monsoon precipitation over the Indian subcontinent during January 2001 to December 2005 using the ECHAM5.5-HAM GCM . To start with, the model was evaluated using satellite retrievals. The model simulated AOD at 550 nm captures the variability both in time (inter-seasonal variability) and space (distribution patterns) over the Indian

subcontinent. The seasonal mean anomalies (PD-PI) in aerosol optical depth and its climate effects were computed as the differences between an experiment with the present-day (PD) aerosol emissions and an experiment with pre-industrial (PI) aerosol emissions, averaged for 5 years for the period from January 2001 to December 2005 (i.e. Δ = PD-PI). The model simulates significant changes (PD-PI) in clear-sky surface dimming (> -6 Wm-2), which agrees well with the observed trends over the Indian region. Statistically significant reduction in surface shortwave flux is simulated by the model from an enhanced PD anthropogenic aerosol emissions over the Indian subcontinent. The low-altitude surface cooling was caused primarily by the increase in the BC absorption of the solar radiation. Statistically significant decreasing surface precipitation results from the enhanced anthropogenic aerosol (PD-PI) are simulated only for the SW monsoon season over the CNI region. This simulated trend is consistent with the trend analysis using observed rainfall values. However the magnitude of present-day precipitation was not well simulated. Stratiform cloud drop increased number concentration and decreased sizes, induced by aerosols, leads to increased aerosol indirect forcing, which enhances lower tropospheric stability and reduction in convective rainfall calculated by the model. Such meso-scale effects, of aerosol modulation of monsoon rainfall, need further investigation.

Attempt has been made to understand the capability of regional climate model RegCM4 to simulate the mineral dust transport over India. Simulations were carried out for the period 1 Dec 2008 to 31 Dec 2009, but analysis has been done for the entire year 2009 leaving the first month as spin up time. Monthly variations of AOD_d within 30 km domain containing each Aerosol Robotic Network (AERONET) site are compared with mean monthly coarse mode AOD (AOD_c) from AERONET. The seasonal variability of AOD_d is well captured by the model. Simulations were also carried out for both natural and anthropogenic aerosols at 50 km resolution for the period Nov 2008 to Dec 2010. The atmospheric burden of individual species (dust, BC, OC and sulfate) is examined. Although the model is able to simulate the dust transport appreciably well, the anthropogenic load was observed to be biased low (compared to in-situ observations). Further, simulations were carried out for both natural and anthropogenic aerosols at 50 km resolution for the period Nov 2008 to Dec 2010 using RegCM to examine 3-D aerosol distribution over India and seasonal variability. The atmospheric burden of individual species (dust, BC, OC and sulfate) is examined. Although the model is able to simulate the dust transport appreciably well, the anthropogenic load was observed to be biased low (compared to in-situ observations). In another study related to aerosols, an analytical framework was developed to estimate the contribution of clouds to the observed T_S trend through perturbation of the radiation balance. The framework has been applied to the seven homogeneous surface temperature zones of India - Western Himalaya, East coast, West coast, Northwest, Northeast, North-central and Interior Peninsula. MERRA reanalysis data and RegCM outputs are analyzed and inter-compared. RegCM is able to reproduce the monthly pattern of total cloud fraction over India with over estimation over Central-northeast and under estimation over the Arabian Sea and Bay of Bengal (by 10-25%).

Since North East India (NEI) is very vulnerable to global changes and also this region is least studied, here attempt has been made to examine the changes in climatic parameters of temperature and precipitation in NEI under the IPCC A1B scenario as a case study. It is found that RegCM3 is able to simulate the trends in annual mean temperature and annual mean precipitation and extreme temperature events during the

period 1971-2005. The simulations in to the future project rise in the annual mean temperature and rainfall. In future, there may be more enhancements in the warm events than the cold events.

ii) Global Climate Model Products

Bias correction in GCM products

It is well known that all GCMs have their own biases. In this study Canadian GCM, CGCM3 simulations during the historical period are used to bias correct the surface temperatures in the 20C3M simulations and then also correct their projections. Bias corrections are made as described in Chapter-2. As the observed temperature at 1º resolution are available from 1969 to 2000, the period 1969 to 1984 was selected as training period and 1985 to 2000 was selected as testing period. It is found that the predicted and observed values of temperature for the period of study (1985-2000) match at each grid point at 1° resolution for the entire India. Projected fields under scenarios SRES A2, A1B and B1 are analysed for the 21st century divided into three time slices each of 30 years. The time slices are made for the periods 2020s, 2050s and 2080s. The variations of mean, minimum and maximum temperatures for the referred time slices are examined. Results indicate that the projected temperature values have gradual increase with time. To get some quantitative idea about actual rise in the temperature with respect to 20C3M, the differences between the A2 projections of mean temperature at various time slices and 20C3M mean temperatures are examined.

Treatment of aerosols in GCM

In this study, the spatial distribution of the ECHAM5.5-HAM model-simulated seasonal mean AODs averaged over 5 years (2001 to 2005) has been evaluated using MODIS-derived Terra and Aqua satellite combined AOD values. The model broadly captures AOD distributions during all different seasons over the Indian region. In the monsoon season, high AOD values are found over the IGP, NWI and CNI regions consistently in model and satellite retrievals, albeit too far south in the GCM. This maximum arises because of an enhanced transport of dust aerosols from desert regions of Arabia, Africa and Thar (Rajasthan), and also of sea salt from the ocean. The AOD composition was found to be dominated by dust aerosols, followed by sulfate, OC, and sea salt aerosols during this season. During the inter-monsoon season, high AOD are found over the northern parts of the IGP. The composition of total AOD was dominated by sulfate followed by OC and BC aerosols during this season. In summary, seasonal and spatial variability of the model simulated AOD broadly captures the MODIS-observed variability over the Indian region. In particular, the model simulated AOD was relatively well predicted during the SW monsoon (JJAS) and inter-monsoon seasons (with a certain geographical displacement), but significantly underpredicted locally by up to a factor of 2 during the NE monsoon because of the uncertainties in regional emission inventories and pre-monsoon dust emission fluxes.

The sensitivity of the climate response anthropogenic aerosol emissions over the Indian subcontinent is also evaluated and discussed. The focus is on the differences between the experiment with the present-day (PD) and the pre-industrial (PI) aerosol emissions, averaged for 5 years for the period from January 2001 to December 2005. The seasonal mean changes (PD-PI) in total precipitation is negative over most of the Indian subcontinent, but generally small. Precipitation changes are found to be statistically significant (95% confidence level based on a student's t-test analysis) only for SW

monsoon season, and only over the CNI region. Seasonal mean precipitation changes are not statistically significant in all the other three seasons. There is decrease in SW monsoon rainfall (JJAS) over the CNI which corresponds well with the trend analysis in the observed rainfall from 1951-2003. But some of the finer regional features seen in the observed rainfall trends were not captured in the model which may be arising because of low model horizontal resolution (180 km). Also, because of the model set-up, changes near the coasts in the simulation are limited since the prescribed SST boundary conditions remain the same in both, PD and PI simulations. In this pair of simulations, the large-scale meteorology is also prescribed by nudging towards re-analysis data.

iii) Characteristics of Extreme Rainfall Events

The frequency and occurrence of low to medium, heavy, very heavy and extremely heavy rainfall over eastern India is quantified in the context of climate change. The analysis is made by using the daily rainfall values during 2006-2100 from different IPCC AR5 models in the RCP 2.6, RCP 4.5 and RCP 8.5 scenarios. The comparison is made with the historical runs of these models from 1860-2005. A new diagnostics as described in Chapter2, is proposed to examine the relation between the Indian summer monsoon rainfall and the ENSO events. The modulation in the frequency of the active and break spells during these events is demonstrated. The nature of extreme rainfall (and no rainfall) in this context is also investigated.

Chapter-1

Introduction

At present, the most important topic of discussion all over the world is the perceived changes in Earth's climate. Climate change encompasses several areas of science and its impacts are over almost all sectors of our society; water, agriculture and health being in the top category. The impacts of climate change are very difficult to quantify because of the uncertainties involved in projecting the future climate at different spatial scales. During the last half century or so there has been tremendous effort to understand the deterministic aspects of weather and climate and enhance the accuracy of forecasts at different time scales with the help of technological advancements in instrumentation for making observations and computing power numerical simulations.

Future climate is simulated using coupled Atmosphere-Ocean General Circulation Models (AOGCMs) for scenarios that encompass a range of emissions. These models have been developed over the last few decades. The variations between models in their representation of physics and dynamics result in differences in the simulated climate and represent the uncertainty in our state of knowledge (Tebaldi and Knutti, 2007). The uncertainty that arises from differences in initial conditions (for a single model) and the uncertainty from differences in the models themselves are quite different. The range of model simulations of future climate that are used in impact assessments and adaptation studies therefore influence the uncertainty they capture. Using a single model's projections (even with multiple realizations) does not capture the uncertainty in our knowledge of key physical processes and gives a false sense of certainty about the future. The use of a single model will result in its systematic errors influencing the climate change impacts projected and therefore the adaptation options considered.

The need for high spatial resolution (of the order tens of kilo-meters or finer) model simulations in order to carry out regional analysis adds another layer of complexity. The AOGCMs that are available today are too coarse for this purpose as they are nominally at about 100-150Km square grids. One way of getting closer to the desired resolution is through a downscaling procedure (dynamical or statistical) that produces the desired resolution. Each of these approaches is fraught with scientific questions. For example, in dynamical downscaling using Regional Climate Models (RCMs) errors can be introduced due to a lack of interaction with the larger global scale processes. This can introduce additional errors in the downscaled climate and therefore add to the uncertainty. The quantification of the errors in the two steps is the motivation behind Coordinated Regional Downscaling Experiment (CORDEX). These simulations also depend on the availability of high frequency snapshot data from the AOGCMs to drive the RCM boundary conditions. The issue with statistical downscaling is that the statistical relations may not hold in a future climate. However, this needs to be explored in more detail.

Another way of providing the high resolution data required for the impacts and adaptation community is to run high-resolution Atmospheric General Circulation Models (AGCMs) using coarse AOGCM simulated SST, sea-ice and snow as boundary conditions. However, just as in the case of RCMs, this adds to the underlying AOGCM errors thereby introducing another layer of uncertainty. The uncertainties arising are

likely to be different depending on the choice of strategy to arrive at high resolution. The various techniques discussed are however the only options available till such time AOGCMs are routinely run at the desired resolution (~10 Km or less) – an unlikely prospect in the near future given that there are not even coarse resolution AOGCM simulations being carried out routinely in India. In the meantime, quantifying the uncertainties arising from each of these methodologies will provide decision makers and the impacts and adaptation community with a truer picture of the future climate over India.

One of the major areas where the climate models have made improvement between the third and fourth IPCC assessment is the treatment of the interactions of aerosols and clouds with climate due to availability of in-situ and remote sensing data that help better characterization across the globe. These data have reduced the uncertainty in direct climate forcing, but large uncertainty still exists at the regional level because of assumptions associated with sub-grid scale parameterizations. Thus the sensitivity of regional climate to these parameterized dynamic and physical processes (e.g. change in cloud cover and cloud optical depth due to increasing aerosol concentration) and the associated uncertainties in direct, indirect and semi-direct radiative forcing need to be assessed for improved forecast of future climate. This can be achieved by evaluating the model performances and upgrading the GCM parameterization using observations at various spatial scales (Li et al., 2010).

Despite the improvements, many issues remain unresolved and uncertainties remain especially when regional climate changes are considered. Unless we quantify these uncertainties, the projected results cannot be properly interpreted and suitable scientific and technological strategies cannot be formulated for adaptation and mitigation measures. A large coordinated effort is required to address this problem. With the progress in understanding the science of climate change, there is an urgent need to prepare a scientific/technical workforce that can utilize the existing scientific information for the betterment of society through the use of state-of-the-art technology such as satellites and powerful computers. To take advantage of such scientific findings and technical tools, we need more skilled manpower. The manpower problem can only be resolved by creating a human resource development program.

1.1 State-of-the-art Research on Climate Change and Modelling

Various international efforts have been made to arrive at the question of uncertainty in future climate. The uncertainties in regional predictions (ranging from seasonal to climate time-scale) have been addressed through projects such as DEMETER and ENSEMBLES. More recently, recognizing the need to examine the uncertainties in regional downscaling techniques, the World Climate Research program has initiated a framework called Coordinated Regional Downscaling Experiment (CORDEX) aimed at improving coordinated international efforts in regional climate downscaling techniques.
Many regional climate models are already available. Multi-decadal high resolution climate change simulations over East Asia were performed by Gao et al. (2008) using the Abdus Salam International Centre for Theoretical Physics (ICTP) Regional Climate Model version3 (RegCM3) nested within the NASA/NCAR global model FvGCM. They had two sets of simulations at 20-km grid spacing for present day and future climate (IPCC A2 scenario). The changes in the mean precipitation during the monsoon season (May to September) over China were analyzed and the results of RegCM3 and FvGCM

inter-compared. Simulation of the present day precipitation by the RegCM3 shows a better performance than that of the driving FvGCM in terms of both spatial pattern and amount. The FvGCM simulates a predominant increase of precipitation over the region, whereas the RegCM3 shows extended areas of decrease. They also found that RegCM3 simulated changes were in better agreement with observed precipitation trends over East Asia. Based on their results they have suggested that high resolution models are needed to better investigate future climate projections over China and East Asia.

Sylla et al. (2009) examined the ability of the latest version of RegCM3 at 50km resolution to reproduce seasonal mean climatology, annual cycle and inter-annual variability over the entire African continent and different climate sub-regions using the new European Center for Medium Range Weather Forecast (ECMWF) ERA-interim (0.75^0x0.75^0) gridded reanalysis as initial and lateral boundary conditions. Seasonal mean values of zonal wind profile, temperature, precipitation and associated low level circulations were shown to be realistically simulated, although the regional model still shows some deficiencies. The regional model has captured fairly well the main circulations influencing the African continent, such as the monsoon flow in the lower troposphere, the African Easterly Jet and Tropical Easterly Jet in the mid and upper troposphere for the boreal summer north of the equator. In the austral summer, the Subtropical Jet Stream, the low level easterlies and the mid and upper troposphere easterlies were also captured. The important systematic errors in the model simulations are an overestimate of the strength of the monsoon flow and an underestimate and slight northward displacement of the AEJ core compared to the driving ERA-interim reanalysis. Simulated seasonal rainfall climatology is found to be in consistent with the observations. The RegCM3 captures the spatial variability of rainfall, the north–south migration of the ITCZ and the associated low level circulation reasonably well.

Diffenbaugh et al. (2006) have examined the response of summer precipitation to mid-Holocene insolation forcing and insolation-induced changes in sea surface temperature using a high-resolution nested climate modeling system RegCM3 (Pal et al., 2007) and the NCAR Community Climate System Model (CCSM3) (Collins et al., 2006) at 55km resolution over continental US. They found that mid-Holocene insolation forcing results in drier-than-present conditions over the central continental United States (U.S.) and northern Rocky Mountains, as well as wetter-than-present conditions over the Atlantic seaboard and northwestern Great Plains. Changes in summer precipitation are dominated by changes in large-scale processes, with similar patterns of change in the global and nested models.

Ying et al. (2009) studied a fine scale analysis of the climate change signal over East Asia from the CMIP3 ensemble based on the regional climate change index (RCCI) introduced by Giorgi (2006). They have calculated the RCCI to investigate hot-spots under 21st century global warming over East Asia on a 1-degree resolution grid from the ensemble of CMIP3 simulations for the B1, A1B, and A2 IPCC emission scenarios. They found that, as a whole East Asia does not show a large RCCI compared to other regions of the world. It still includes clearly identifiable sub-regions with high RCCI values (i.e., sub-regional scale hot-spots). It may be noted that East Asia is not identified as a prominent climate change hot-spot by Giorgi, (2006). More specifically, they have identified five such hot-spots, three in the northern China-Mongolia areas, one in the eastern China, and one in the Tibetan Plateau.

Quantifying the impact of aerosols and clouds on radiation and climate is another major source of uncertainty in all climate models. Improved aerosol modules that include all the major anthropogenic and natural species and their size distributions throughout the lifetime in GCMs have reduced the uncertainty in direct climate forcing significantly. Several studies have explored the sensitivity of direct climate forcing to current parameterization uncertainties in GCMs (*Kinne et al*., 2006). Model results are constrained to obtain present-day aerosol distribution consistent to the satellite observations. However, most GCMs continue to fail to reproduce the spatial distribution of aerosols and under-predict the aerosol optical depth in India (*Ganguly et al.*, 2009) due to large uncertainty stemming from complex aerosol characteristics and poor emission inventories. The indirect and semi-direct effects are more complex, and their poor treatments in the GCMs, primarily due to lack of statistically robust observational evidence, make it difficult to project climate change at regional scale. Recent approaches to tackle this problem involve assessments of the climate models through intercomparison with observations (*Quaas et al.*, 2009). It has been suggested to derive statistical relationships for different cloud systems in response to varying aerosol characteristics at various spatial scales (*Stevens and Feingold*, 2009), which will improve the sub-grid scale parameterization. Similar efforts are needed in the Indian region, where strong seasonal cycle of atmospheric circulation makes it difficult to disentangle meteorological influence from aerosol influence on clouds and climate.

Given the range of unanswered questions in climate change predictions and in view of their importance, a much larger research effort is needed for which existing manpower is not adequate. Realizing the need, many developed countries have started capacity building programs on “Climate Change Education”. One prime example is United States of America, where agencies like NSF, NASA and NCAR have launched outreach programs with focus on climate change to engage and stimulate young research scholars. Similar programs were also initiated in Australia and many countries in Europe. These programs aimed at to improve understanding of the science of climate change and implement new approaches to adapt and mitigate the climate change in near future. The objectives were envisioned to be achieved by preparing the young researchers and creating awareness among general public that will lead to development of appropriate strategies in dealing with climate change. The programs contain capsule training modules to educate young researchers in the university through interactive portal website, science workshops and visual media. Financial support in the form of scholarships and awards are provided to generate excitement among the young scientific workforce and engage them in various public awareness activities. The programs are being operated at national to county level and are funded by state and federal government agencies.

The study of regional climate change is increasingly becoming important for accurate assessment of impacts on different sectors of the society. For such studies the regional climate models are the most convenient tools provided the uncertainties are computed with reasonable accuracy. Although several studies have been conducted for regional climate change assessments for countries in Europe and USA, the same is in very infant stage in India. Since India is very vulnerable to climate changes, more emphasis should be given on the study of regional climate changes using available models.

The National Communication (NATCOMM) process has resulted in the HadCM3 simulations being carried out at IITM Pune, where Rupa Kumar et al. (2006) conducted experiments using the Hadley Centre regional climate models HadRM3H/Providing REgional Climates for Impacts Studies (PRECIS) for the Indian region using HadCM as initial and boundary conditions with 0.44^0x0.44^0 resolution in Baseline (1961-90), A2 Scenario (2071-2100) and B2 Scenario (2071-2100). The model captured the important regional climate information on summer monsoon rainfall which was missing in its parent GCM simulations. These climate scenarios are being used for impact assessment studies in hydrology, agriculture and other related fields. Amongst the regional models, PRECIS is the only model used for the climate change scenarios and impact assessment studies in India, to some extent. However, since each model has its own uncertainties and it is not yet known which one is a good model for a particular domain, it is essential to run another regional model, the RegCM3 in the climate mode.

These realizations are available for assessment of uncertainty in future climate – both as simulated by the AOGCM and the downscaled output from the RCM. One serious limitation of the above exercise is that the full range of uncertainty is possibly not captured by using a single model. Beyond these studies, the IPCC AR4 models have been available for uncertainty assessment (*Christensen et al.*, 2007). The impacts and adaptation studies that have come out of these do not seem to have taken the range of possible outcomes into account. They have focused on using one realization and in the process end up coming up with answers that contain no uncertainty information.

During the last ten years, tremendous efforts were made to acquire in-situ and remote sensing data for improved characterization of aerosols and clouds in India. These data have definitely reduced the uncertainty in direct aerosol radiative forcing, but not up to the desired level, because of many assumptions that are still to be evaluated with observations. Thus the sensitivity of regional climate due to direct, indirect and semi-direct forcing and the associated uncertainties need to be assessed for improved forecast of future climate, which can only be achieved by evaluating the model performances and upgrade the GCM parameterization using observations (*Li et al.*, 2010). This is even more important for regions like India, where monsoon precipitation is possibly being affected by aerosol forcing (*Ramanathan et al.*, 2005; *Lau et al.*, 2006), but the quantification of the processes are debated and unresolved.

Unlike the USA or other developed countries, India does not have a dedicated curriculum on human resource development for climate change research. This has led to a deficit of skilled manpower and lack of a strong coordination between academic institutions and government organizations are the major challenges our country is facing in developing strategies for climate change. In our country 'Weather and Climate' is taught in very few institutions as a subject on its own, that too only at postgraduate level. To cater to the increasing demands it is essential to encourage students to choose this subject as a career option through coordinated training programs, especially in modelling.

1.2 Research initiatives undertaken under National Mission on Strategic Knowledge for Climate Change (NMSKCC) as part of Climate Change programme (CCP) of DST

Details of each project run by different PIs in Climate Modelling theme

Project 1:

Major R&D Project on "Modelling Regional Climate Change : Addressing Scientific Uncertainties and Capacity Building Needs" (DST/CCP/PR/11/2011(G) dated 22.3.2012)

S.K. Dash, Krishna Mirle Achutarao and Sagnik Dey
Centre for Atmospheric Sciences, IIT Delhi, Hauz Khas, New Delhi-110016 and
U.C. Mohanty
School of Earth Ocean & Climate Sciences, IIT Bhubaneswar

Project 2:

DST's Centre for Excellence in Climate Studies

Kaustubh Salvi, Subimal Ghosh, Ribu Cherian and Chandra Venkataraman
Indian Institute of Technology Bombay, Powai, Mumbai-400076

Project 3:

Major R&D Project on "Study of Extreme Rainfall Events Over India in the Context of Climate Change" (Ref No: DST/CCP/PR/15/2011(G)

Suneet Dwivedi and Avinash C Pandey
K Banerjee Centre of Atmospheric and Ocean Studies, University of Allahabad, Allahabad, 211002

Chapter-2

Project Objectives and Methods of Approach

2.1 Project wise Objectives

Project 1:

- The objectives of the project operational at IIT Delhi are to understand the uncertainties in projections of climate in the Indian region
  a) as simulated by multiple AOGCMs
  b) as simulated by regional climate models at high resolution
  c) as simulated by dynamical and statistical downscaling
  d) due to treatment of aerosols in the climate models
- The other objective of IIT Delhi project is to create skilled manpower by providing hands-on training on the operations of the global and regional climate models

Project 2:

- The Indian Institute of Technology Bombay's Centre for Excellence in Climate Studies (IITB-CECS), supported by the Government of India, DST-Climate Change Programme, was created in January 2012, with a mandate to *"Undertake interdisciplinary education and research to develop a scientific understanding of regional climate change and connect it to impacts (socio-economic, environment, resources) and effective response (technology and adaptation)."* An important objective of the IITB-CECS is to provide critical assessments to support governmental policy and decision response to climate change mitigation. The specific objectives are:
- To understand various climatic variables and their impact on precipitation.
- To understand the downscaling techniques.
- To apply the bias correction technique and validate the temperature projections for various SRES scenarios.
- To simulate high resolution (1º Lat × 1º Long) temperature projections for 21st century.
- To apply 'Statistical Downscaling' methodology and simulate high resolution (0.5º Lat × 0.5º Long) rainfall projections for 2020s, 2050s, and 2080s time period for various SRES scenarios.
- To compare the influence of high level predictors on rainfall projections as compared to surface level predictors.

Project 3:

- The objectives of Allahabad University project is to study the long-term trends in the extreme rainfall events over India by using station as well as gridded data and to investigate the observed discrepancies, especially over Indo-Gangetic plains (UP, Bihar, Punjab, Haryana, West Bengal).
- Further, the model outputs of few selected AR4/IPCC models which are found to perform better for the Indian monsoon simulation shall be subjected to a similar study, to see, how close they are capable of capturing the spatial variability of trends

in the extreme rainfall events. In addition to this, the efficacy of satellite products in capturing the extreme rainfall events shall also be investigated, where possible.

2.2 Methods of Approach

Project 1:

The National Center for Atmospheric Research (NCAR) Community Atmospheric Model (CAM) Versions 4 and 5 (part of the Community Earth System Model) are now installed and these are running on the two HPC clusters at CAS. In addition, some computer time has been arranged at CDAC, Pune and test runs have been successfully carried out. Climate change and uncertainty analysis for selected Indian region is carried with respect to present time (1971-1990) and for the future (2020-2099) by dividing it into four time-slices of 20 years each. We provide three measures of uncertainty. The first is a simple measure of 'Reliability Ensemble Averaging' (REA, Giorgi & Mearns (2002)) and 'Reliability Ensemble Averaging Upgraded' (REAUpgraded, Ying Xu et al. 2010) are used. Based on different merits and demerits suggested in literature, we compared these with simple 'Multi-Model Ensemble Averaging'. REA weights the ensemble model based on two criteria, a model's ability to simulate the present day mean climate termed as 'Model Performance criteria' and the distance of each model simulated future change from Multi-Model ensemble change termed as 'Convergence Criteria 'because the distance is iteratively checked to be minimum from the multi-model ensemble change. REA weights are based on the models above criteria for a single atmospheric variable, whereas in Upgraded REA weighing approach is extended for multivariable, multi statistics and multiple characteristics. In essence, this means, a model is weighted higher if it simulates both temperature and precipitation (or any other combination of variables) well. Also, the "Convergence Criteria" is replaced with model's ability to simulate the interannual variability of temperature and precipitation. Interannual variability is measured in terms of multiple statistics. Introduction of effective number of models for a threshold change for unbiased estimation of uncertainty range, while original REA weights outliers low, thus gives a downward biased estimation as explained in literature.

The uncertainty in regional climate model simulations arises due to several sources. Use of different GCM forcings as initial conditions and different parameterization schemes are the two most important sources of such climate uncertainty. Current study is aimed at examining the differences in response to similar GCM forcings in the regional climate model RegCM4.3 with two different cumulus convection parameterization schemes over the ocean. The global coupled climate earth system models, GFDL-ESM2M and MPI-ESM-MR obtained from CMIP5 archive constitute the two anthropogenic emission forcings. MIT-Emanuel convective parameterization scheme has been used over the land in all the experiments. Over the ocean, experiments are designed using both Emanuel and Grell convection schemes. RegCM4.3 has been integrated for the south Asia CORDEX domain at 50 km resolution starting from the initial condition of 1st Jan 1970 and the climate simulation continued till 1st Jan 2100.

Boundary forcings of GFDL and MPI are obtained for control experiments and two emission scenarios RCP4.5 and RCP8.5. Here RCP stands for Representative

Concentration Pathways. Following experiments are conducted with two different GCM forcings and two convective schemes using RegCM4.3.

1) GFDL forcing with Emanuel convective scheme both over land and ocean (EE)
   i) Historical run over the period 1970-2005: RCM-GFRF-EE
   ii) Future RCP4.5 scenario over the period 2006-2099: RCM-GF45-EE
   iii) Future RCP8.5 scenario over the period 2006-2099: RCM-GF85-EE

2) GFDL forcing with Emanuel convective scheme over land and Grell over ocean (EG)
   i) Historical run over the period 1970-2005: RCM-GFRF-EG
   ii) Future RCP4.5 scenario over the period 2006-2099: RCM-GF45-EG
   iii) Future RCP8.5 scenario over the period 2006-2099: RCM-GF85-EG

3) MPI forcing with Emanuel convective scheme over land and Grell over ocean (EG)
   i) Historical run over the period 1970-2005: RCM-MPRF-EG
   ii) Future RCP8.5 scenario over the period 2006-2099 RCM-MP85-EG

Using two selected GCM boundary forcings, the RegCM4.3 is integrated starting from the initial conditions of 1st January 1970 till November 2005 for the control experiments and further restarted using the boundary conditions of emission scenarios till the end of 1st January 2100 spanning 130 years at 50 km resolution. First five years spin-up period are discarded for the analysis of model simulated data.

In the third component of the first project by IIT Delhi, the NCMRWF global spectral model (T80) and ICTP regional climate model RegCM have been used. T80 model is the climate version of the medium-range weather forecast model of NCMRWF and is being used for preparation of seasonal predictions of monsoon in real-time. The model is global spectral model with 80 waves in Triangular truncation equivalent to 1.4° × 1.4° horizontal grid resolutions. In the vertical, the model has 18 sigma layers. Deep convection is modelled by a fairly basic Kuo-Anthes type of scheme.

The RegCM4.1.1 standard model configuration consists of 18 vertical sigma levels in which five levels at approximately 40, 110, 310, 730, and 1400 m are in the lower troposphere (within 1.5 km from surface, Giorgi and Bates (1989). The physical parameterization schemes used in the present study include the mass flux cumulus cloud scheme of with Fritch–Chappell closure, nonlocal boundary scheme and radiative transfer of the NCAR CCM3. The land-surface processes are described via Community Land Model (CLM). The model is integrated from 1st November to 28th (29th for a leap year) of February of each year, for a period of 28 years (1982-2010). The model horizontal resolution is 30 km which extends from 28°E -128°E and 30°S - 56°N. The initial and lateral boundary conditions are provided from NCMRWF T80 model available at 1.4°×1.4° resolution. Optimal Interpolation SST (version 2, NOAA_OISST_V2) data of NOAA at 1°×1° resolution are provided to the model. Other geophysical parameters obtained from USGS at 10 min resolution are used as surface conditions to the model. The Model simulated results are validated with the NNRP2 reanalysis and IMD gridded precipitation data sets.

Uncertainty in climate forcing due to aerosols can be attributed to two reasons: (i) Model simulation of 3-D aerosol field in comparison to the observations (satellites and in-situ) may have uncertainty due to (a) uncertainty in emission inventory and (b) bias in simulated meteorological fields that redistributes aerosols spatially (ii) Aerosol-induced changes in cloud properties also lead to indirect radiative forcing. Errors in simulated cloud fields also contribute to uncertainty in climate forcing. To asses these two issues, regional climate model RegCM version 4.1 has been used to simulate aerosol (natural and anthropogenic) distribution over India. The results are evaluated against observations. Simultaneously, an analytical framework has been developed to link the radiative forcing at top of the atmosphere to the observed surface temperature trends to further understand the implications for climate projections.

Project 2:

Every model has its own bias as against the actual observation. It is important to remove the bias from the GCM output for projecting the future hydrologic and climatic scenario correctly. Standardization (Wilby et al., 2004) is used to reduce systematic biases in the mean and variances of GCM predictors relative to the observations or NCEP/NCAR data. The procedure typically involves subtraction of mean and division by standard deviation of the predictor variable for a pre defined baseline period for both NCEP/NCAR and GCM output.

The other methodology by Li et al. (2010) is quartile based mapping method on cumulative distribution functions of observed, training and testing data. In case of ideal scenario, the observed time series of temperature and GCM simulated time series of temperature for the same location (node) would actually overlap each other. But because of bias, the GCM simulated time series shows a similar pattern as that of observed one but would not coincide with it as in Figure 1. The time series in blue colour actually represents the GCM simulated data and the time series in red represents the observed data for the same node. Bias is clearly seen.

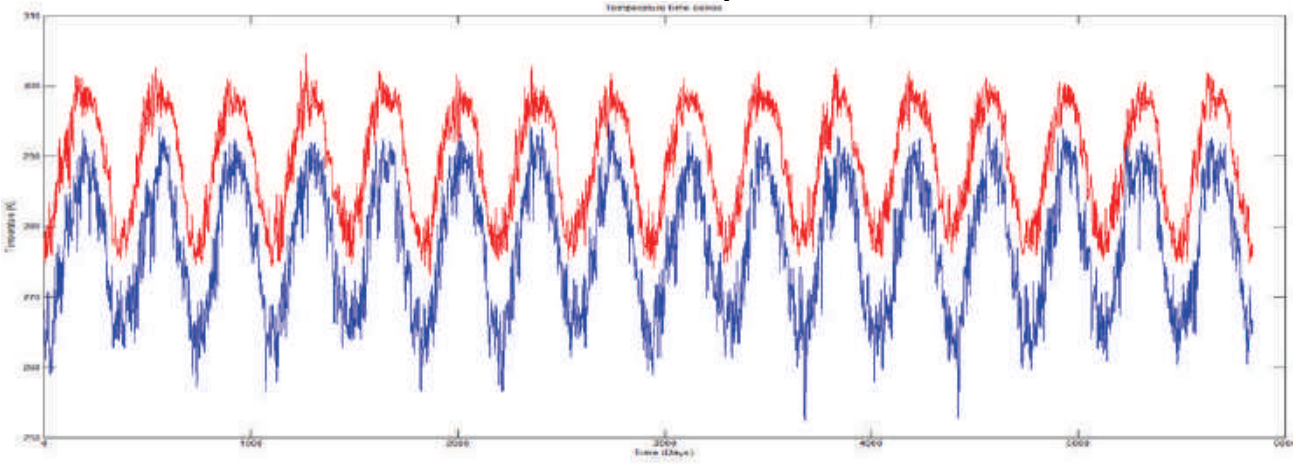

Figure 1: Bias in observed and GCM simulated Data

Following are the steps which have been repeated for every node to get the bias corrected data. Figure 2 shows a pictorial representation of the bias correction methodology. Time series of observed and GCM simulated temperature fields for the same node are used for the training period.

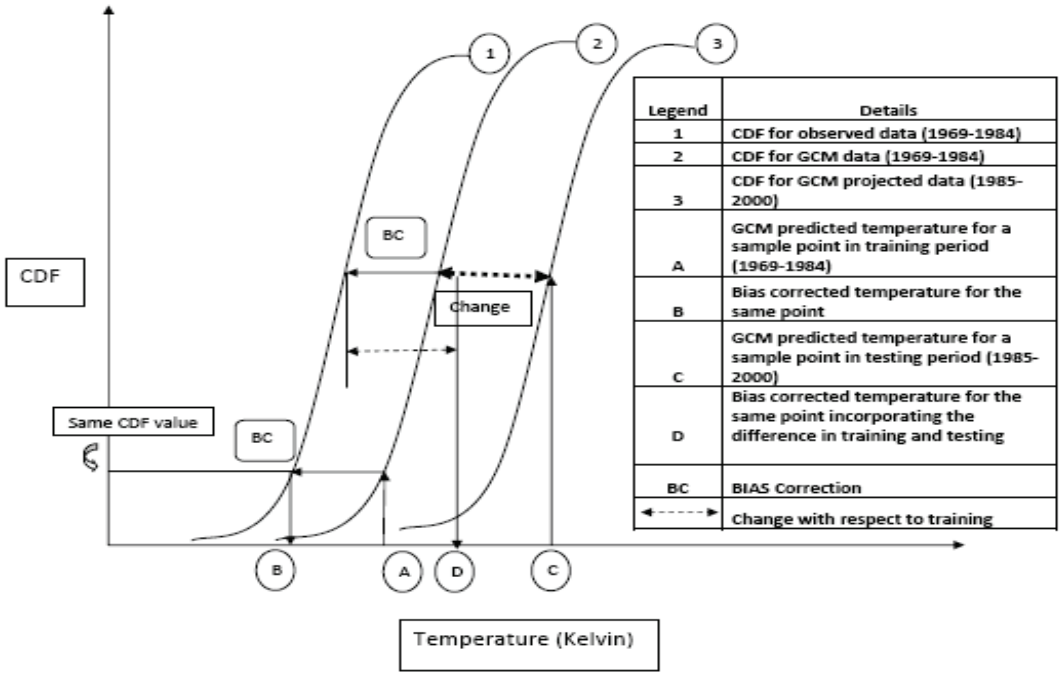

Figure 2: Pictorial representation of Quantile based remapping Bias correction methodology

First of all the same probability distribution for both the time series is fitted. In this study, we have used 'Gamma' distribution as it proved to be the best fit. (Highest AIC value). Let the distribution parameters for the observed time series be $P1_{observed}$ and $P2_{observed}$. Similarly let the parameters for the GCM simulated time series be $P1_{GCM}$ and $P2_{GCM}$. As a next step the CDF values for both the time series using corresponding parameters are computed. Let the CDF for observed time series be $CDF_{observed}$ and CDF for GCM simulated time series be CDF_{GCM}. Finally using CDF_{GCM} and parameters $P1_{observed}$ and $P2_{observed}$, generate the corrected time series values. This procedure just replaces the GCM simulated value by an observed value whose quantile values are equal.

In order to correct the bias in case of future data one needs (1) GCM simulated temperature time series for future (to be corrected; observed data is not available for this period) (2) GCM simulated temperature time series for the same node for training period (observed data is available of this training period) (3) Observed temperature time series at the same node for training period. In this case first the same probability distribution for all the time series is fitted. Again we have used 'Gamma' distribution as it proved to be the best fit. (Highest AIC value). Let the distribution parameters for the observed time series be $P1_{observed}$ and $P2_{observed}$. Similarly let the parameters for the GCM simulated time series for training be $P1_{GCM\_train}$ and $P2_{GCM\_train}$ and the parameters for the future time series (testing period) be $P1_{GCM\_test}$ and $P2_{GCM\_test}$. In the second step the CDFs for all the three time series using their respective parameters are computed. Let the CDF for observed time series be $CDF_{observed}$ and CDF for GCM simulated time series for training period be CDF_{GCM_train} and CDF for GCM simulated time series for future (testing) period be CDF_{GCM_test}. Then a time series using the CDF_{GCM_test} and parameters $P1_{GCM\_train}$ and $P2_{GCM\_train}$ is generated. These time series values from the GCM simulated time series for future (testing) period are subtracted. This difference can be treated as the climate change. This step is essential because we cannot directly

correct the future time series using past observed data. (We did this for the training period time series because the observed data was available for the same period.) Finally, using CDF_{GCM_test} and the parameters $P1_{observed}$ and $P2_{observed}$, the new time series is obtained and the difference calculated in the previous step to this time series is added. This is the bias corrected time series for future.

The above mentioned methodology is applied to Canadian GCM, CGCM3, with 1969-1984 as training data and 1985-2000 as testing data using 20C3M simulations. The future projections are done dividing the 21st century in to four slices each of 30 years. Figure 3 shows the bias corrected temperature time series in green colour.

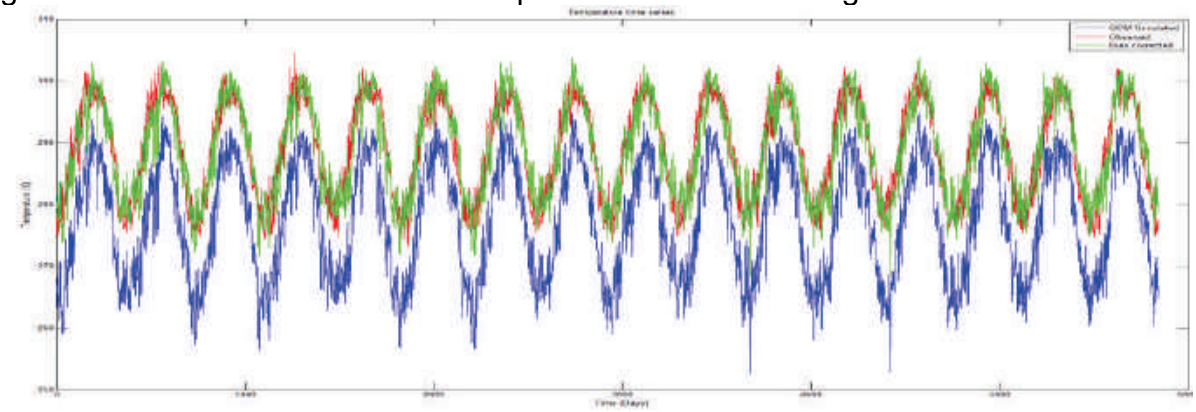

Figure 3: Bias corrected temperature at one node

The focus of this study is to assess the direct and indirect effects of anthropogenic aerosols on south Asian climate, with a focus on precipitation, using the general circulation model European Centre for Medium-Range Weather Forecasts (ECMWF) - Hamburg Model, ECHAM, version 5.5, extended by the Hamburg aerosol module, HAM). The influence of anthropogenic aerosols on seasonal monsoon rainfall patterns was investigated using present-day (PD) and pre-industrial (PI, 1750) aerosol emission inventories. A new, regionally-validated aerosol emission dataset for present-day emissions was used, with better model resolution of 180 km, more detailed cloud microphysics description and a realistic mix of natural and anthropogenic aerosols. A seasonal trend analysis from January 2001 to December 2005 was made of model-simulated aerosol distributions, radiative effects, atmospheric heating patterns and monsoon precipitation. The model-simulated aerosol optical depth (AOD) and precipitation patterns were evaluated seasonally using satellite retrievals. The influence of circulation patterns on aerosol induced precipitation changes over the Indian region was evaluated.

In the current study, the CART Analysis is used to (1) Obtain the relationship between the PCA processed predictors and rainfall states for training period (2) Generate future rainfall states using the developed relationship and PCA processed predictors for testing period (simulated by GCM) with as assumption that the relationship developed for training period holds good for future as well. Once the future states are simulated, using Kernel regression the future rainfall is projected. CART Analysis is an iterative process of splitting the data into partitions, and then splitting it up further on each of the branches. The steps involved in building CART are as follows:

- Initially, place all observations in the training set (the pre-classified records that are used to determine the structure of the tree) at the root node. This node is considered

impure or heterogeneous, since it contains all observations. The goal is to devise a rule that initially breaks up these observations and creates groups or binary nodes that are internally more homogeneous than the root node.

- Starting with the first variable, split a variable at all of its possible split points (at all of the values the variable assumes in the sample). At each possible split point of the variable, the sample splits into two binary or child nodes.
- Apply goodness-of-split criteria to each split point and evaluate the reduction in impurity or heterogeneity due to the split.
- Select the best split on the variable as that split for which reduction in impurity is the highest.
- Repeat steps (2)–(4) for each of the remaining variable at the root node and rank all of the 'best' splits on each variable according to the reduction in impurity achieved by each split.
- Select the variable and its best split point that reduces most of the impurity of the root or parent node.
- Assign classes to these nodes according to a rule that minimizes misclassification cost.
- Repeatedly apply steps (2)–(7) to each non-terminal child node at each of the successive stages.
- Continue the splitting process and build a larger tree. The largest tree can be achieved if the splitting process continues until every observation constitutes a terminal node.
- Prune the results using cross-validation and create a sequence of nested tree, and select the optimal tree based on minimum cross-validation error rate.

The advantages of using the CART model are:

- It makes no distributional assumption of any kind, either on dependent or on independent variables. No predictor variable in CART is assumed to follow any kind of statistical distribution;
- The predictor variables in CART can be a mixture of categorical, interval, and continuous;
- CART is not affected by outliers, colinearities, heteroscedasticity or distributional error structure that affect parametric procedures;
- CART has the ability to detect and reveal interactions in the dataset;
- CART is invariant under monotonic transformation of independent variables; and
- CART effectively deals with higher-dimensional data.

In the study related to aerosols in GCMs (under project2 at IIT Bombay) the model simulations were performed with prescribed present-day climatological observed sea surface temperature (SST) and sea ice concentration (SIC) using the monthly varying atmospheric model intercomparison project (AMIP) data sets, and with prescribed present-day long-lived green house gas concentrations, ozone, and land-surface properties. The simulations differ only from the emissions of anthropogenic aerosol and aerosol precursor gases (BC, OC and SO_2). In the control run the pre-industrial (PI, 1750) anthropogenic aerosol emission inventory (*Dentener et al.*, 2006) is used, while in the experiment simulations the present-day (PD) anthropogenic aerosol emissions are used (see Table 1). In both PD and PI runs, nudged simulations were performed, in which the large-scale meteorological fields were constrained using European Centre for Medium Weather Forecast (ECMWF) re-analysis data sets. To analyse the effect of

circulation changes, an ensemble of three non-nudged simulations was also carried out for both PI and PD aerosol emissions.

Table 1: Summary of emission data used in present-day (PD) and pre-industrial (PI) simulations

Experiment name	Simulated years	Prescribed emissions (DMS, dust, and sea salt are calculated)
Pre-Industrial (PI)	5 years (2001-2005)	1750 anthropogenic emissions (Dentener et al., 2006)
Present-day (PD)	5 years (2001-2005)	SO_2, BC and OC (AERONET + INDIA) fixed at year 2000 levels

In this study, SSTs and SICs were used to isolate and examine the effects of anthropogenic aerosols on the atmospheric heating and precipitation patterns, without the complexity of a fully coupled ocean-atmosphere model. By applying the observed SSTs as the lower boundary condition, most of the uncertainties associated with the lower-boundary forcing (which may arise from the use of a mixed-layer ocean or a fully coupled ocean model) do not come into picture. The feedback of SST changes from aerosol surface cooling was not considered in this study. This is to reduce the complexity in the effects of aerosols on precipitation patterns.

Aerosol emissions, based on the AEROCOM emission inventory (*Dentener et al.*, 2006) of the year 2000 are combined with regional emission inventories available over India (*Reddy and Venkataraman*, 2002; *Venkataraman et al.*, 2005; *Venkataraman et al*., 2006). The combined emission dataset was used for residential, transport, industry and agricultural residue burning emission sectors. AEROCOM global emissions of SO_2 for these sectors are from *Cofala et al.*, (2005) and BC and OM global emissions are from *Bond et al.*, (2004). Global fire emission data (GFED) was used for forest burning emission sectors. Volcanic emissions of SO_2 are included (*Andres and Kasgnoc*, 1998). Dust and sea salt emissions were calculated online (*Tegen et al.*, 2002) using the ECHAM 10m winds speed.

Each of the above simulations covers 5 years (2001 to 2005) after a spin-up of three months to initialize aerosol fields. In this study, the analysis was carried out separately for four different seasons i.e. north east monsoon (NE, November-December-January; NDJ), pre-monsoon or dry season (February, March, April, May; FMAM), south west monsoon (SW, June, July, August, September; JJAS), and inter-monsoon or post-monsoon (October) over the Indian region. The seasonal climatology of model simulated aerosol optical depth (AOD) and its regional climate effects over the Indian subcontinent during the period 2001 to 2005 are discussed in the following sections.

Project 3:

In Project 3 at Allahabad University, the standard statistical methodologies are used for trend analysis and mapping of remote sensing data. The nonlinear dynamical rules are used for active/break spell analysis of the rainfall during El Nino and La Nina years. The annual time series of different rainfall indices are constructed from each model's output for statistical trend analysis. The trend analysis uses non-parametric Mann-Kendall test, z-statistics and Sen's slope. The non parametric tests are taken into consideration over the parametric ones since they evade the problems raised by skewness of data. The

Mann-Kendall test is preferred for trend detection when various stations are tested in a single study.

The rainfall categories are classified in the following manner as per the definition of India Meteorological Department:

- Low to Medium Rainfall: A day is treated under this category, if the rainfall of that day is 2.5 mm or more but less than 64.5 mm.
- Heavy Rainfall: If the rainfall of a day is greater than 64.5 mm but less than 124.5 mm.
- Very Heavy Rainfall: If the rainfall of a day is greater than 124.5 mm but less than 244.5 mm.
- Extremely Heavy Rainfall: If the rainfall of a day is greater than244.5 mm.

Chapter-3

Important Results of Project 1: Modelling Regional Climate Change : Addressing Scientific Uncertainties and Capacity Building Needs

The first project at IIT Delhi has four distinct scientific objectives. Under each of these objectives progress has been made considerably as mentioned briefly under the following items:

3.1 Exploring the uncertainty in multiple AOGCMs

The future changes in temperature and precipitation over India as simulated by Coupled Climate Models under different scenarios (RCP4.5 and RCP8.5) have been investigated in order to understand the uncertainties in these projections. Chaturvedi et al. (2012) have examined the future changes in terms of calculating the average changes to be expected at different times in the future. However, they do not give any indication of the uncertainty in the mean changes in temperature and precipitation, nor do they provide any information of the spread among different models. In this study the uncertainties in these changes have been understood in order to help policymakers make informed decisions. Changes in temperature and precipitation for future time periods are calculated at each grid point and spatially averaged over the Indian land region (6.5N-38.5N, 66.5E-100.5E). Changes are calculated Annually as well as for JJA and DJF seasons. These are presented in the Figures 4 to 8.

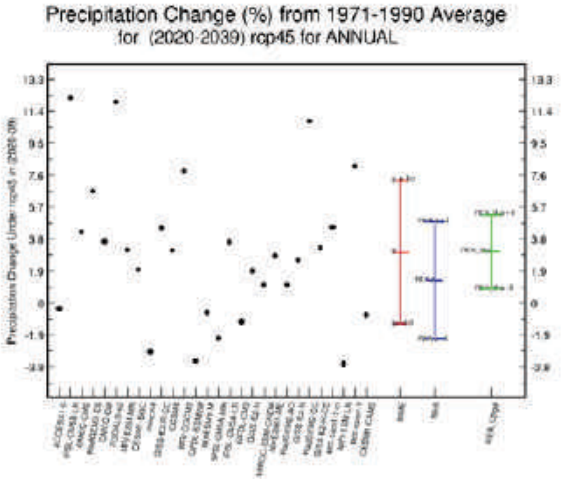

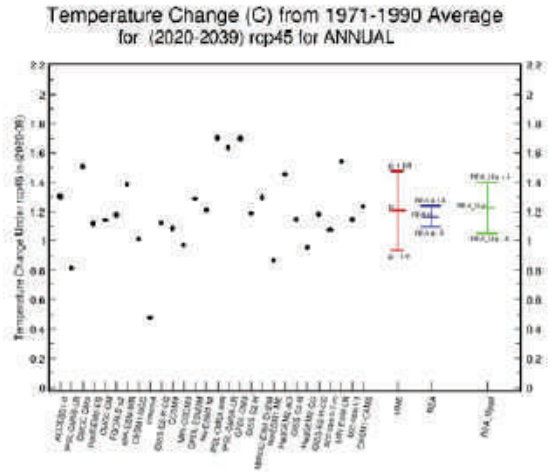

Figure 4: Spatial Multi-Model Ensemble (MME) Mean and weighted change (REA and REA Enhanced) for Annual Average Rainfall (Left panel) and Temperature (Right panel) for the 2020-2039 period under RCP8.5 scenario. Black dots represent area-averaged change over India from the 1971-1990 average as simulated by individual models listed along the X-axis. MME Mean and uncertainty (±standard deviation) are shown as red bar and whisker. The REA mean and uncertainty are shown in blue, while the REA Enhanced mean and uncertainty range are shown in green.

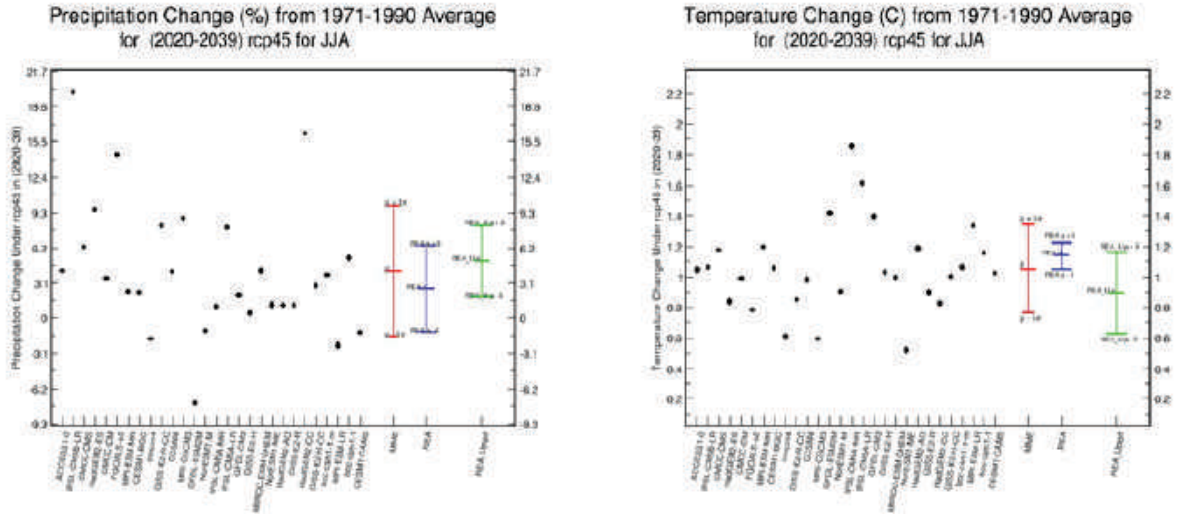

Figure 5: As in Figure 4, but for JJA season change

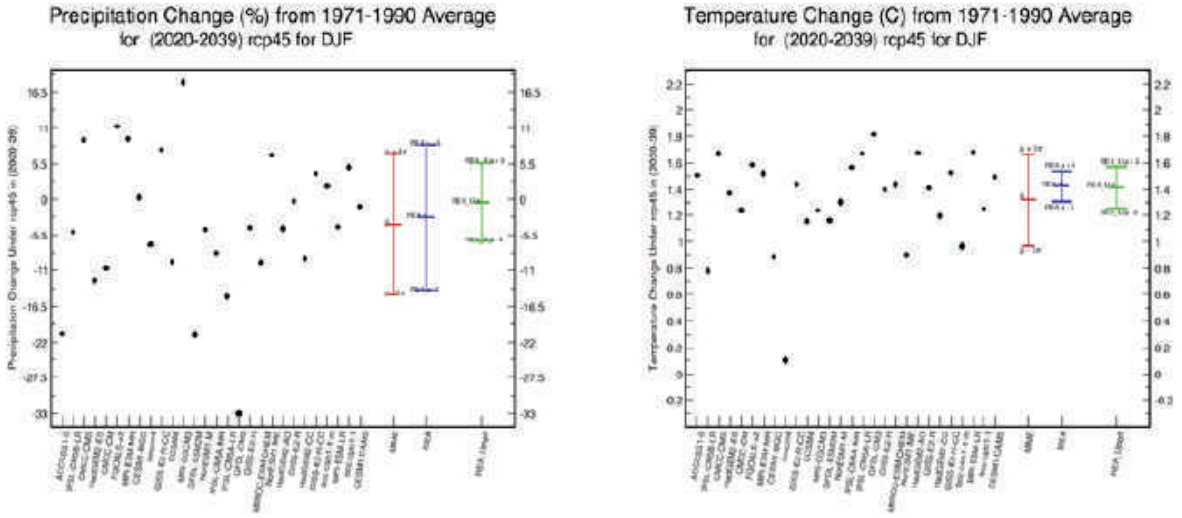

Figure 6: As in Figure 4, but for DJF season change

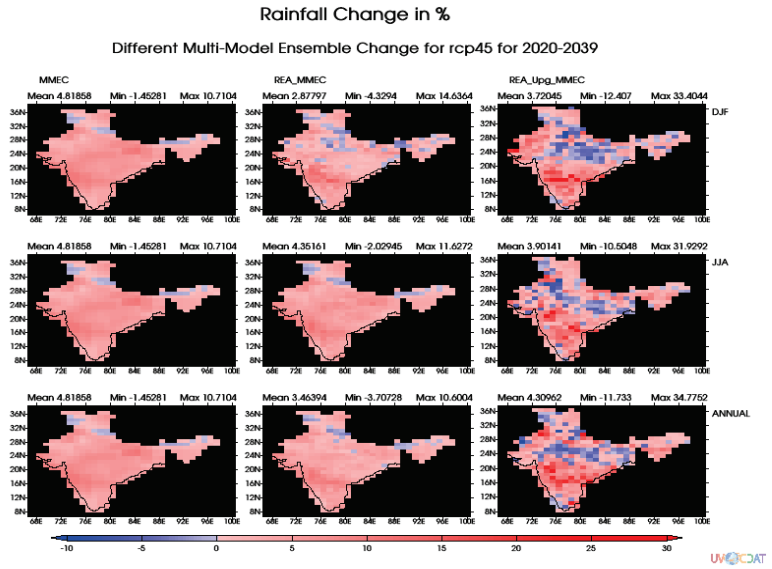

Figure 7: Projected change in mean rainfall over India under RCP4.5 for the 2020-2039 period. The rows show changes for DJF(top), JJA(middle) and Annual(bottom) respectively. The left column shows the mean change with models equally weighted; Middle column shows REA weighted change; Right column shows REA Upgraded change.

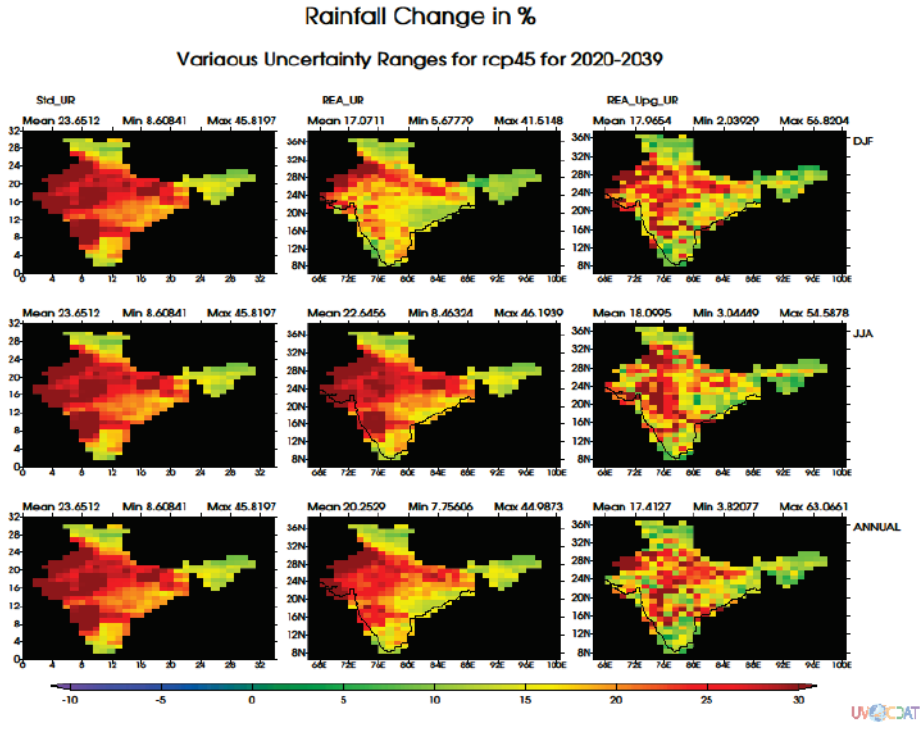

Figure 8: As in Figure 7, but for uncertainty range as described in Figure 4

3.2 Examining the uncertainties in the regional climate models

3.2.1 Model and Simulations

The regional climate model RegCM4 is used for this study. The model is described and documented in detail by Giorgi et al. (2012). In brief, RegCM4 is a hydrostatic & compressible model that runs on Arakawa B-grid and employs an explicit time splitting scheme. The model includes multiple physics options, and for the experiment presented here it uses sigma-p coordinates with 18 levels in the vertical. For the calculation of radiative transfer it uses the NCAR CCM3 radiation package. Land surface processes are simulated via the Biosphere-Atmosphere Transfer Scheme (BATS; Dickinson et. al. 1993), while boundary layer processes are parameterized using the non-local formulation of Holtslag et al. (1990). For convection, the Emanuel scheme (Emanuel and Zivkovitch 1999) and Grell (1993) schemes are used over land and ocean, respectively. Large-scale precipitation is represented by the subgrid explicit moisture scheme (SUBEX) of Pal et al. (2000). The surface elevation and land cover data are obtained from the United States Geological Survey Global Land Cover Characterization (GLCC).

The model was integrated from 1st January 1970 till 31st December 2099 at 50 km horizontal resolution over the South Asia CORDEX domain, which covers a broad South Asia region and adjacent ocean areas 10^{o} E to 130^{o} E and 22^{o} S to 49^{o} N. Here CMIP5 GFDL-ESM2M and MPI-ESM-MR simulations (from IPCC AR5) are used to produce the initial and lateral boundary conditions. The simulations consist of two phases; phase 1 is the historical period covering from 1970 till 2005, and phase 2 is for the future (2006-2100) under RCP4.5 (low end) and RCP8.5 (high end). The RegCM4 configuration and driving GCM were selected after an extensive set of preliminary experiments showed them to provide a realistic representation of the South Asia climate in present day conditions.

3.2.2 Model Verification and Validation

Before analyzing the future projections, it is essential to verify if the model is able to simulate the present monsoon conditions satisfactorily. Towards this purpose, simulated rainfall by both the global and regional climate models is validated against the IMD0.5 gridded rainfall (only over Indian land points) and GPCP rainfall over the entire South Asia domain for the reference period. The seasonal (JJAS) mean rainfall from RegCM4, GFDL and GPCP are shown in Figure 9. The left column shows the 1979-1988 mean rainfall, the middle column shows the 1995-2004 mean rainfall, while the right column shows the difference between the two means, which measures possible changes within the reference period.

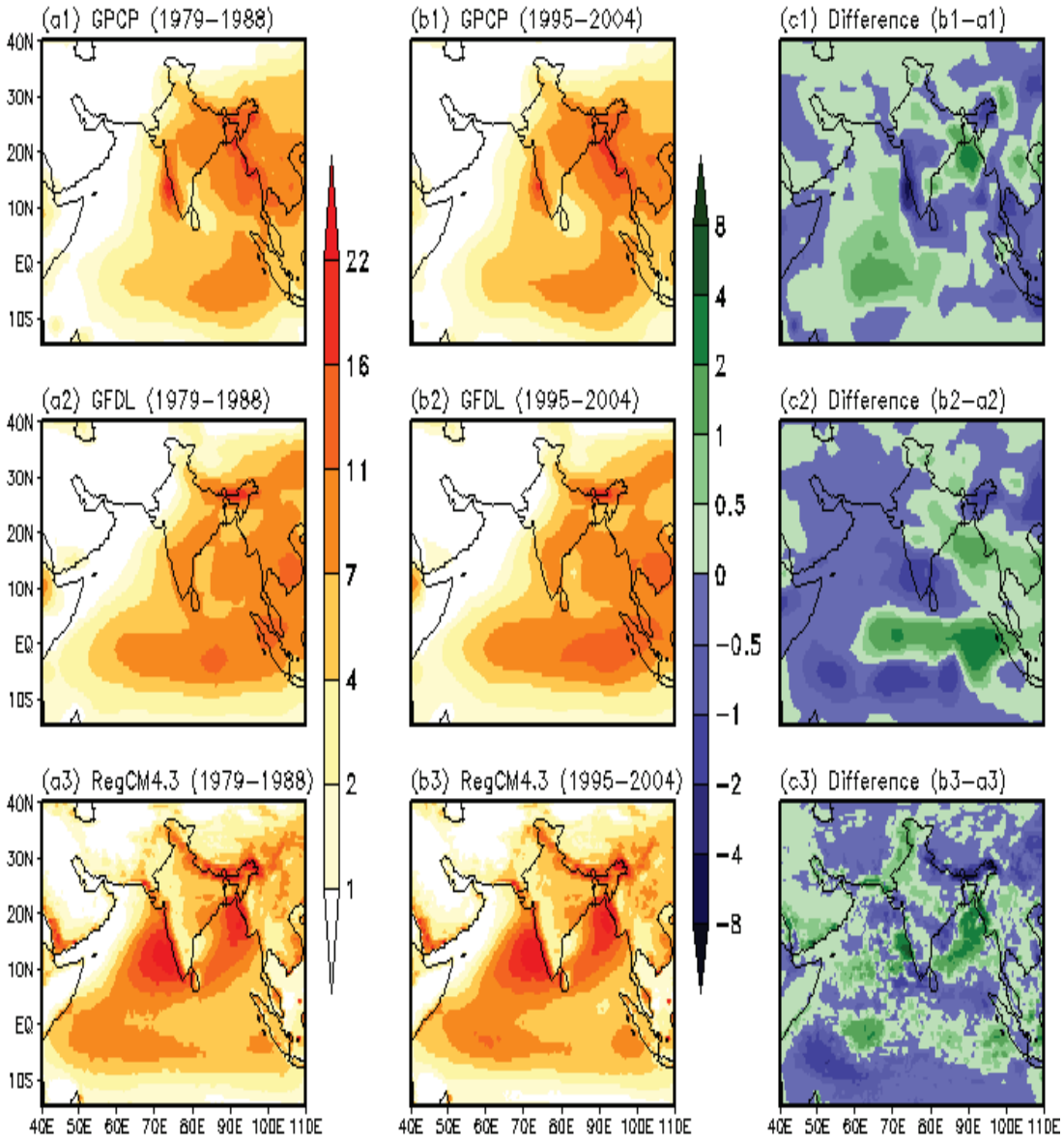

Figure 9: 10 years mean JJAS rainfall (mm/day) in the vicinity of Indian summer monsoon region, and the difference in rainfall between first and last decades during 1979 to 2004. The top panel represents the represents GPCP rainfall,

middle panel represents GFDL rainfall and the bottom panel represents RegCM4.3 simulated rainfall

The starting year is chosen as 1979 since the GPCP rainfall data are available from that year. From the left and middle columns, it appears that, although the regional model has some biases (i.e. overestimation of rainfall over the Arabian Sea, and western equatorial Indian Ocean, and underestimation over the eastern equatorial Indian Ocean), it largely captures the spatial distribution of rainfall over the Indian monsoon region. The occurrence of maximum rainfall over the head of Bay of Bengal, its extension up to south of the equator between 80^0 E and 100^0 E, and the secondary maxima over the western coast of India are captured well. The spatial distribution of rainfall over the Indian subcontinent is captured satisfactorily. The wet zones over the eastern and northeastern parts of India, as well as over the Himalayas and the dry zones over northwestern India and east coast of peninsular India are well simulated by the model. For the GFDL model, the seasonal rainfall is underestimated over the Arabian Sea, northwest and central India, and the Western Ghats, while it is overestimated over the equatorial Indian Ocean in both the decades. By and large, the regional model simulates satisfactorily the primary features of the seasonal mean rainfall well.

An interesting issue is to examine whether the model, despite the fact that we are analyzing only one realization here, captures the change in rainfall during the reference period. This may be expected if this change is related to the forcing by increasing greenhouse gases and would provide increasing confidence in the ability of the models to simulate greenhouse gas driven precipitation changes. Figure 9.c1 displays the change in rainfall from the observations. We can note a decrease in rainfall over central and northeastern India, as well as over the Himalayas and west coast of peninsular India, with an increase in rainfall over the Gangetic plain, northwest India, head of the Bay of Bengal, and western part of the equatorial Indian Ocean. As seen in Figure 9.c3, there is a similar reduction in rainfall over central and northeastern India and over the Himalayas, and an increase in rainfall over the Gangetic plain, northwest India, head of Bay of Bengal, and western part of the equatorial Indian Ocean. However, over the west coast of peninsular India, the model fails to simulate the decrease in rainfall. Similarly, over the Himalayas the model overestimates the reduction in rainfall. The GFDL rainfall doesn't simulate the increase of rainfall over the Arabian Sea and eastern part of Indian Ocean but, it reproduces the same increasing (decreasing) pattern over Bay of Bengal (Peninsular India) as in the observations (Figure 9.c2). Figure 10 compares simulated precipitation changes during the reference period with observed ones from the IMD0.5 dataset. The RegCM4 is able to reproduce the IMD observed pattern over the northern part of Uttar Pradesh, Bihar, Odisha, Vidarva, Kutch and Arunachal Pradesh. Over these regions, both the RegCM4 and the IMD0.5 observations show a decrease of rainfall by about 1 to 2 mm/day (Figure 10 c). In GFDL the northwest, western part, peninsular India and Western Ghats show decreasing pattern in rainfall which is not present in the IMD0.5 data. The entire western part of the country shows decreasing pattern whereas the eastern part indicates increasing pattern in rainfall.

This comparative study provides two important indications: First, the regional model can reproduce the spatial distribution of monsoon precipitation over the Indian land mass (correlations between RegCM4 and observed patterns are 0.77 for GPCP and 0.62 for IMD0.5), with some improvements compared to the driving global model (correlations between GFDL and observed patterns are 0.72 for GPCP and 0.36 for IMD0.5)

particularly in terms of change patterns; second, despite the use of a single realization, the model is capable of capturing some aspects of the observed precipitation trends during the reference period, which implies that these might indeed be due to greenhouse gas forcing. Figure 11 shows a validation analysis for lower level and upper level winds by comparison with NCEP reanalysis data. The regional model satisfactorily simulates the location of the Somali jet and upper level easterly jet. The Somali jet is underestimated in the GFDL model, but the regional model realistically captures the cross-equatorial flow, and south equatorial easterlies in the lower troposphere (Figure 11 a1 & a3). The model agrees well with the weakening of low level westerlies over the Arabian Sea (Figure 11 b1 & b3), which the GFDL fails to simulate (Figure 11 b1 & b2). Similar inference has been found from the upper level wind circulation. The regional model shows that the strength of the easterly jet and Tibetan anticyclone has weakened in the last three decades of the 21st century, which is well supported by the NCEP/NCAR reanalysis (Figure 11 d1 & d3). On the contrary, the global GFDL model shows a sign of strengthening (Figure 11 d1 & d2). In general, the wind circulation is better represented in the RegCM4.3 than in the GFDL which forces the regional model. The pattern correlation coefficients over the whole domain between the model simulated lower level wind and the NCEP/NCAR wind during the first and last decades of the period of study are 0.76 and 0.82 respectively. Similar pattern correlation coefficients for the upper level winds are 0.90 and 0.93 respectively. Overall, RegCM4.3 does a fairly good job in the reference period, particularly over India. These comparative analyses of the circulation pattern and precipitation over India thus leads to the conclusion that RegCM4 driven by the GFDL GCM is of sufficient quality for its further use to project future changes in South Asia monsoon climate.

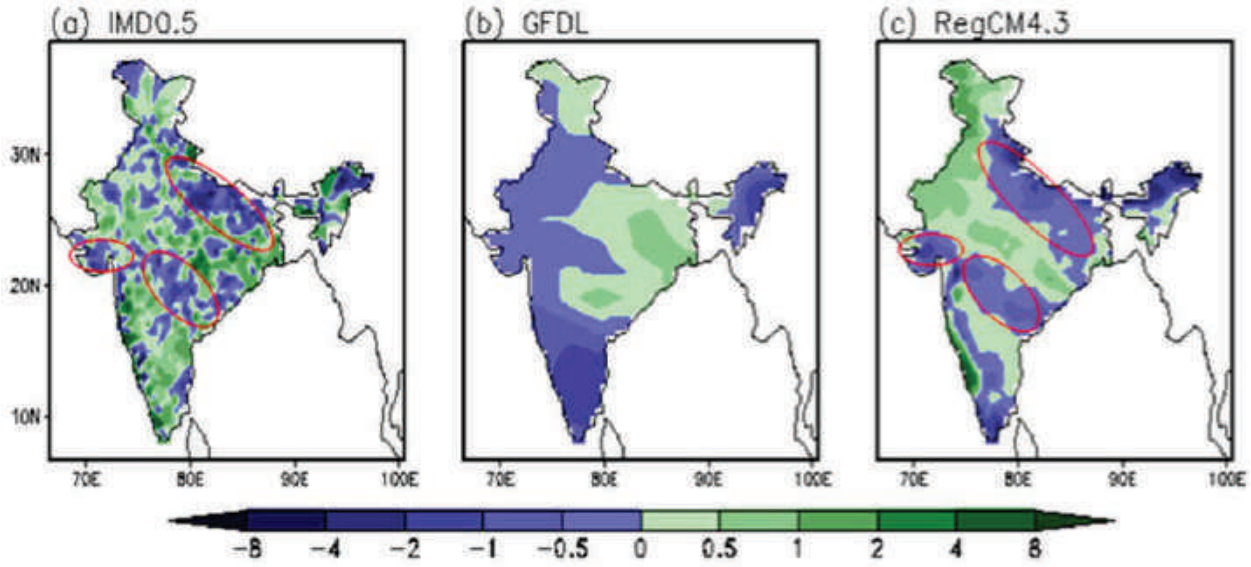

Figure 10: Decadal JJAS rainfall (mm/day) difference between first and last decades during 1979 to 2004 over the Indian land points in (a) IMD0.5, (b) GFDL and (c) RegCM4.3

Comparison of model simulations indicates differences in the summer monsoon mean precipitation distribution mainly over the Northwest region and the southern tip of the Peninsular India. These regional differences contribute to the uncertainties associated with the estimation of future all India precipitation. When Emanuel scheme is used over the ocean, the low level jet is weak over the Arabian Sea. In this case, moisture influx to

the land is dominated by strong anonymous easterlies from the Bay of Bengal. However, in both the experiments when Grell scheme is used over the ocean, the south westerly flow over the Arabian Sea is well captured. Thus the Grell scheme over the ocean improves the mean pattern of westerly flow over India and hence the summer monsoon rainfall simulated by RegCM4.3.

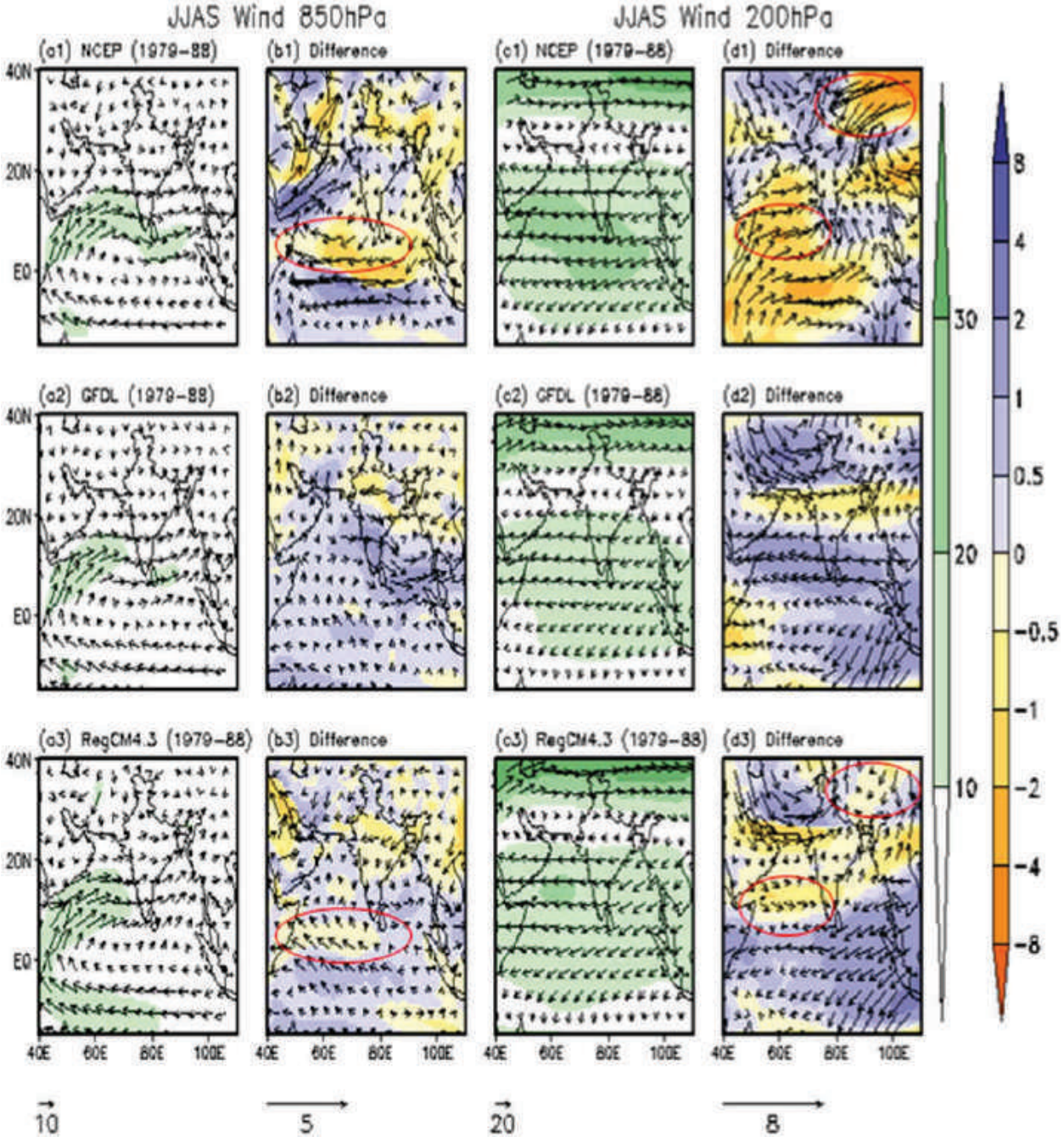

Figure 11: 10 years mean JJAS wind (m/s) at 850hPa and 200hPa in the vicinity of Indian summer monsoon region, and the difference between first and last

decades during 1979 to 2004. The top panel represents the NCEP/NCAR, middle panel represents GFDL and the bottom panel represents RegCM4.3 simulated wind. First two columns represent wind at 850hPa and other two represents wind at 200hPa.

3.2.3 Future Projections of Monsoon Rainfall

Here we examine the simulated future changes in rainfall over the Indian subcontinent and its adjoining regions under the RCP4.5 and RCP8.5 scenarios. As mentioned we analyze fours time slices, each of 30 years length, i.e. 1975-2004, 2010-2039, 2040-2069, and 2070-2099. The periods are respectively termed as historical (or reference), near-future, mid-future, and far-future. As discussed earlier, the period 1975-2004 has been used as reference (historical period) for model validation. The future projected changes are also obtained by taking the difference from the mean during the reference period. JJAS mean rainfall for the reference period and the far future as simulated by RegCM4 and the corresponding global model GFDL are shown in Figure 12 (a – d). Future changes in the seasonal mean rainfall with respect to the reference period are also shown in Figure 12 (e, f, g) as projected by RegCM4 and in Figure 12 (h, i, j) by GFDL. A notable systematic change in rainfall is found the farther we go into the future the larger is the change. For instance, rainfall over central India, the equatorial- and northern- Indian Ocean show a progressive reduction; on the contrary precipitation shows a steady increase over the Arabian Sea, northern Bay of Bengal and the Himalayas. The changes are in the range of 4-8 mm/day, which are about 30% of their mean values. Over the maritime continent, precipitation also decreases progressively as we proceed in time. On the other hand, there is a marginal increase in rainfall over northwest India in the mid-future, which is not found in the far-future. Since most of the projected changes are progressive in nature – spatial patterns of rainfall in the near-future and mid-future fall in between those of the reference and far-future spatial periods – we analyze the differences between the reference and far-future periods in greater detail. We also note that the comparison of the difference fields (Figure 12 e – g and h – j) brings out the effects of downscaling by RegCM4. In the global model the region of decrease in projected rainfall extends to northern India whereas, following as per the observed decrease in rainfall (Figure 11), the regional model shows a progressive reduction in rainfall over central India.

The projected changes under the RCP4.5 scenario are in general consistent with those seen in RCP 8.5 one i.e. in the future there will be more rainfall over the Arabian Sea, Bay of Bengal, and Himalayas, and less rainfall over India, equatorial Indian Ocean and northern Indian Ocean (Figure 13). However, there are two notable differences unlike in RCP8.5, no increase of rainfall is found over northwest India and the region of drying is located over East India i.e. over Odisha, West Bengal, Chhattisgarh, Jharkhand, and eastern part of Madhya Pradesh. Secondly, there is a difference in the magnitude between the two scenarios. In the near future, the global model indicates more pronounced decrease in the RCP4.5 scenario, probably a result of the effect of multi-decadal variability in the model. On the other hand, the regional model projects a progressive decrease in rainfall (Figure 13 e – g) consistently with the RCP8.5 (Figure 13 e – g).

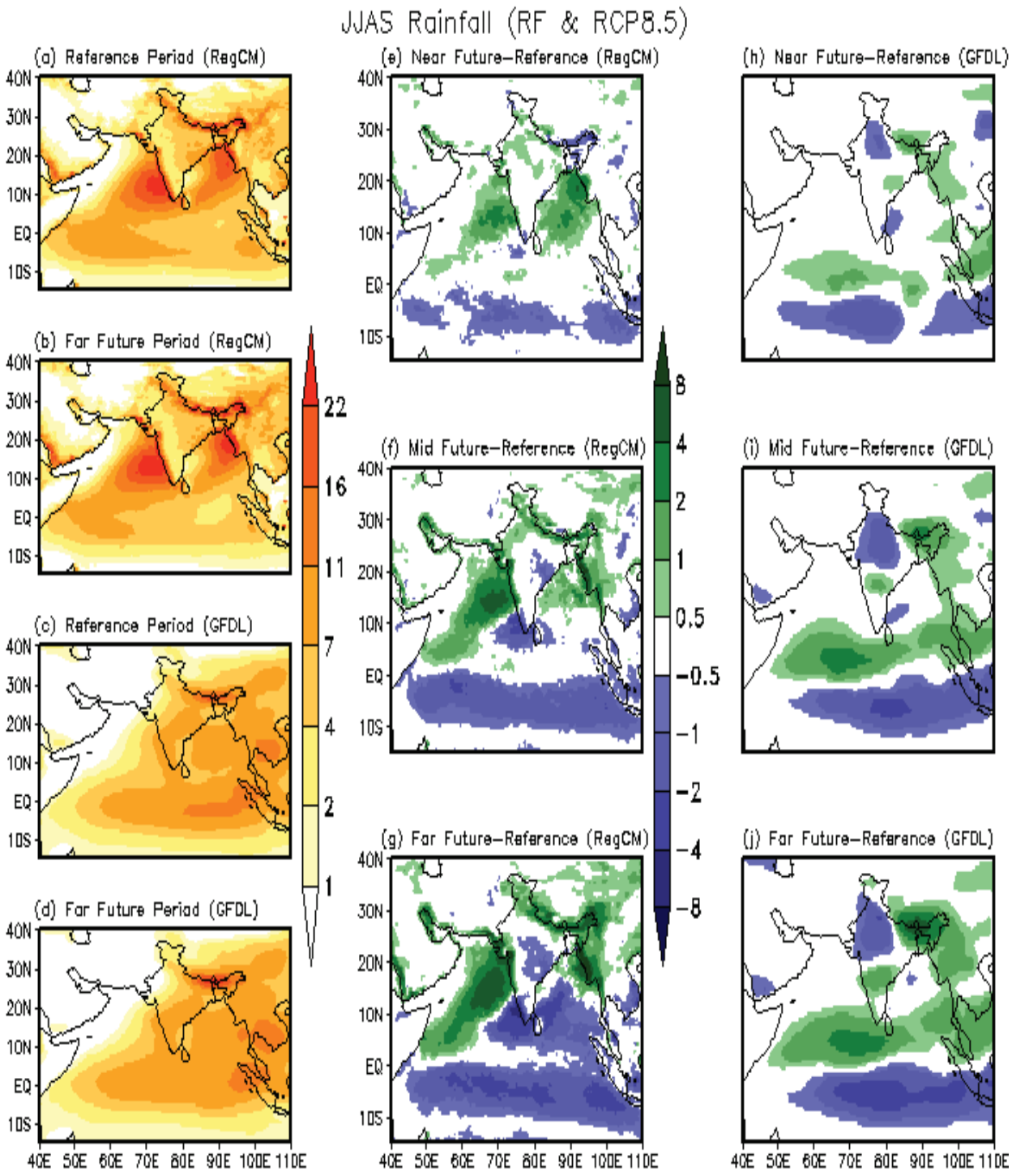

Figure 12: Climatological mean JJAS rainfall (mm/day) in the vicinity of Indian summer monsoon region during present (1975 to 2004), near future (2010 to 2039), mid future (2040 to 2069) and far future (2070 to 2099) periods in RCP8.5 as simulated by the model. The middle and right panel shows the difference between the reference and future periods

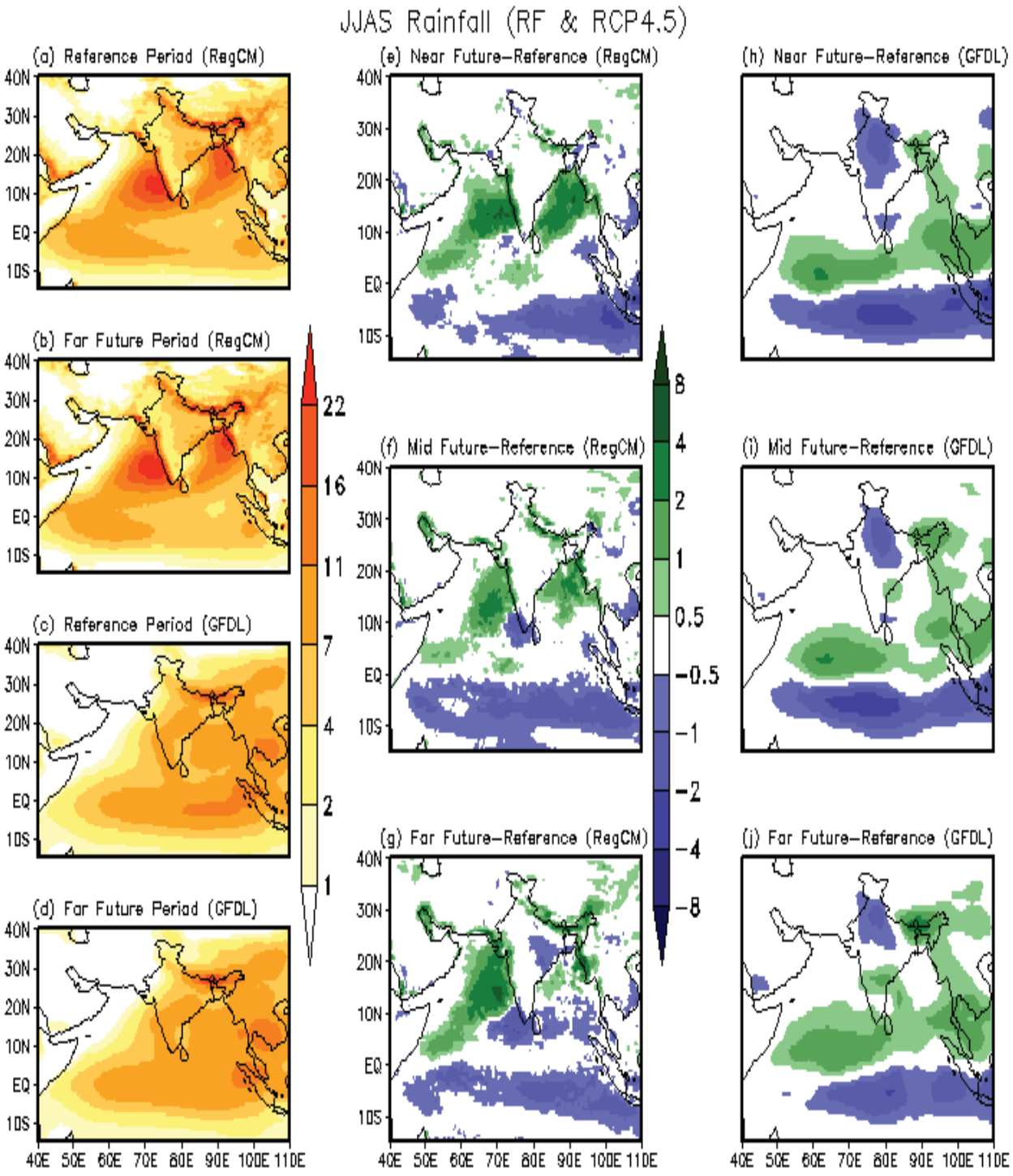

Figure 13: Climatological mean JJAS rainfall (mm/day) in the vicinity of Indian summer monsoon region during present (1975 to 2004), near future (2010 to 2039), mid future (2040 to 2069) and far future (2070 to 2099) in RCP4.5 scenarios

as simulated by GFDL-ESM2M. The middle and right panel shows the difference between the reference and future periods

In this study, RegCM4 has been integrated over the South Asia CORDEX domain under the RCP4.5 and 8.5 scenarios using GFDL-ESM2M CMIP5 lateral meteorological forcing. The regional model performance in simulating the Indian summer monsoon circulation and rainfall was first validated over the reference period 1975-2004 using observed rainfall from different sources, including GPCP and IMD0.5 gridded precipitation data and wind data from the NCEP/NCAR reanalysis. RegCM4 is found to satisfactorily simulate the main characteristics of the Indian summer monsoon rainfall distribution over the region: the occurrence of maximum rainfall over the head of Bay of Bengal, its extension south of the equator between 80^0 E and 100^0 E, and the secondary maxima over the western coast of India. The spatial distribution of rainfall over the Indian subcontinent is also adequately captured, with wet zones over the eastern and northeastern parts of India and the dry zones over northwest India and east coast of peninsular India. More importantly, despite the use of a single experiment, the model captures various features of the observed changes in rainfall during the last decades. Compared to the driving global model, the RegCM4 improved the spatial distribution of monsoon precipitation and the representation of observed changes.

The future projections for both RCP4.5 and 8.5 scenarios reveal a systematic change over most of the Indian sub-continent which increases with time, consisting of a weakening of monsoon precipitation over central India and the northern and equatorial Indian Ocean. On the other hand, increased precipitation is projected over the Arabian Sea, and the northern Bay of Bengal. The changes are in the range of 4-8 mm/day, which are about 30% of their mean present day values. Comparison between the global forcing fields and the downscaled fields shows that RegCM4 is able to resolve regional circulation and rainfall features and their future changes more consistently with observations than the global model. We also discussed how these changes in monsoon precipitation are related to changes in evaporation and moisture convergence.

The two main results we highlight are i) the ability of RegCM4 to reproduce areas of decreased monsoon precipitation found in the historical period; and ii) the simulation of an increasing monsoon precipitation reduction over mid-continental India, the main agricultural region of the country, over some sub-regions in disagreement with the driving GCM. In particular, the latter conclusion is in line with observed monsoon precipitation trends but in disagreement with most global model projections (e.g. Christensen et al. 2007). The main caveat of these two conclusions is that we used a single regional model driven by a single global model. An ensemble is needed to provide more robustness to this result, and we plan to compare our projection with other available ones within the CORDEX framework.

3.3 Temperature and precipitation changes in the North-East India and their future projections

North East India (NEI) comprising eight states is very vulnerable to global changes and is least studied. In this study the present day climatic conditions prevailing in NEI are examined based on IMD gridded data and actual observations of meteorological stations in the region. Further, Regional Climate Model version 3 (RegCM3) is used to examine the changes in climatic parameters of temperature and precipitation in NEI

under the IPCC A1B scenario. First of all, the present-day simulations (1971-2005) are compared against the IMD gridded datasets to validate the model performance. It is found that RegCM3 is able to simulate the trends in annual mean temperature and annual mean precipitation for the period 1971-2005. However, there is overestimation of rainfall simulated by the model. Major portion of NEI shows a wet bias in the model precipitation. The simulated annual mean temperature for the region shows a good correlation with those in the gridded temperature values. The extreme temperature events based on IMD gridded datasets of daily maximum and daily minimum temperature are also examined. Results indicate that during the years 1971-2005, the occurrence of warm nights was more frequent than the warm days in summer months. The simulations to the future years indicate rise in the annual mean temperature as well as in the annual mean rainfall. Projections based on RegCM3 simulations indicate more rise in the warm events than the cold events.

3.3.1 *Downscaling NCMRWF seasonal forecast*

The downscaling experiment over northwest India has been conducted by nesting the regional climate model (RegCM) with the NCMRWF global spectral model for a period of 28 years (1982–2010) at a horizontal resolution of 30 km. The winter season climate is first compared with observations to study the downscaling skill of RegCM over the northwest India. The results indicate that the wintertime climatology of precipitation and winds at different pressure levels, and their interannual variability are more accurately simulated by the T80 driven RegCM than the T80 itself. Composite analysis for extreme precipitation years suggests that the precipitation and circulation features simulated by the T80 driven RegCM shows better skill compared to T80. A complete and statistically robust analysis also suggests that downscaling provides a credible means to improve GCM climate simulations.

The observed climatology of precipitation (mm/day) is depicted in Figure 14 (left panel). It is seen that the maximum value of rainfall occurs during winter over Northern Kashmir, which is in the range of 3.5 - 4.5 mm/day. The T80 model is able to depict the observed features up to certain extent. However, the spatial extent and the intensity are underestimated by the model. On the other hand T80 driven RegCM simulation has brought out the observed climatology spatially and intensity wise better than the T80 model itself. Figure 14 (a-b) (right panel) represents the bias (in %) between the model and observed precipitation. It is seen that the T80 model shows the bias pattern, ranging from 50-150% over Jammu and Kashmir (J&K) and Himachal Pradesh (HP) region. On the other hand, the T80_RegCM model has stronger bias over eastern part of J&K.

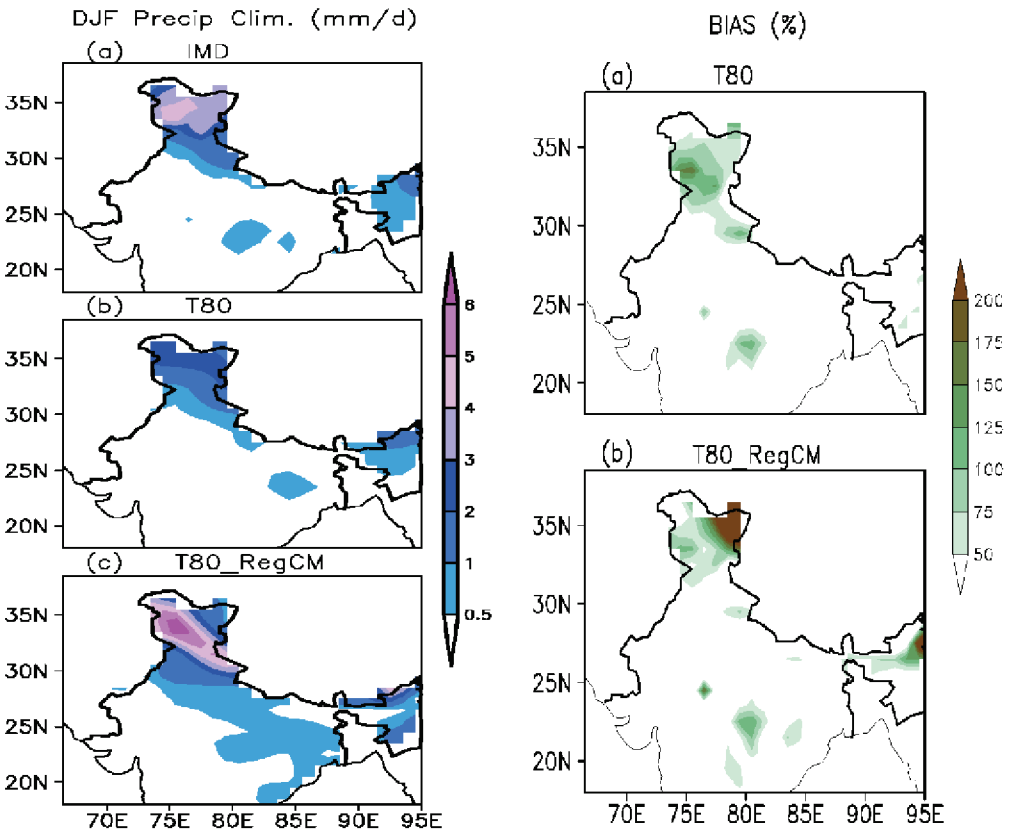

Figure 14: Observed and model simulated climatology of precipitation (mm/day) and bias (%) in December-February during 1982-2009

A composite analysis has been carried out for precipitation by computing the precipitation anomaly pattern during excess/deficit rainfall years.The years having standardized precipitation anomaly greater than 1 are considered as excess years, while years having less than -1 standardized precipitation anomalies are termed as deficit years. Therefore, among 33 years, there are 4 years in the category of excess precipitation (1991-92, 1994-95, 1995-96, 1997-98) and 4 deficit precipitation (1984-85, 1996-97, 2000-01, 2008-09) years. Figure 15 shows observed and model simulated wind and precipitation difference between excess and deficit years. It is seen that over entire domain of interest, a coherent positive precipitation pattern has emerged and the positive difference ranges from 0.2 to 0.6 mm/day. In case of composite analysis of wind, the observation shows anomaly of strong westerlies (~ 2.5 m/s) over central part of India succeeded by cyclonic flow due to hindrance of Himalayas. As already mentioned precipitation occurs over northern parts of India when Western Disturbances (WDs) pass over the region forming cyclonic anomaly over J&K and adjoining regions. This feature is well brought out in T80 driven RegCM simulation compared to T80 model itself.

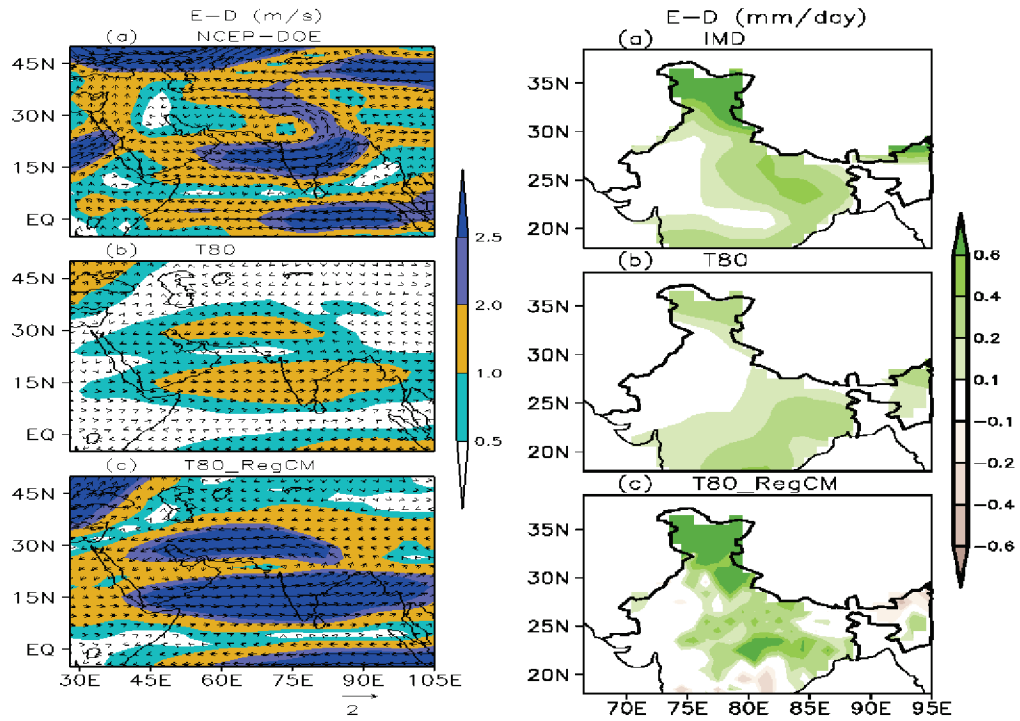

Figure 15: Observed and model simulated composite wind (m/sec) difference (Excess-Deficit) and precipitation (mm/day)

To examine how well the distribution of model-simulated values correspond to the distribution of observed values a box-whisker plot (Figure 16) has been drawn for the domain of interest. Boxes indicate the 25th to 75th percentiles of the distribution, while the whiskers show the full width of the distribution. It is noticed that the distribution of the T80 driven RegCM model-simulated values are closer to the distribution of observed values compared to T80 model itself.

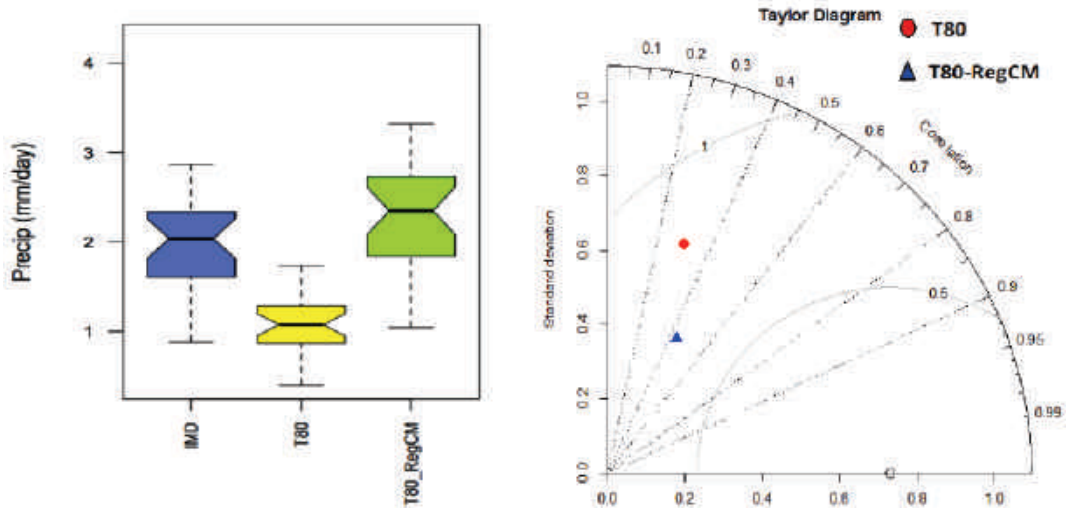

Figure 16: Left panel: Distribution of observed and model simulated precipitation (mm/day) for 1982-2010 box-whisker plot. Right panel: Taylor diagram for the prediction skill of model over NWI

A Taylor diagram is also presented in the right panel of Figure 16. In this diagram the skill of T80 and T80 driven RegCM for prediction of rainfall during winter in terms of correlation, root mean square error (RMSE) and standard deviation is shown. The figure clearly indicates the significant correlation skill of T80 driven RegCM with less RMSE as compared to T80 model itself.

Equitable Threat Score (ETS) is a skill metric, which is generally used for Yes/No forecast. ETS is defined as:

$$ETS = \frac{(H - H_\lambda)}{(H + M + F - H_\lambda)}, \qquad \text{where} \qquad H_\lambda = \frac{(H + M) \times (M + F)}{T} \tag{1}$$

Here M, H and F are the number of misses, the number of hits and the number of false alarms for each category; hits due to random chance are denoted by H_λ and T is the total number of events. ETS varies from −0.33 to 1. ETS = 0 indicates no skill and ETS = 1 indicates perfect skill in prediction. As the maximum values of precipitation from the observation during the study period (1982–2010) vary from 2 to 3 mm/day, three thresholds, 2, 2.5 and 3 mm/day are taken for calculating ETS. It is seen that in all thresholds ETS values of T80_RegCM is higher than T80.

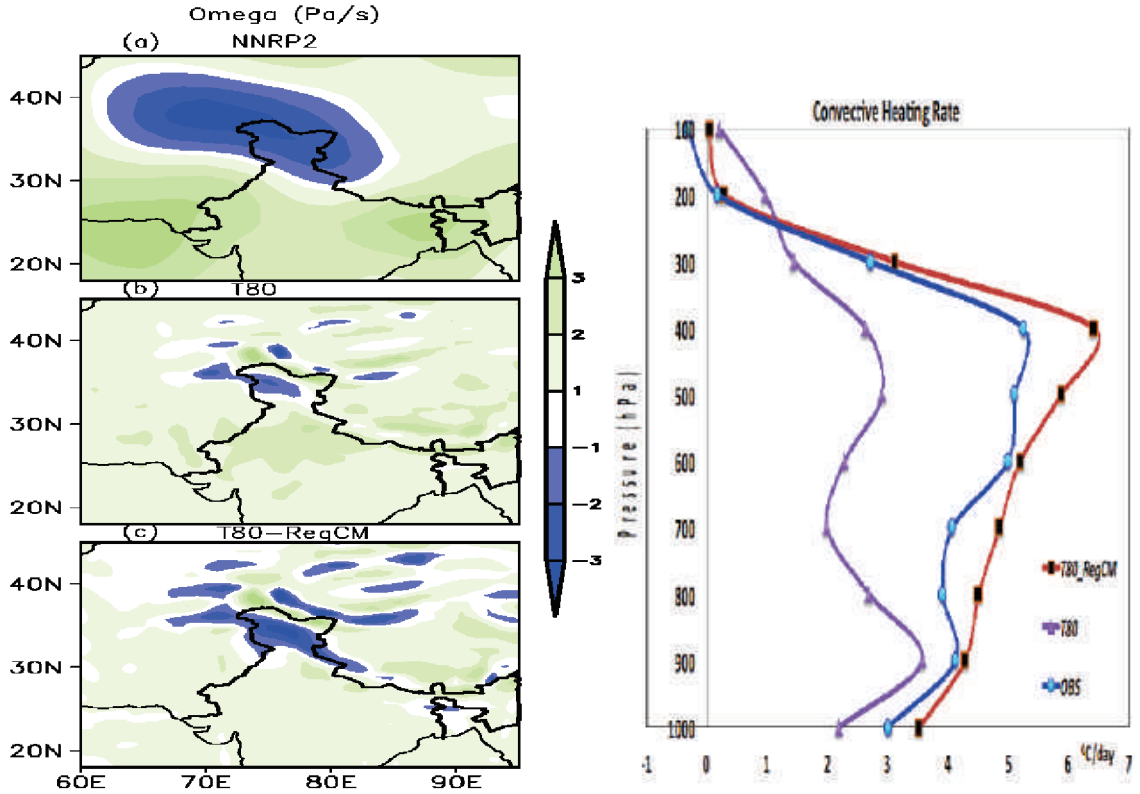

Figure 17: Observed and model simulated vertical pressure velocity (Pa/s) in the left hand panel and convective heating rate in the right hand panel

The vertical velocity (omega), which is one of the important upper air parameters, plays major role in the model dynamics for precipitation simulation. Therefore, it would be of interest to study the performance of the T80 and T80 driven RegCM model in representing vertical velocity. For this purpose, vertical velocity (hereafter referred as omega) at 500 hPa obtained from NNRP2 reanalysis, T80 and T80 driven RegCM

model simulations is analyzed and shown in Figure 17. It is seen from the figure that omega is negative in reanalysis over western parts of Himalaya during the winter season. T80 and T80 driven RegCM are able to bring out negative omega over that regions. However the area with negative omega is lesser in the model as compared to the reanalysis. Fig. 17 indicates that the area with stronger vertical velocity over that region is represented well in T80 driven RegCM model simulation compared to the T80 model itself. Further study on the convective heating rate has been carried out to get a deep insight on why T80 driven RegCM simulation is showing better representation of precipitation compared to the T80 model itself. The convective heating rate is calculated for T80 and T80 driven RegCM and the vertical profiles are also shown in Figure 17. It is noticed from the diagram that the convective heating rate is 5.3 ºC /day at 400 hPa in NNRP2 reanalysis. The convective heating maximum at 400 hPa is well brought out in T80 driven RegCM simulation (6.4 ºC/day) compared to T80 model (3 ºC /day) itself. Overall, simulation of precipitation is better in the T80 driven RegCM experiment compared to T80 model itself due to better representation of vertical velocity and convective heating rates.

3.4 Treatment of aerosols in regional climate model

3.4.1 Mineral dust transport over India

This study aims at understanding the capability of regional climate model RegCM 4.1 to simulate dust transport over India. RegCM4.1 is a hydrostatic sigma vertical coordinate model with a built-in module for simulating natural aerosols like mineral dust (Zakey et al., 2006) and anthropogenic aerosols (Solmon et al., 2006). The dust module includes dust emission, dry and wet deposition, transport and estimation of dust optical depth (AOD_d) and DDRF. The soil characteristics in each model grid cell are considered from United States Department of Agriculture textural classification. Dust mobilization is parameterized as function of wind speed exceeding a threshold value, surface roughness, minimum friction velocity (Marticorena and Bergametti, 1995) and soil moisture (Fecan et al., 1999). Horizontal mass flux is parameterized in terms of friction velocity (Sun et al., 2012). The dust particles are represented by four size bins - 0.1-1.0 μm, 1.0-2.5 μm, 2.5-5.0 μm and 5.0-20 μm (Zakey et al., 2006). The first two size bins represent fine mode dust and the last two bins represent coarse mode dust. τ_d is calculated following Mie theory, while radiative flux estimation follows NCAR-CCM scheme (Kiehl et al., 1996) that uses δ-Eddington approximate. The LW DDRF has been estimated using parameterization of Kiehl et al. (1996). Land surface processes are represented through Biosphere-Atmosphere Transfer (BATS) scheme (Dickinson et al., 1993). The dust scheme in relation to the BATS scheme becomes effective in the model for the grid cells dominated by desert and semi-desert land cover. The planetary boundary layer and cumulus convection schemes are represented by Holtslag et al. (1990) and Grell (1993) respectively. The model includes a large scale, resolvable subgrid explicit moisture scheme SUBEX (Pal et al., 2000). The study domain covered the area bounded by 4°N-48° N, 37° E-107° E. Simulations were carried out at 30 km × 30 km horizontal resolution on 18 vertical sigma levels with the model top set at 50 hPa in both the domains. The initial and lateral boundary conditions were extracted from the NCEP/NCAR (2.5° × 2.5°) reanalysis data for the atmospheric variables, where lateral boundary conditions are updated every six hours. Simulations were carried out for the period 1 Dec 2008 to 31 Dec 2009, but analysis has been done for the entire year 2009 leaving the first month as spin up time. The year 2009 was chosen because of the availability of Aerosol Robotic Network (AERONET) data at maximum 5 sites in India.

ARFI data do not provide estimates of fine and coarse mode optical depth and hence are not used for validation. Other than AERONET, multi-sensor data (OMI and CALIPSO) are also used to evaluate the dust transport qualitatively.

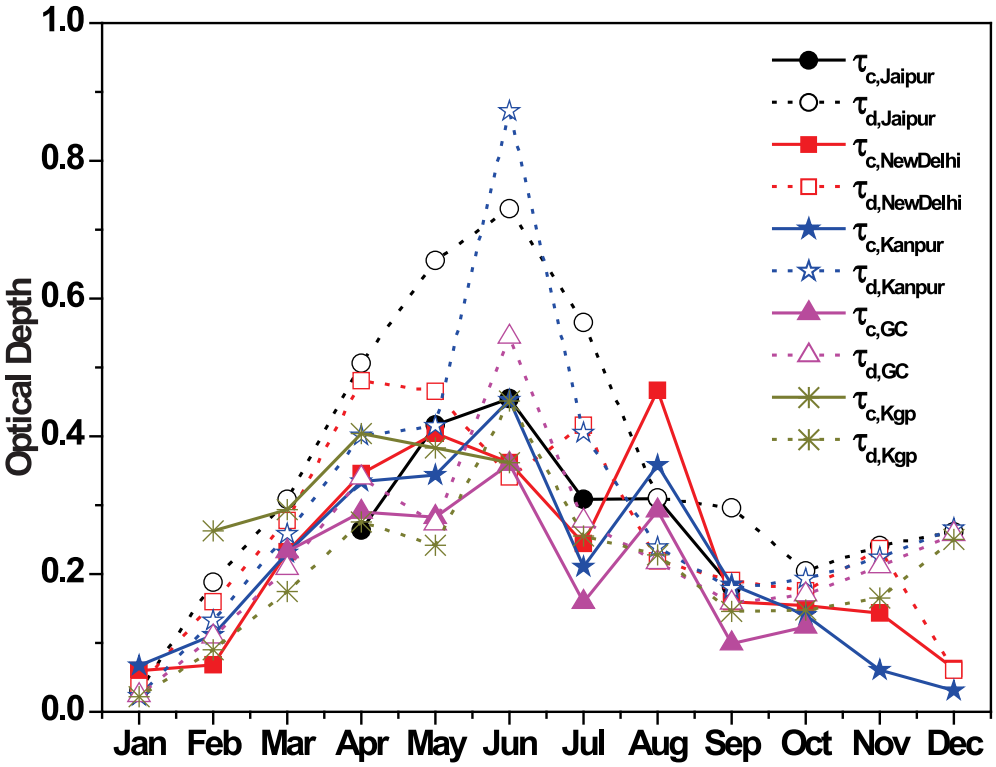

Figure 18: Monthly variations of RegCM-simulated dust optical depth, τ_d and AERONET-retrieved coarse mode optical depth, τ_c at Jaipur, New Delhi, Kanpur, Gandhi College (GC) and Kharagpur (Kgp)

Monthly variations of AOD_d within 30 km domain containing each AERONET site are compared with mean monthly coarse mode AOD (AOD_c) from AERONET. It must be noted that the above comparison is not a direct comparison. AERONET retrieval of fine mode fraction depends on spectral dependence of *AOD* and does not use any fixed cut-off size (O'Neill et al., 2003). Figure 18 shows monthly variations of AOD_d (shown by dotted lines) and AOD_c (shown by solid lines and used as surrogate to dust optical depth) at these five AERONET sites. The seasonal variability of AOD_d is well captured by the model. For example, the model replicates the increase in τ_c from March reaching a peak in May-June followed by a decrease at all the sites. However, simulated AOD_d is overestimated relative to AERONET-retrieved AOD_c, particularly during the pre-monsoon season when the dust transport peaks. This overestimation increases as we move away from the source region to Kanpur, Gandhi College and Kharagpur compared to the other two sites. This difference may be attributed to three factors. Firstly, the dust emission in the model depends on regional soil characteristics and hence only major arid/desert regions contribute to dust load. Secondly, high bias in wind speed by the model may lead to an overestimation in dust emission. Lastly, as the dust is transported along the IGB, large particles keep settling down due to dry deposition. Hence the model-simulated AOD_d at AERONET sites away from the desert sources is

mostly contributed by fine mode dust. This is not uncommon and has been observed in other places also (e.g. Tao et al., 2013).

The vertical distributions of AOD_d along the transport path of IGB are averaged over the entire pre-monsoon season and represented as longitude-altitude cross section along 28º N latitude in Figure 19. Dust particles are mostly transported at 700-850 hPa altitude over the IGB with a reduction in τ_d by 50-60% as they settle down away from the source (Figure 19a). The model-simulated vertical distribution of dust during the peak transport season is qualitatively evaluated against vertical distributions of frequency occurrences of dust based on CALIPSO-PDR values. CALIPSO profiles below 950 hPa are not considered due to large error in the retrieval (Misra et al., 2012). Presence of cirrus clouds at altitude above 500 hPa even in the pre-monsoon season (Meenu et al., 2011) may also influence the PDR retrieval as the cloud droplets are highly non-spherical and hence the PDR profiles are restricted up to 500 hPa. The vertical resolution of CALISPO is very high (~15 hPa). However, since our interest is to qualitatively compare the model simulated vertical distributions of dust, the vertical resolution of day and night time CALIPSO profiles is degraded to 50 hPa to smooth out the profiles for clarity. Mean PDR values greater than 0.35 confirm the presence of dust at that altitude (Shimizu et al., 2004; Liu et al., 2008). The general patterns of day and night time profiles of dust frequency occurrence are similar. The longitudinal (Figure 19c) gradient obtained by combining all day and night profiles along the IGB shows a decrease in dust occurrence from west to east at 700-850 hPa, supporting the model simulated gradient. The latitudinal gradient along 79º E longitude (Figure 4.2d) clearly demonstrates accumulation of dust (dust frequency>25%) over the IGB and Himalayan foothills at ~700-850 hPa altitude, similar to model simulation shown in Figure 19b.

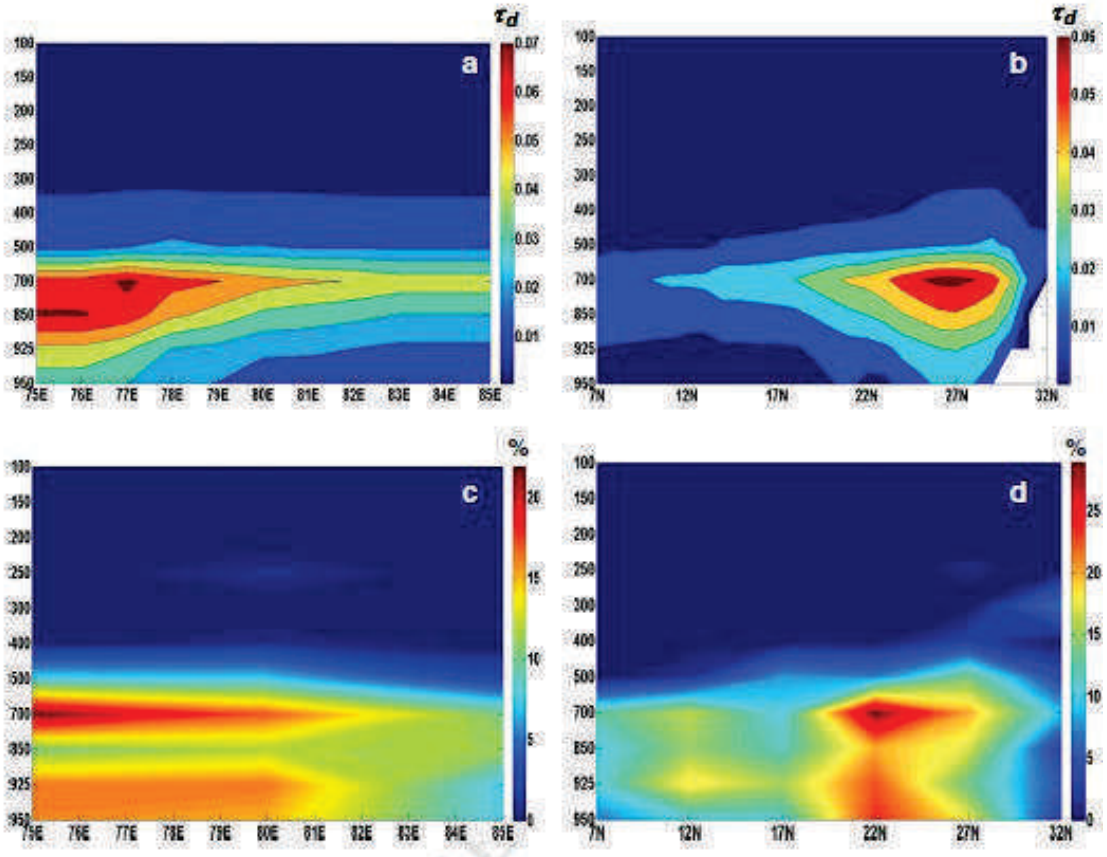

Figure 19: Vertical distributions of AOD_d (shown as τ_d) as simulated by RegCM (a) along the dust transport corridor over the IGB and (b) its laitudinal gradient across India, and vertical distributions of frequency occurrences of dust (in %) as observed by CALIPSO (c) along the transport corridor and (d) the latitudinal gradient

3.4.2 3-D aerosol distribution over India and seasonal variability

Simulations were carried out for both natural and anthropogenic aerosols at 50 km resolution for the period Nov 2008 to Dec 2010, with the first two months considered as spin up. The atmospheric burden of individual species (dust, BC, OC and sulfate) is examined. The 3-D distribution of total aerosols is shown in Figure 20 for all the seasons. Although the model is able to simulate the dust transport appreciably well, the anthropogenic load is observed to be biased low (compared to in-situ observations).

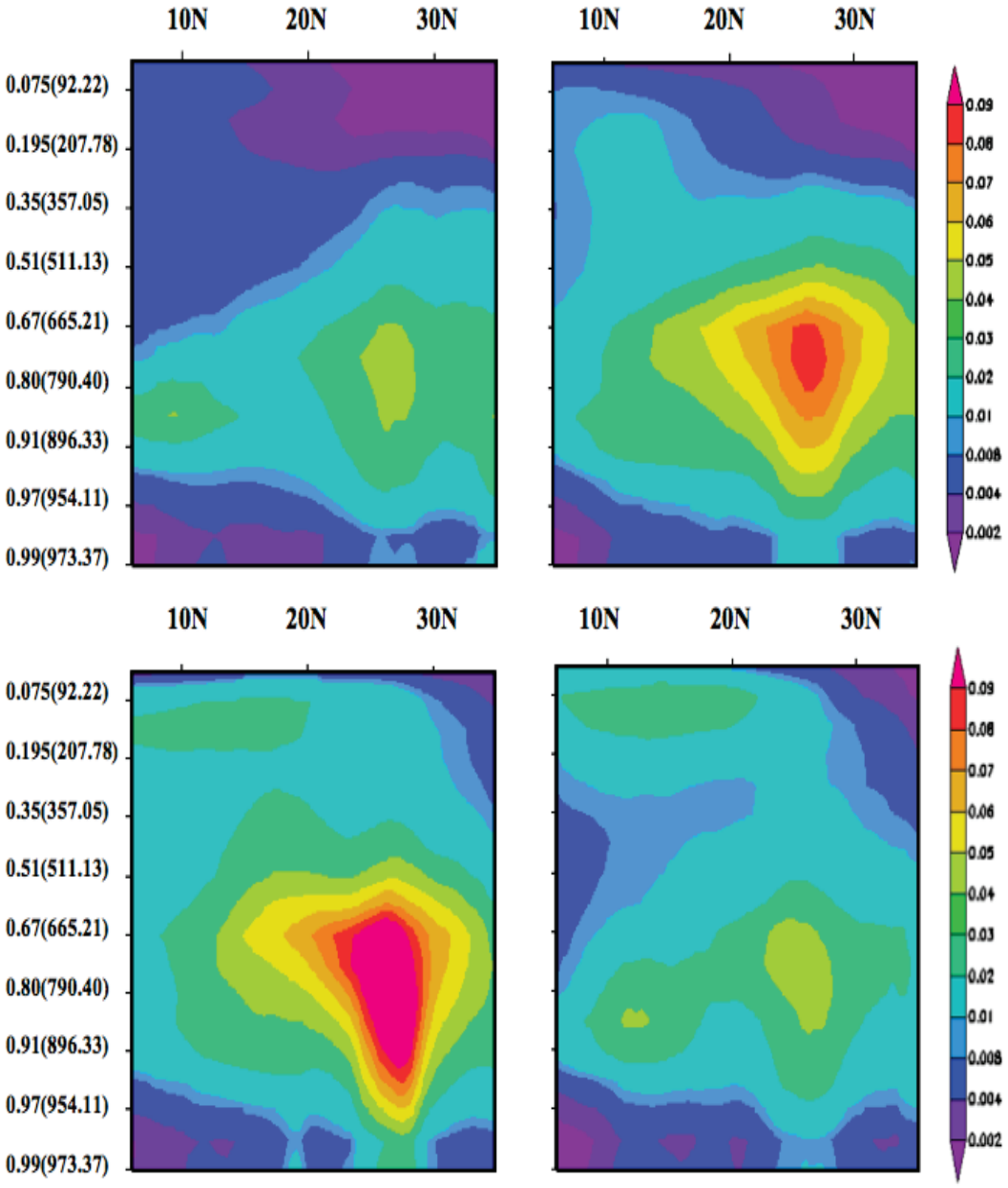

Figure 20: Three Dimensional distribution of RegCM simulated mean seasonal AOD during the winter (Dec-Feb, top left), pre-monsoon (Mar-May, top right), monsoon (Jun-Sep, bottom left) and post-monsoon (Oct-Nov, bottom right) seasons

3.4.3 Analytical framework for examining the link between cloud radiative forcing (CRF) and surface temperature (T_S) trend

An analytical framework has been developed to estimate the contribution of clouds to the observed T_S trend through perturbation of the radiation balance. The framework has been applied to the seven homogeneous surface temperature zones of India (Figure 21) - Western Himalaya, East coast, West coast, Northwest, Northeast, North-central and Interior Peninsula. These regions, demarcated by the climatological features of T_S, show different T_S trends during day and night time in different seasons (Table 2). For example, the night time increase of T_S in Western Himalaya is almost double relative to the daytime increase during the monsoon season. Such spatial and seasonal heterogeneity in T_S trends cannot be explained only by increasing greenhouse gas concentration. To examine the possible impact of CRF at TOA on the observed T_S trends in these regions, first we develop a mathematical framework. T_S can be changed by perturbing the radiation balance at TOA due to cloud (hereafter referred to as ΔT_S^{Cld}). The perturbation in the net radiation by clouds, expressed in form of ΔCRF, can be linked to ΔT_S^{cld} through a cloud sensitivity term (λ_{Cld}):

$$\Delta T_S^{Cld} = \lambda_{Cld} \Delta CRF \qquad (2)$$

λ_{Cld} (°C/W m^{-2}) can be defined as the change in T_S per unit change in CRF. Positive (negative) λ_{Cld} implies an increment of T_S for a positive (negative) change in CRF. The analytical form of λ_{Cld} is derived from the fundamental definition of CRF as follows:

$$\lambda_{Cld} = \frac{\Delta T_S / \Delta t}{(S_0/4)(\Delta \alpha_d / \Delta t) + (\alpha_d/4)(\Delta S_0/\Delta t) + A_1(\Delta f_C/\Delta t) + B_1(\Delta T_{Cld}/\Delta t) + C_1(\Delta T_S/\Delta t)} \qquad (3)$$

where the terms A_1, B_1, C_1 are region specific. λ_{Cld} is a function of incoming solar radiation at TOA (S_0) and temporal changes (expressed in terms of the rate of change per unit time, Δt) of T_S, cloud top temperature (T_{Cld}), cloud fraction (f_c) and difference of 'clear-sky' and 'all-sky' albedo (α_d). Note that the dependence of λ_{Cld} on the 'T_S trend' term (i.e. $\Delta T_S/\Delta t$) in the numerator of the equation (3) implies that any change in T_S due to cloud will also impact λ_{Cld}, thereby the framework considers cloud radiative feedback in estimating cloud-induced changes in T_S.

Two different data sets are analyzed to calculate λ_{Cld} for all seven homogenous T_S zones of India for the time period 2000-2012. f_c and T_{cld} data are taken from Moderate Resolution Imaging Spectroradiometer (MODIS), while the CRF data are obtained from Cloud and the Earth's radiant energy system (CERES). MODIS, onboard EOS-Terra satellite, is a 36 channel scanning radiometer that continuously retrieves cloud

parameters globally since March 2000. The cloud property retrieval depends critically on the calibration of L1B radiance at TOA and proper accounting of surface reflectance in cloud masking at 1 km resolution. Cloud products at level-2 are reported at 10 km resolution, which is further regrouped into 1°×1° gridded global level-3 data. CERES, which is flying onboard the same Terra satellite, is a key part of NASA's Earth Observation System serving as continuation for the Earth Radiation Budget Experiment. Product from CERES gives double accuracy in the estimates of radiative fluxes due to the improvements to the input fluxes, scene identification, and new models of the solar zenith angle dependence of albedo as a function of the new angular distribution model (ADM) scene types. Analysis has been carried out at the spatial resolution of 1°×1°. The linear trends of f_c and T_{Cld} are deseasonalized with respect to mean values for the available period of observations. Total changes in T_S at the seven homogeneous zones during the period 2000-2012 are estimated (Table 2) using the T_S trends reported in the literature. With reference to equation (1), ΔCRF is calculated from the linear trend value of net CRF (sum of SW CRF and LW CRF) estimated for each of the zones separately for day and night time. λ_{Cld} values for both day and night are estimated for each of the homogeneous zones (summarized in Table 2) using the linear trends of f_c, T_{Cld} and α_d. f_c shows spatially heterogeneous temporal patterns, while T_{Cld} shows increasing trend for all regions except NW and WH for both day and night. Daytime (night time) temperature T_{Cld} increases significantly by 1.53^0 C per decade (1.63^0 C per decade). But in NW, daytime (night time) temperature T_{Cld} decreases by 0.42^0 C per decade (0.56^0 C per decade). SW-CRF has increased significantly over the same period for all the homogenous surface temperature zones. For example, SW CRF has increased by 6.65 Wm^{-2} per decade in the EC. While daytime net CRF has been found to be increased over all the homogenous zones, night time CRF shows a mixed trend. Night time CRF increases by 4.46 Wm^{-2} per decade in North West but decreases by 1.99 Wm^{-2} per decade in the EC. Average night time CRF has larger value than the average daytime CRF in all homogenous zones (Figure 21). It is found that λ_{Cld} values are consistent in sign for both day and night. All zones have negative λ_{Cld} except WH and NW. During night time, clouds contributed in the range 15-51% to T_S trends in all the zones except NC and WC (Table 3). In daytime, only NW and WH contribute to 79% and 38% of the T_S trend. Otherwise, the negative values of ΔT_S^{cld} suggests a reduction into cloud-induced temperature trend. This further implies that the T_S would have increased rapidly during daytime, if the clouds were not present. The suppressed diurnal variation in T_S due to a smaller rate of daytime T_S increase relative to night time may be attributed to the long term trends in cloud characteristics.

Table 2: λ_{Cld} (in K m^2 W^{-1}) values for both day and night time over the seven homogeneous surface temperature zones in India

Zones	Day	Night
North West	0.052	0.029
North Central	-0.141	-0.220

North East	-0.020	-0.023
West Coast	-0.237	-0.641
Interior Peninsula	-0.025	-0.019
Western Himalaya	0.031	0.051
East Coast	-0.081	-0.023

Table 3: Surface temperature change (K) due to cloud

Zones	Day		Night	
	ΔT_S	ΔT_S^{Cld}	ΔT_S	ΔT_S^{Cld}
North West	0.377	0.298 (79%)	0.325	0.166 (51%)
North Central	0.169	-0.280	0.325	-0.215
North East	0.182	-0.117	0.351	0.054 (15.4%)
West Coast	0.299	-0.702	0.234	-0.167
Interior Peninsula	0.195	-0.188	0.13	0.028 (21.3%)
Western Himalaya	0.689	0.263 (38%)	0.416	0.058 (13.9%)
East Coast	0.221	-0.488	0.234	0.058 (24.9%)

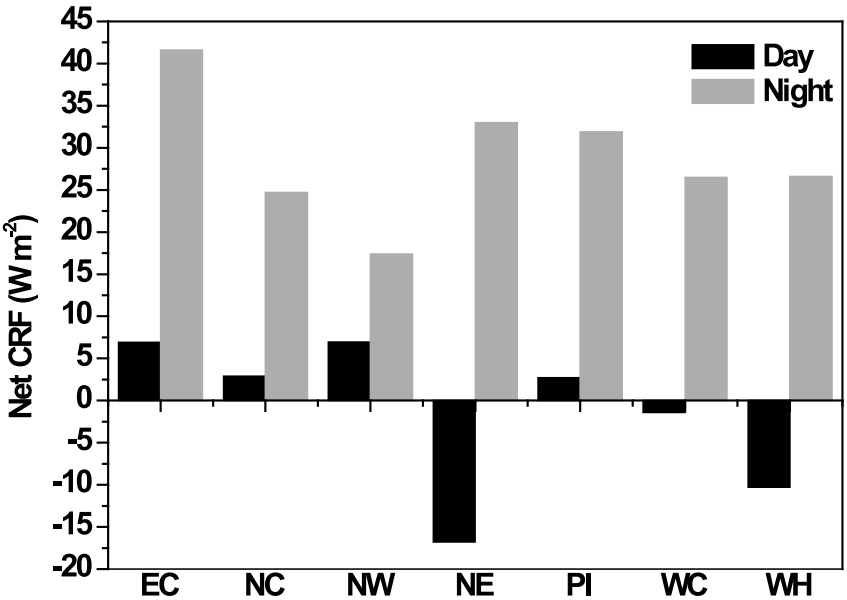

Figure 21: Net CRF over the seven homogeneous temperature zones (EC = east coast, NC = north-central, NW = northwest, NE = northeast, PI = peninsular India, WC = west coast, WH = western Himalaya) in India

3.4.4 Long-term changes in cloud field over India

To understand the long-term changes in cloud characteristics, MERRA reanalysis data and RegCM outputs are analyzed and inter-compared. First, cloud fraction climatology (for 30 years) over the homogeneous rainfall zones and the oceans adjoining the Indian landmass are established (Figure 22). RegCM is able to reproduce the monthly pattern of total cloud fraction over India. However, there is a consistent under-estimation by RegCM over the Arabian Sea and Bay of Bengal (by 10-25%). The inter-comparison over the land reveals different pattern. For example, RegCM slightly over-estimates cloudiness over Central-northeast (primarily the polluted and populated Indo-Gangetic basin) during non-monsoon months, while it over-estimates cloudiness during the monsoon season (Jun-Sep) relative to MERRA. On contrary, RegCM under-estimates total cloudiness in all the months in Northwest, Peninsular and West-central India throughout the year. Previously, Dash et al. (2013) have examined the performance of RegCM in simulating Indian summer monsoon rainfall and observed that monsoon rainfall is overestimated by RegCM in the Northwest, Central-northeast and Peninsular India, Arabian Sea and Bay of Bengal, while it has a dry bias in the West-central India. Despite of lower cloudiness, the model produces higher rainfall than the reanalysis data in these regions, which implies that the convection scheme of the model is not suitable for Indian region. Since the model does not consider aerosol indirect effect, which could have resulted in increased cloudiness, the cloud formation in response to the dynamic changes in the atmospheric is too strong.

Examination of the temporal change of cloudiness over the Indian monsoon region reveals that the cloudiness has been decreasing in the last 30 years (Figure 23). Mean decadal cloudiness during the monsoon decreased by 3.4±1% over the last three decades, which is quite significant given the fact that bulk of the rainfall in India occurred during the monsoon. Recently, Eastman and Warren (2013) have reported a global decreasing trend in annual cloudiness by analyzing in-situ observations across the world, including India, where the magnitude is larger than the global trend. This reduction is primarily attributed to the decrease in cumuliform clouds (typically found in the monsoon season). Large reduction is clearly observed in the reanalysis data (Figure 23) during the last two decades, especially over the oceans and central and peninsular India. All these analysis point out in favour of the hypothesis of a weakening monsoon circulation (Ramanathan et al., 2005; Bollasina et al., 2011).

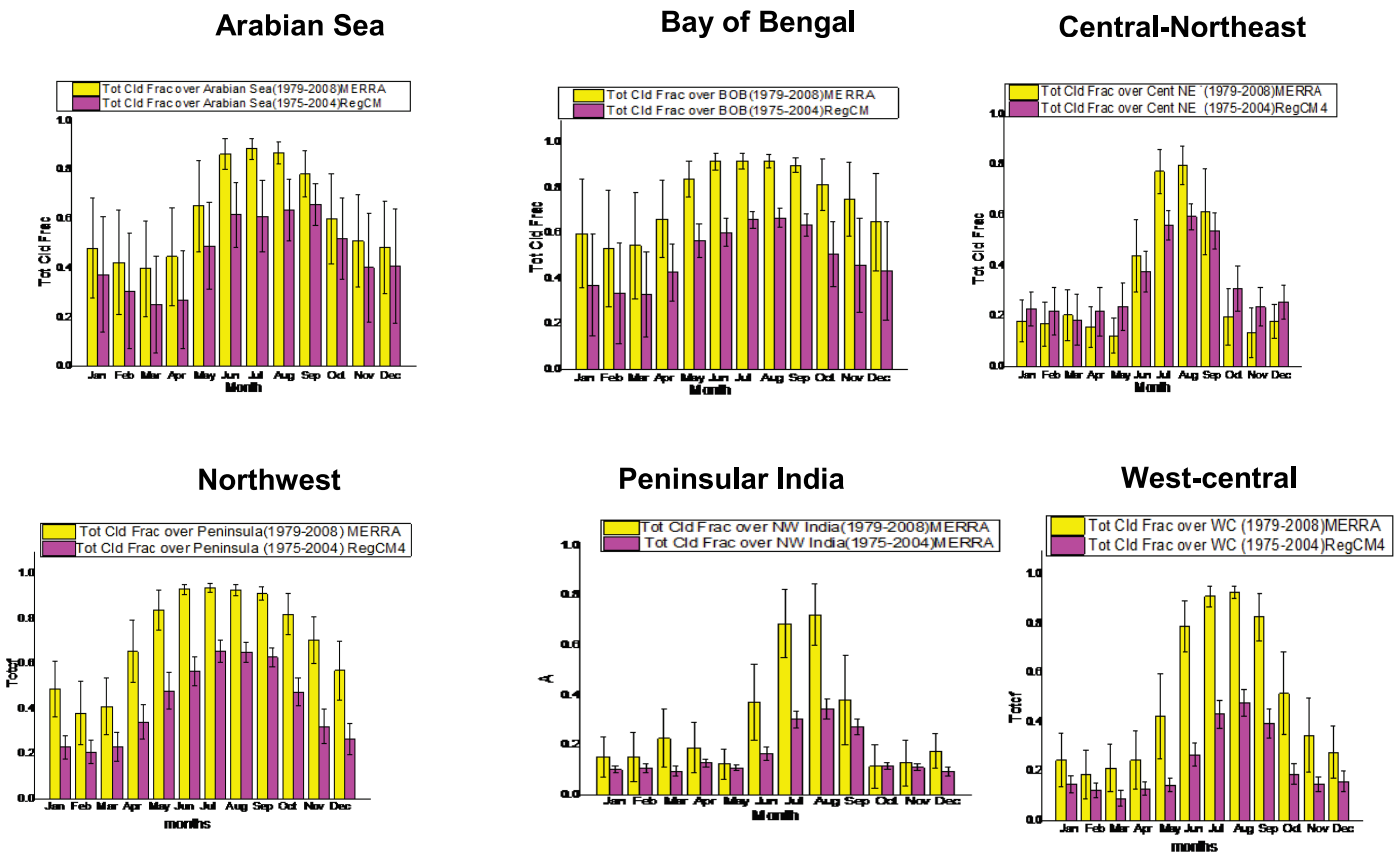

Figure 22: Total cloud fraction monthly climatology over the homogeneous rainfall zones (Central-Northeast, Northwest, Peninsular India and West-central) and the oceans (Arabian Sea and Bay of Bengal) from RegCM and MERRA reanalysis

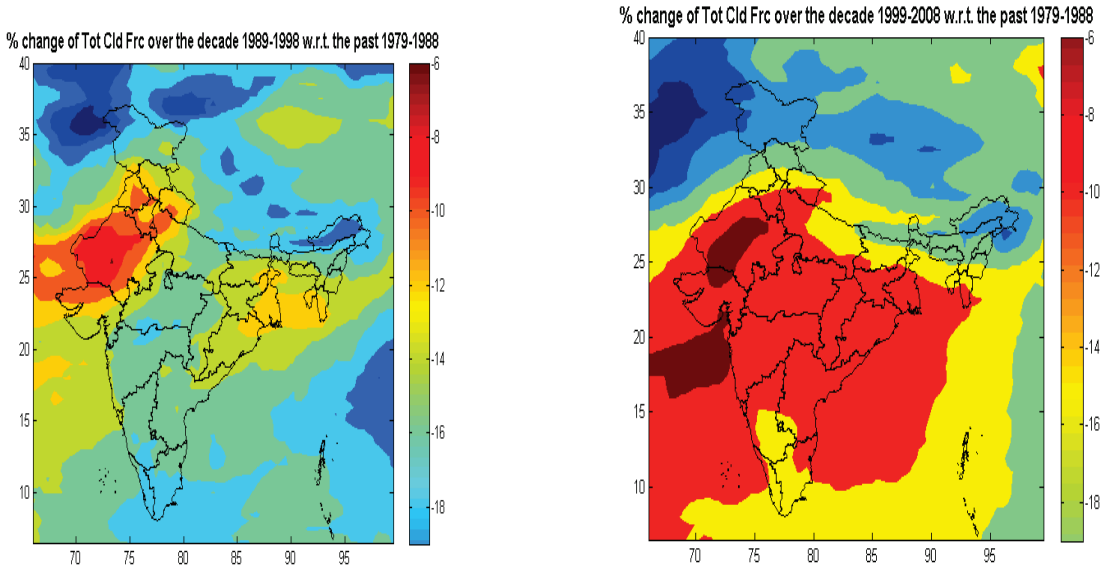

Figure 23: Relative change (in %) of monsoon cloudiness (a) during 1989-1998 and (b) 1999-2008 with respect to the period 1979-1988 as derived from MERRA reanalysis data

Chapter-4

Important Results of Project 2
DST CENTRE OF EXCELLENCE IN CLIMATE STUDIES

4.1 Bias correction in GCM products

The bias correction of 20C3M scenario has been done here. As the observed temperature data at 1º resolution are available from 1969 to 2000, the period 1969 to 1984 was selected as training period and 1985 to 2000 was selected as testing period. The predicted values of temperature and observed value of the temperature for testing period (1985-2000) are matching for each grid point at 1° resolution for entire India. Following are the plots depicting the temperature values for maximum daily temperature, mean daily temperature and minimum daily temperature for GCM. predicted and observed values. The plot (Figure 24) shows the comparison between mean of daily maximum temperature projected by GCM and observed maximum temperature.

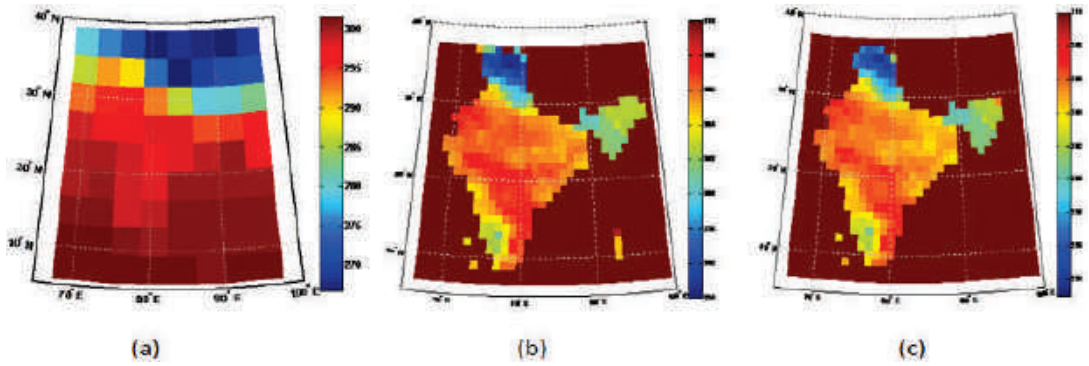

Figure 24: Comparison of average of daily maximum temperature between observed values and bias corrected GCM products for testing period (1985-2000) (a): GCM projected mean of daily maximum temperature without any correction and at 3.75º resolution; (b)GCM projected, bias corrected mean of daily maximum temperature at 1º resolution; (c) Observed mean of daily maximum temperature at 1º.

Figure 24(b) and (c) show that the mean of bias corrected temperature is matching with that of observed data except at northern part of Himalaya and Northeast part in India. This is mainly because the observed temperature data (Source: IMD) is not well interpolated in those regions because of lack of gauge stations in those areas. Figure 25(a), (b) and (c)) show the comparison between averages of daily mean temperature projected by GCM and observed mean temperature. Figure 25(a) contains the projections of GCM for mean temperature without bias correction at 3.75º. The other two plots show a good match except for northern Himalayan region and Northeast part of India.

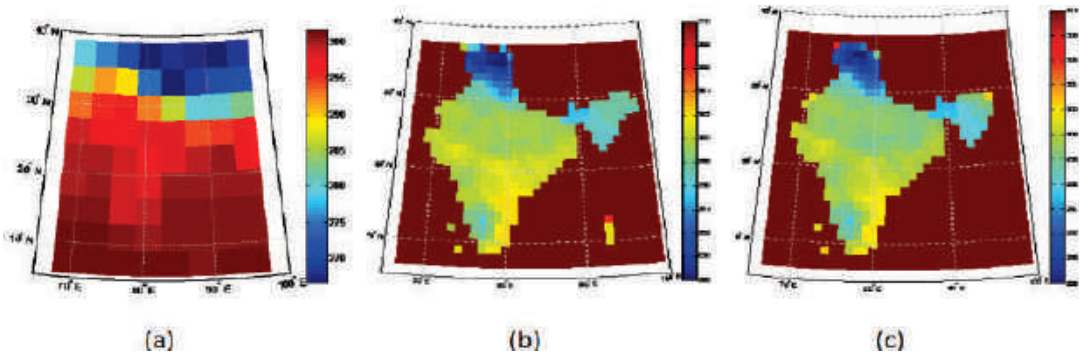

Figure 25: Comparison of average of daily mean temperature between observed values and bias corrected GCM products for testing period (1985-2000) (a): GCM projected mean of daily mean temperature without any correction and at 3.75º resolution; (b) GCM projected, bias corrected mean of daily mean temperature at 1º resolution; (c) Observed mean of daily mean temperature at 1º.

Figure 26 (a), (b) and (c)) show the comparison between average of daily minimum temperature projected by GCM and observed minimum temperature. Figure 26(a)) contains the projections of GCM for minimum temperature without bias correction at 3.75º. The other two plots show a good match except for northern Himalayan region and Northeast part of India.

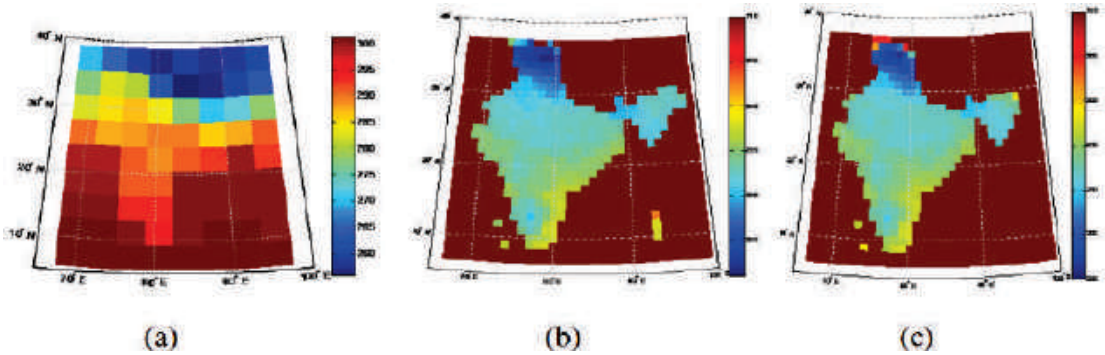

Figure 26: Comparison of average of daily minimum temperature between observed values and bias corrected GCM products for testing period (1985-2000), (a):GCM projected mean of daily minimum temperature without any correction and at 3.75º resolution; (b)GCM projected, bias corrected mean of daily minimum temperature at 1º resolution; (c)Observed mean of daily minimum temperature at 1º.

4.1.1 SRESA2 Scenario

For A2 scenario, the 21st century time period is divided into three time slices each of 30 years. The time slices are 2020s, 2050s and 2080s. Figure 27 shows the variation of mean, minimum and maximum temperature for the referred time slices. The projected temperature values show gradual increase with time.

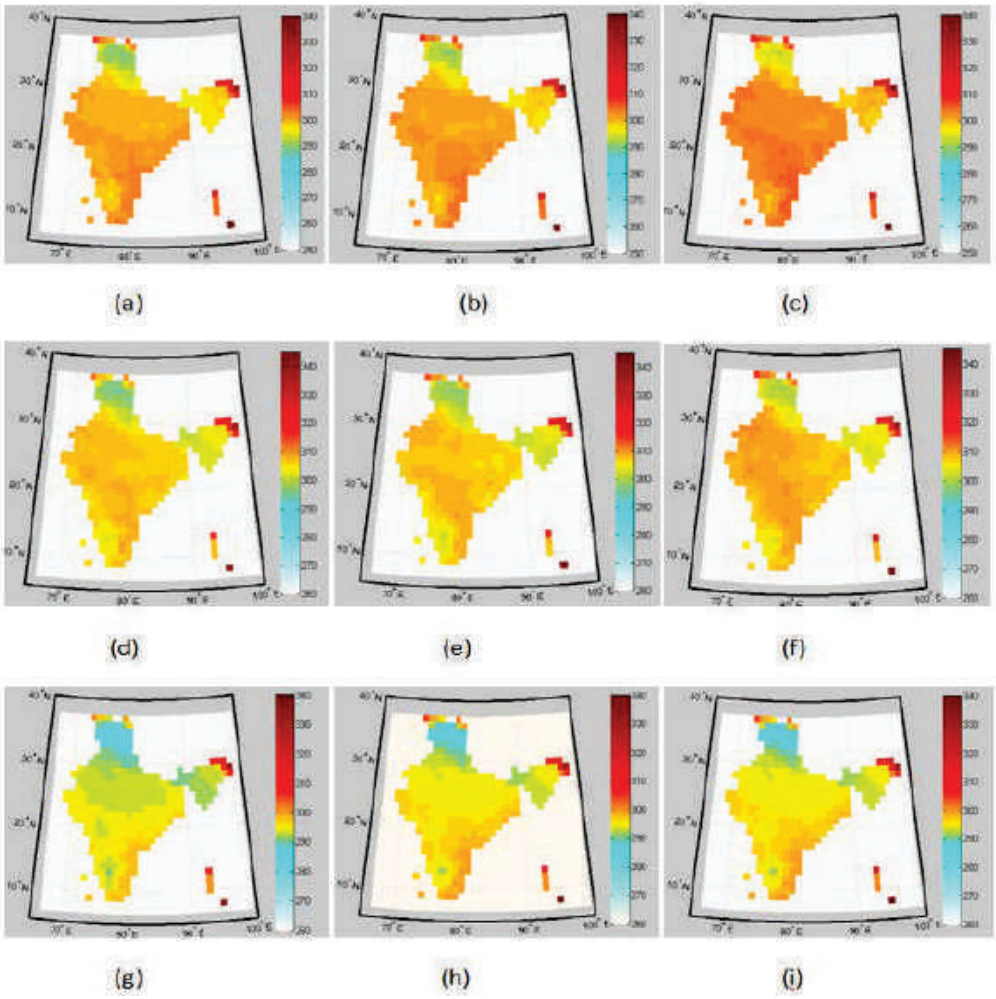

Figure 27: Temperature projected for 21st Century using Bias Correction for SRESA2 [8(a): Mean of Daily maximum temperature (2011-2040); (b): Mean of Daily maximum temperature (2041-2070); (c): Mean of Daily maximum temperature (2071-2100); (d): Mean of Daily mean temperature (2011-2040); (e): Mean of Daily mean temperature (2041-2070); (f): Mean of Daily mean temperature (2071-2100); (g): Mean of Daily minimum temperature (2011-2040); (h): Mean of Daily minimum temperature (2041-2070); (i): Mean of Daily minimum temperature (2071-2100).

4.1.2 SRESA1B Scenario

For A1B scenario, the 21st century time period is divided into three time slices each of 30 years. The time slices are 2020s, 2050s and 2080s. Figure 28 shows the variation of mean, minimum and maximum temperature for the referred time slices. The projected temperature values show gradual increase with time.

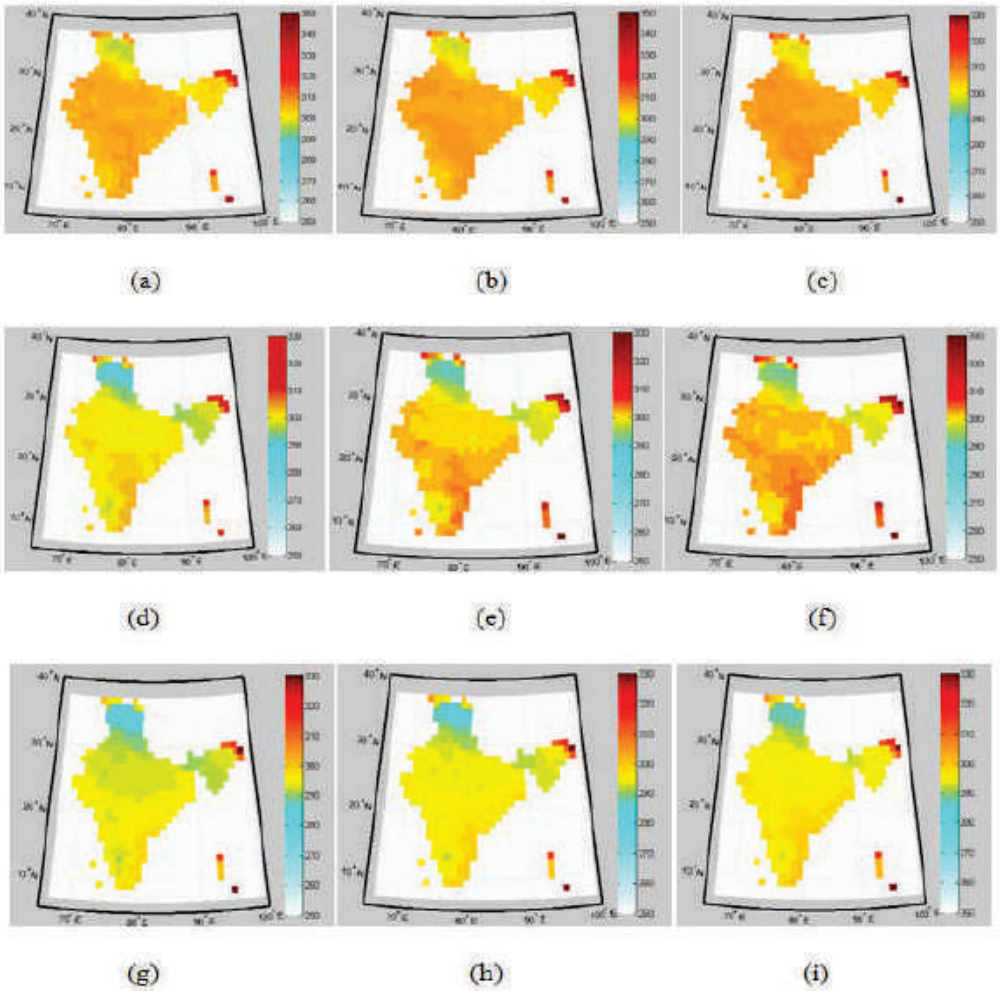

Figure 28: Temperature projected for 21st Century using Bias Correction for SRESA1B, (a): Mean of Daily maximum temperature (2011-2040); (b): Mean of Daily maximum temperature (2041-2070); (c): Mean of Daily maximum temperature (2071-2100); (d): Mean of Daily mean temperature (2011-2040); (e): Mean of Daily mean temperature (2041-2070); (f): Mean of Daily mean temperature (2071-2100); (g): Mean of Daily minimum temperature (2011-2040); (h): Mean of Daily minimum temperature (2041-2070); (i): Mean of Daily minimum temperature (2071-2100).

To get some quantitative idea about actual rise in the temperature with respect to 20C3M projections, the difference between the A2 projections for mean temperature at various time slices and 20C3M mean temperature projections are plotted in Figure 29.

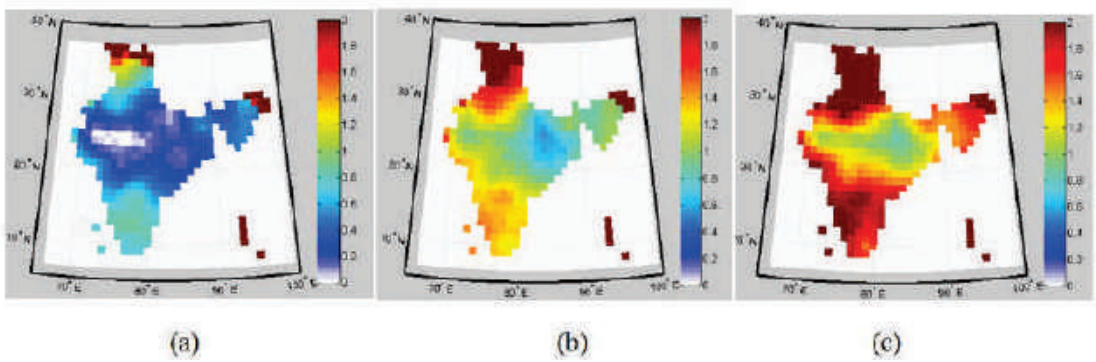

Figure 29: Difference between the A1B projections for mean temperature and 20C3M mean temperature, (a):Difference between the A1B projections for mean temperature and 20C3M mean temperature 2011-2040; (b):Difference between the A1B projections for mean temperature and 20C3M mean temperature 2041-2070; (c): Difference between the A1B projections for mean temperature and 20C3M mean temperature 2071-2100.

To check the temperature variation trend, at one particular grid point 28.5 Latitude and 72.5 Longitude, the maximum temperature time series is plotted for entire 21st century. The trend line shows that there is increase in temperature. Figure 30 shows the time series for maximum and minimum temperatures.

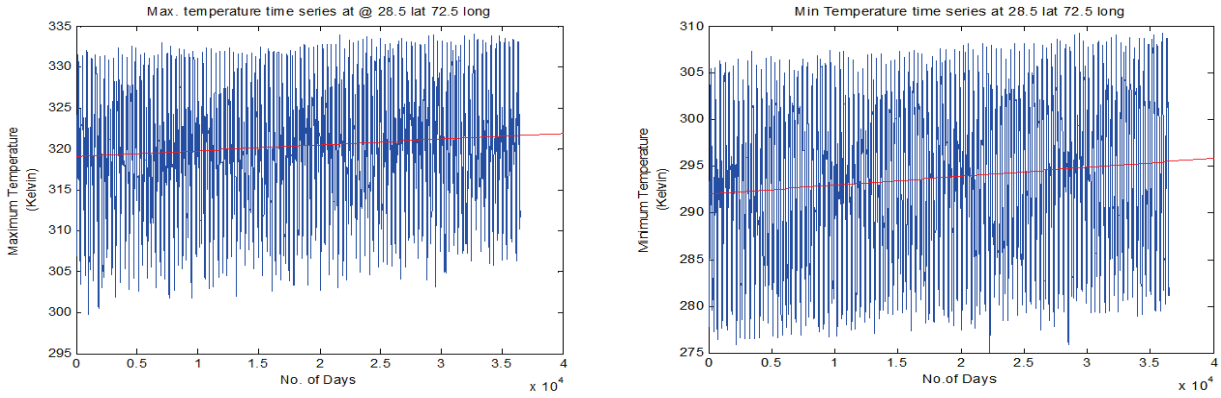

Figure 30: Temporal variation of daily maximum and minimum temperature at 28.5º lat and 72.5º long

4.1.3 SRESB1 Scenario

For B1 scenario, the 21st century time period is divided into three time slices each of 30 years. The time slices are 2020s, 2050s and 2080s. Figure 31 shows the variation of mean, minimum and maximum temperature for the referred time slices. The projected temperature values show gradual increase with time.

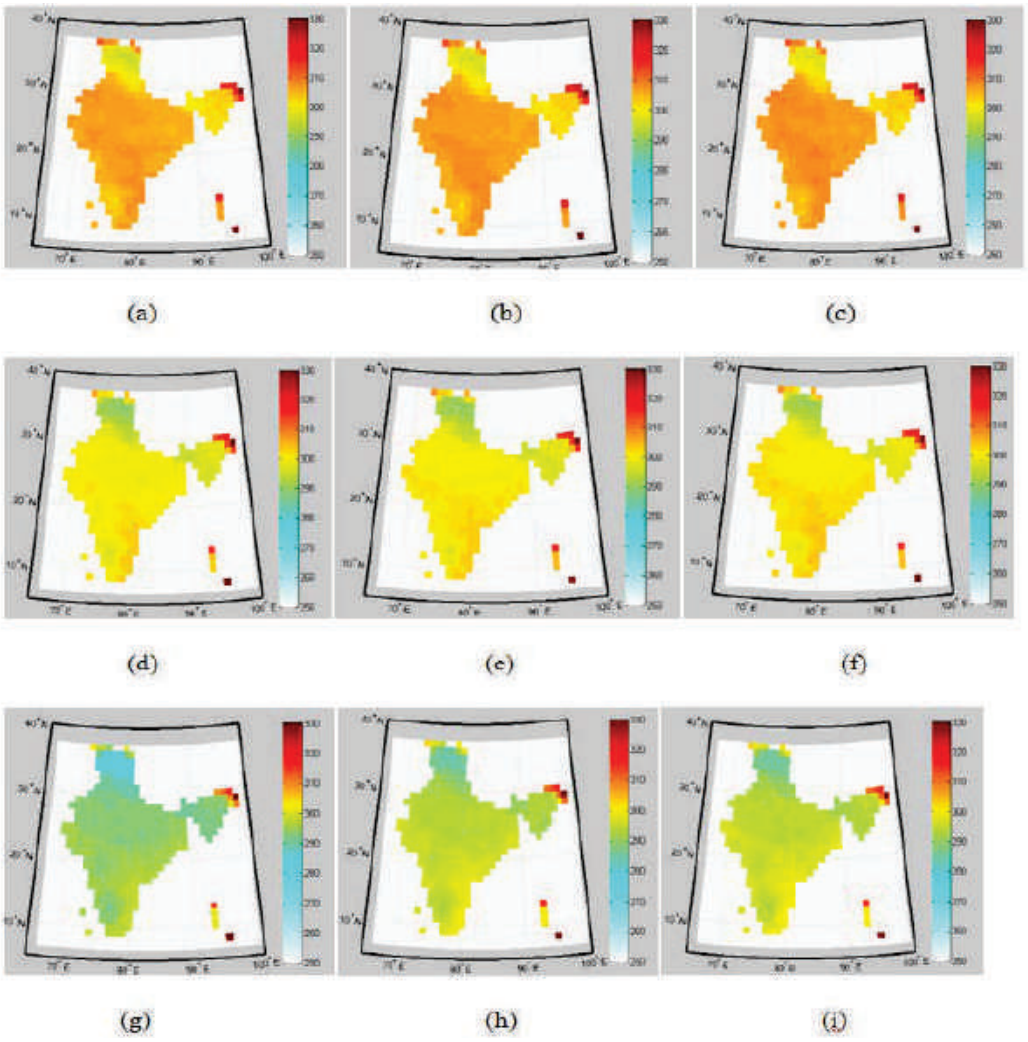

Figure 31: Temperature projected for 21st Century using Bias Correction for SRESB1, (a): Mean of Daily maximum temperature (2011-2040); (b): Mean of Daily maximum temperature (2041-2070); (c): Mean of Daily maximum temperature (2071-2100); (d): Mean of Daily mean temperature (2011-2040); (e): Mean of Daily mean temperature (2041-2070); 12(f): Mean of Daily mean temperature (2071-2100); (g): Mean of Daily minimum temperature (2011-2040); (h): Mean of Daily minimum temperature (2041-2070); (i): Mean of Daily minimum temperature (2071-2100).

4.2 Treatment of aerosols in a GCM

The spatial distribution of ECHAM model-simulated seasonal mean AODs averaged over 5 years (2001 to 2005) was evaluated using MODIS-derived Terra and Aqua satellite combined AOD values (Figure 32). The model broadly captures AOD distributions during all different seasons over the Indian region. During the NE monsoon season, high AOD (0.2 to 0.4) is found over the Indo-Gangetic Plain (IGP) and central-north India (CNI), with substantially lower values in the model compared to the satellite retrievals, but with a similar southwest – northeast gradient. The local maximum in AOD was previously observed from satellites (*Di Girolamo et al.*, 2004; *Jethva et al.*, 2005; *Ramachandran and Cherian*, 2008) and ground-based observations (*Singh et al.*, 2004; *Tripathi et al.*, 2006). The predicted northeastern maximum is from high anthropogenic emissions (mainly for sulfate and organic carbon) (Figure 33). The contribution of fine mode aerosols, such as sulfate, and OC, to the predicted optical depth is dominant during the NE monsoon period (Figure 33). During the pre-monsoon season, AOD patterns change substantially over the Indian subcontinent from an enhancement in dust loading (Figure 32 and Figure 33). This is consistent with the findings from previous studies (*Dey et al., 2004*; *Prasad and Singh*, 2007; *Ramachandran and Cherian*, 2008). High AOD is found over the IGP (24^{o}N-30^{o}N) and CNI (18^{o}N-24^{o}N) regions (Figure 32), but underestimated in magnitude by the model. The model shows a local minimum in the NWI region, where the satellite observations show moderate AOD values. A large influx of desert dust from the western arid and desert regions of Arabia, Africa and Thar (Rajasthan) enhances the dust loading over these regions during the pre-monsoon season (e.g. *Dey et al., 2004*; *Dey and Girolamo*, 2010), and this dust influx may be underestimated by the model (*Cherian et al.*, 2011), most likely from inaccurate representation of soil erodibility factor and soil moisture. Nevertheless, the model shows that dust contribution to total AOD is high (30-40%) during the pre-monsoon period over the IGP and NWI regions (Figure 32). In addition to dust, SO_4 and OC show a significant contribution to total AOD over a large part of the Indian subcontinent (Figure 32). These observations are consistent with the fact that anthropogenic aerosols also contribute significantly to AOD along with dust aerosols over these regions (*Dey and Girolamo*, 2010). It is also known that, in addition to dust storms, open biomass burning peaks during the pre-monsoon season over this regions (e.g. *Vadrevu et al.*, 2011; *Venkataraman et al., 2006*).

In the monsoon season, high AOD values are found over the IGP, NWI and CNI regions (Figure 31), consistently in model and satellite retrievals, albeit too far south in the GCM. This maximum arises because of an enhanced transport of dust aerosols from desert regions of Arabia, Africa and Thar (Rajasthan), and also of sea salt from the ocean (Figure 32). The AOD composition was found to be dominated by dust aerosols, followed by sulfate, OC, and sea salt aerosols during this season (Figure 32). During the inter-monsoon season, high AOD are found over the northern parts of the IGP (Figure 31). The composition of total AOD was dominated by sulfate followed by OC and BC aerosols during this season (Figure 32). It is known that agricultural residue and biofuel burning emissions dominate the aerosol emissions during this season (e.g. *Vadrevu et al.*, 2011; *Bond et al.*, 2004; *Venkataraman et al., 2006*).

In summary, seasonal and spatial variability of the model simulated AOD broadly captures the MODIS-observed variability over the Indian region. In particular, the model simulated AOD was relatively well predicted during the SW monsoon (JJAS) and inter-monsoon seasons (with a certain geographical displacement), but significantly

underpredicted locally by up to a factor of 2 during the NE monsoon because of the uncertainties in regional emission inventories and pre-monsoon dust emission fluxes (*Cherian et al.*, 2011). The broad regional differences of AOD patterns over the Indian subcontinent depend on the anthropogenic (sulfate and OC) and natural (dust) emission sources, but the seasonal variation within the region depends significantly also on the meteorology (dust transport) and topography (Figure 32).

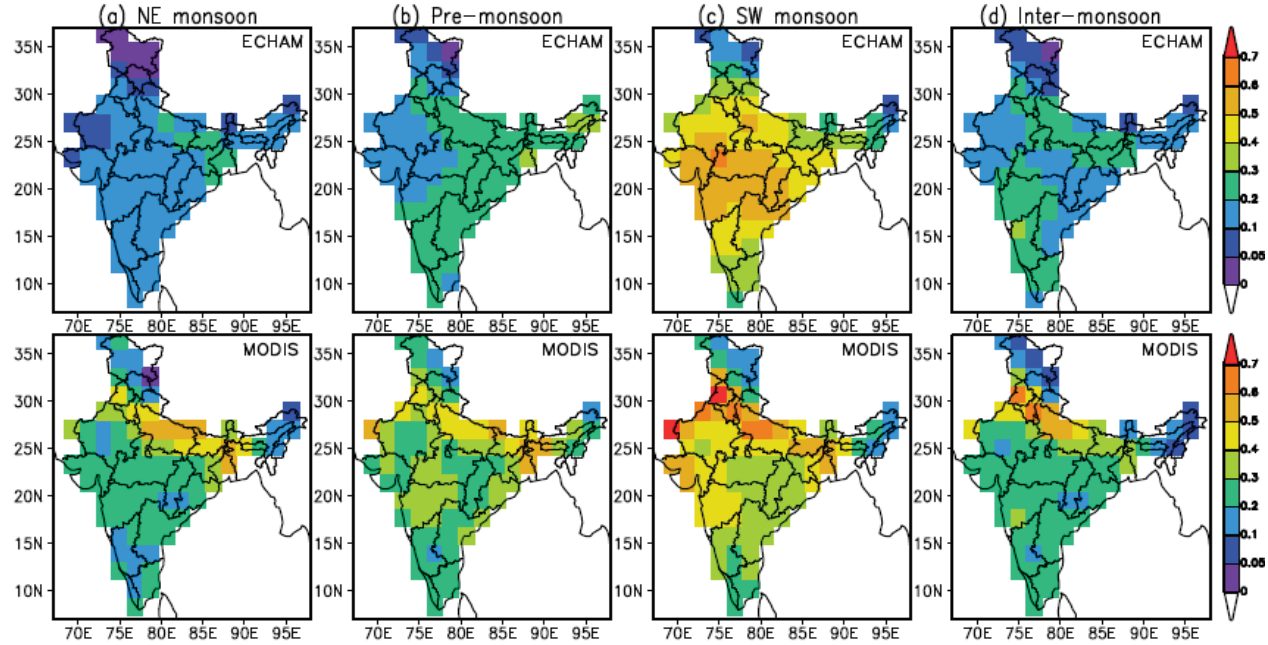

Figure 31: Seasonal mean distribution of ECHAM model simulated aerosol optical depth at 550 nm and MODIS satellite retrievals (January 2001 to December 2005)

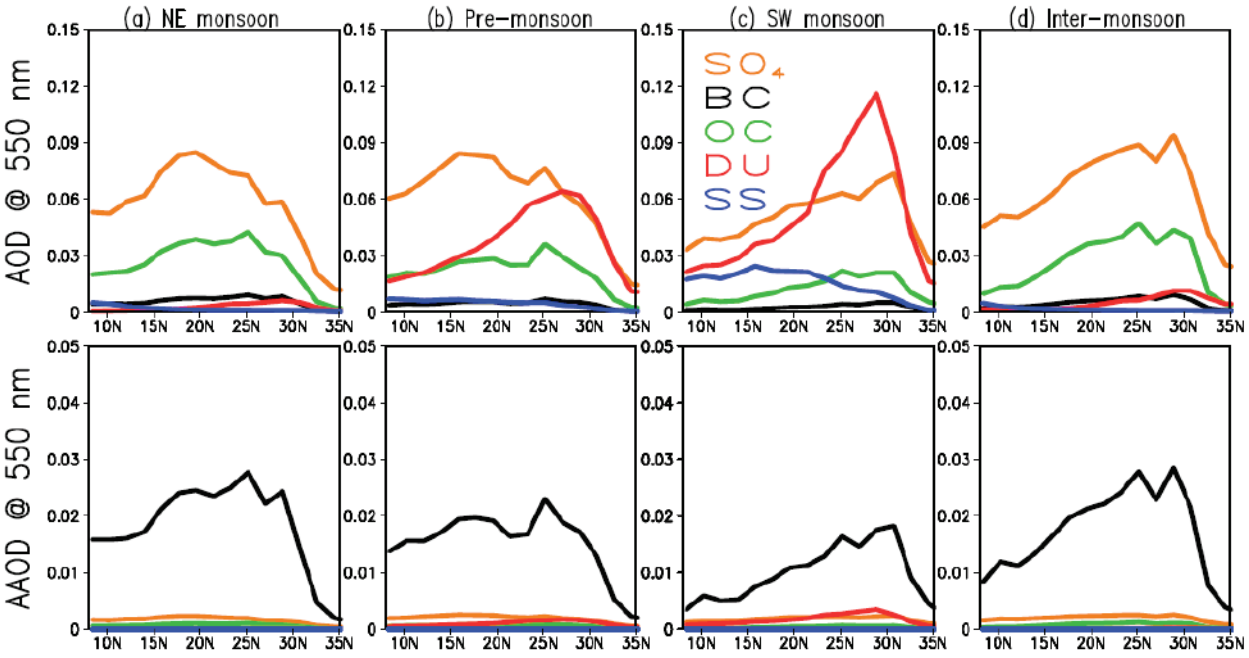

Figure 32: Seasonal zonal mean (68E-98E) ECHAM model simulated contributions by different aerosols species to aerosol optical depth (AOD, top panel) and

absorption aerosol optical depth (AAOD, bottom panel) at 550 nm over the Indian region

4.2.1 Precipitation

The ability of climate models to accurately simulate features of the Indian summer monsoon is crucial for building confidence in future model projections of precipitation response from climate forcing. Climate models that adequately reproduce observed temporal cycles in large-scale features (e.g. monsoon connection with El Niño Southern Oscillation (ENSO)-SST, land-ocean temperature contrast/pressure gradient, and wind circulation patterns) may have a higher degree of credibility in simulating future precipitation perturbations (*Kripalani et al.*, 2007; *Annamalai et al.*, 2007). Recent model inter-comparison studies found that ECHAM model (ECHAM5/MPI-OM) simulates reasonably well the observed seasonal, annual and inter-annual cycle and magnitudes of the Indian summer monsoon precipitation (*Kripalani et al.*, 2007; *Annamalai et al.*, 2007). In addition, the ECHAM model reproduce well the observed ENSO-related SST variability, land-ocean pressure gradient, and the observed SST and rainfall connection (*Kripalani et al.*, 2007; *Annamalai et al.*, 2007).

In this section, the spatial distribution of ECHAM model-simulated seasonal mean precipitation patterns is evaluated against in-situ observed (IMD) precipitation and TRMM satellite derived precipitation values during 2001-2005 (Figure 33). The TRMM rainfall values broadly agree with IMD observed rainfall values in all seasons (Figure 34). The spatial distribution of mean model simulated precipitation (mm/day) broadly captures both the IMD and TRMM observed rainfall patterns over the Indian region in all seasons, while the magnitude of rainfall is not predicted accurately. More than 75% of the annual model simulated rainfall over the Indian subcontinent occurs during the SW monsoon season (i.e. June-September, Figure 33), as observed in previous studies (*Dash et al.*, 2009). The major known rain belt associated with the Indian summer monsoon including the belt extending from west-northwest-ward across the IGP to the head of Bay of Bengal, the equatorial Indian Ocean belt and the western Ghats along the west coast of the peninsula belt (*Gadgil and Sajani*, 1998) is broadly simulated, while the orographic rainfall belt near northern IGP is lacking (Figure 33). However, the inter-seasonal trends are clearly visible in the model simulated rainfall distribution over the Indian region (Figure 33).

Zonal mean rainfall (mm/day) is simulated reasonably well in three different seasons (NE monsoon, pre-monsoon and inter-monsoon season, Figure 34). Convective rainfall was found to be dominant over south and central Indian regions, while large-scale precipitation dominates over the northern Indian regions (Figure 34). During the SW monsoon season, the magnitude of zonal mean rainfall was not predicted accurately; the rainfall values are underestimated by a factor of 2 to 3 (Figure 34). In the SW monsoon season, high rainfall was found over the CNI and NEI regions (Figure 2.3). Model simulated rainfall is especially underestimated (by a factor of 2-3) over the latitudinal band of 19^{o}N – 25^{o}N, where the model shows about equal contributions by both convective and large-scale rainfall values (Figure 34). The magnitude of model simulated rainfall, on the other hand, agrees much better with observations (both in-situ and satellite) over the latitudinal band of 27-30N, which is dominated by large-scale precipitation. In summary, the model broadly captures the observed seasonal rainfall variability both in magnitude and spatial distributions over the Indian region during 2001

to 2005 period, with some underestimation in absolute values, in particular in summer (SW monsoon season).

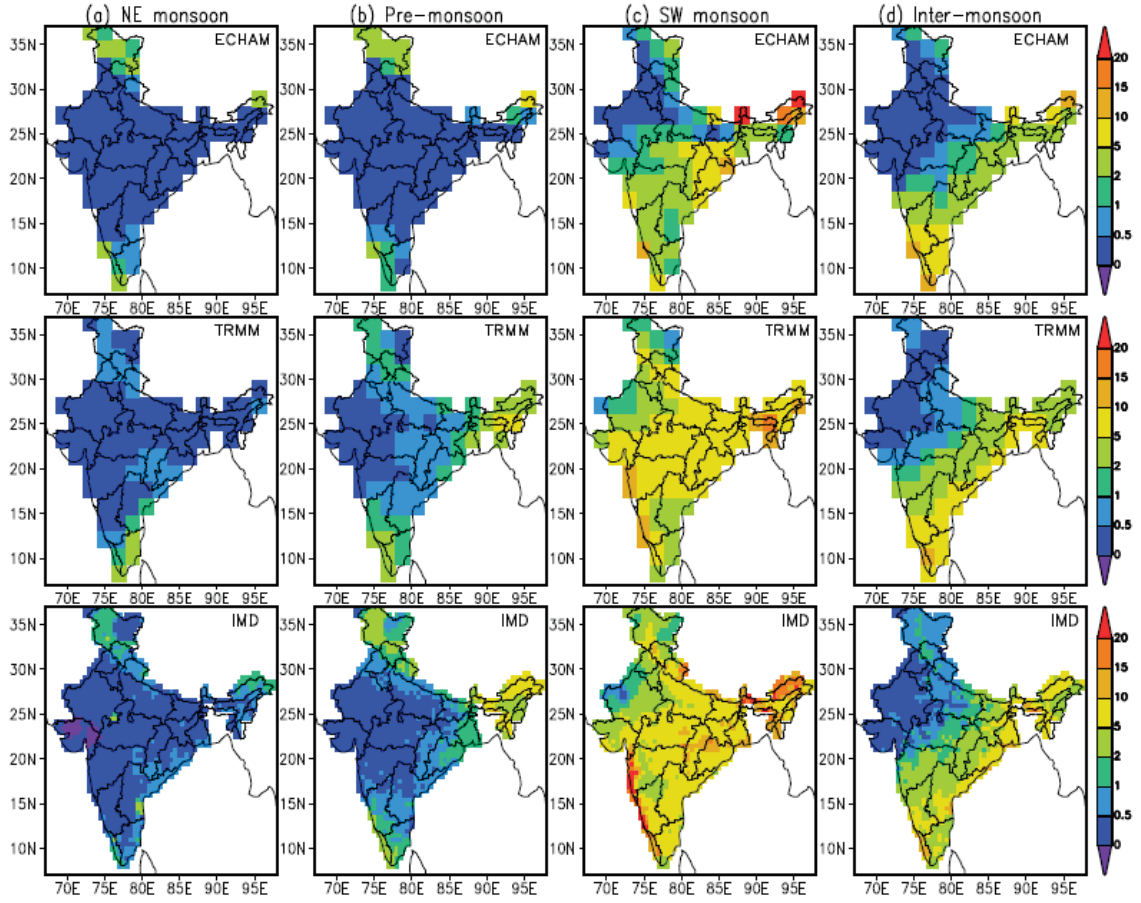

Figure 33: Seasonal mean distribution of the RCHAM model simulated total precipitation (mm/day) against TRMM (0.25°x0.25°) satellite derived rainfall and IMD (0.5°x0.5°) measured rainfall values over the Indian region (January 2001 to December 2005)

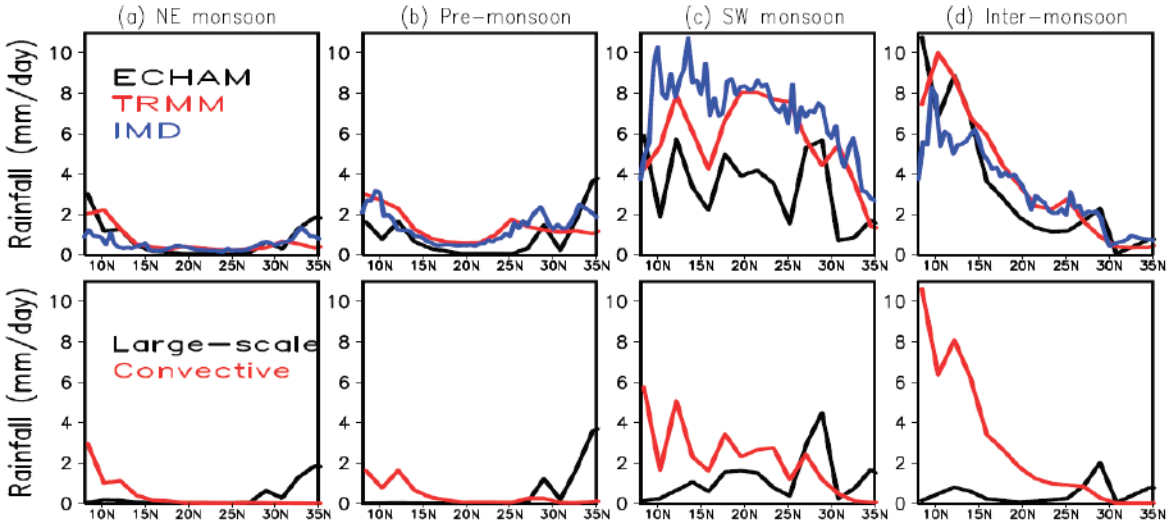

Figure 34: Seasonal zonal mean (68E-98E) ECHAM model simulated rainfall (black, mm/day), in-situ observed (IMD, blue) and satellite-retrieved (TRMM, red) rainfall (top panel) and simulated contributions by large-scale (black) and convective (red) rainfall (mm/day) over the Indian region (bottom panel)

In summary, ECHAM model broadly captures the spatio-temporal variability of AOD and precipitation, but with some caution on the absolute values. For the subsequent analysis of the anthropogenic contribution, this implies that spatial patterns of signals may be more reliable than the absolute magnitudes.

4.2.2 Anthropogenic aerosol emissions induced variability

The sensitivity of the climate response to anthropogenic aerosol emissions over the Indian subcontinent is evaluated and discussed here. In the following analysis, the main focus on the differences between the experiment with the present-day (PD) and the pre-industrial (PI) aerosol emissions, averaged over 5 years for the period from January 2001 to December 2005 (i.e. Δ=PD - PI). It may be noted that the simulations undertaken here are not exactly appropriate to gain insight into the actual time evolution of the AOD and climate response to anthropogenic aerosol emissions. This is because of the fact that the transient changes in anthropogenic aerosols are not considered. The anthropogenic aerosol emissions are kept constant in each year (at the year 2000 level), since the focus of this study is on the climatological, rather than weather, effects.

i) Variability in Aerosol Optical Depth

A mean AOD increase from PD anthropogenic emissions is simulated on the order of 10 – 20 % over the Indian subcontinent (Figure 35). A statistically significant AOD increase (by 0.1 to 0.25 in AOD units) results from PD anthropogenic aerosol emissions is simulated during the biomass burning season (NE monsoon) over the IGP, CNI and south India regions (Figure 35). In the pre-monsoon season, the highest changes in AOD (0.15 to 0.2) are found over the highly populated and industrialized regions (IGP, and CNI), and extending over the east coast into the continent, with a marked northwest – southeast gradient. In the SW monsoon season, the largest changes in AOD (> 0.2) are found over CNI and some parts of the IGP regions. A similar increase in AOD is simulated over the IGP and NWI regions during the Inter-monsoon season (Figure 35). Somewhat smaller changes are found in the NE monsoon and Pre-monsoon season than in SW monsoon season over the CNI region (Figure 35).

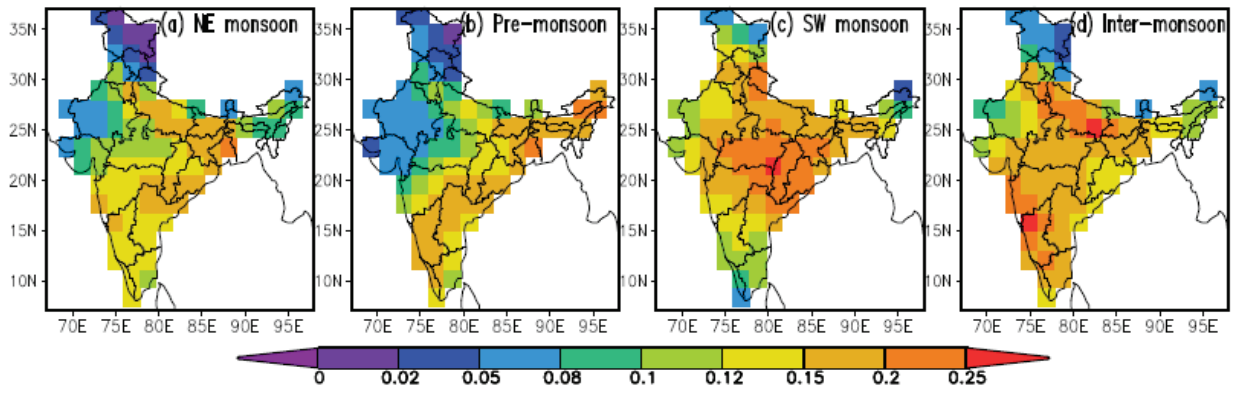

Figure 35: Model simulated seasonal mean AOD anomalies (PD-PI) at 550 nm result from the enhanced anthropogenic aerosol emissions over the Indian subcontinent (January 2001 to December 2005).

ii) Variability in Aerosol Direct Radiative Forcing

The changes in model simulated clear-sky shortwave (SW) radiation fluxes are analysed at the top of the atmosphere (TOA), at the surface (SUR) and within the atmosphere (ATM) to quantify the seasonal differences in the anthropogenic aerosol induced changes in atmospheric heating and surface cooling patterns over the Indian subcontinent (Figure 36). The changes (PD-PI) in clear-sky direct aerosol forcing at the TOA ranges from -0.17 Wm^{-2} (pre-monsoon) to -0.9 Wm^{-2} (inter-monsoon) over the Indian subcontinent (Table 4). The increase in clear-sky atmospheric absorption (6-9 Wm^{-2} in the seasonal mean) can be attributed mainly to the enhanced absorption optical depth in the Indian region. The seasonal mean clear-sky radiative forcing at SUR shows significant cooling (-6.9 to -9.9 Wm^{-2}) over the Indian region (Table 4). The changes in the clear-sky solar radiation at the surface are to a large extent the mirror image of the changes in absorption within the atmosphere, rather than increased sunlight reflection at the TOA, similar to the results of previous studies (*Roeckner et al.*, 2006). Statistically significant regional changes in atmospheric forcing are simulated for the NWI (ranges from 4.7 to 9.1 Wm^{-2}), CNI (ranges from 6.8 to 10.3 Wm^{-2}) and NEI (5.4 to 12.8 W m^{-2}) regions because of enhanced BC aerosols arising from biofuel burning and wild fire emissions. High surface cooling effects (ranging from -11.2 Wm^{-2} to -16.5 Wm^{-2}) are simulated over the high anthropogenic emission source regions (IGP) over the Indian subcontinent during all seasons (Figure 36). This solar dimming effect of anthropogenic aerosols through atmospheric extinction leads to strong surface cooling and atmospheric warming over the high aerosol loading regions (IGP and CNI). The perturbation in Earth's radiation fluxes by the anthropogenic aerosol thus affects the stability of the troposphere over these regions. The changes in clear-sky surface dimming results from PD anthropogenic emissions, locally exceeding -6.95 Wm^{-2}, are consistent with the observed trends in clear-sky solar dimming (-6 Wm^{-2}/decade, averaged over 12 stations) from 1981-2006 over the Indian region (*Padma Kumari and Goswami*, 2010). The surface cooling effect shows a maximum during the NE monsoon season and the Inter-monsoon season precedes the atmospheric warming peak over the Indian region except in the NEI region. This is because the wintertime has a more stable boundary layer and thus enables the surface to respond more to surface forcing than in springtime when the surface is climatologically warmer (Figure 36) and the boundary layer mixing is more active. The shortwave clear-sky aerosol radiative forcing (top-of-the-atmosphere flux change between PI and PD) from enhanced anthropogenic aerosol emissions between PI and PD levels over the Indian region is substantial (Figure 37). The main contributor to atmospheric aerosol absorption is BC aerosols and BC emissions, which have increased by a factor of 8 over the Indian region. The emissions of anthropogenic-influenced scattering aerosol components such SO_2 increased by a factor of 10, while the emissions of OC have had a smaller increase with a factor of two to three (Figure 37). A consequence of the stronger increase in BC is that the enhanced atmospheric heating in different seasons over the Indian region.

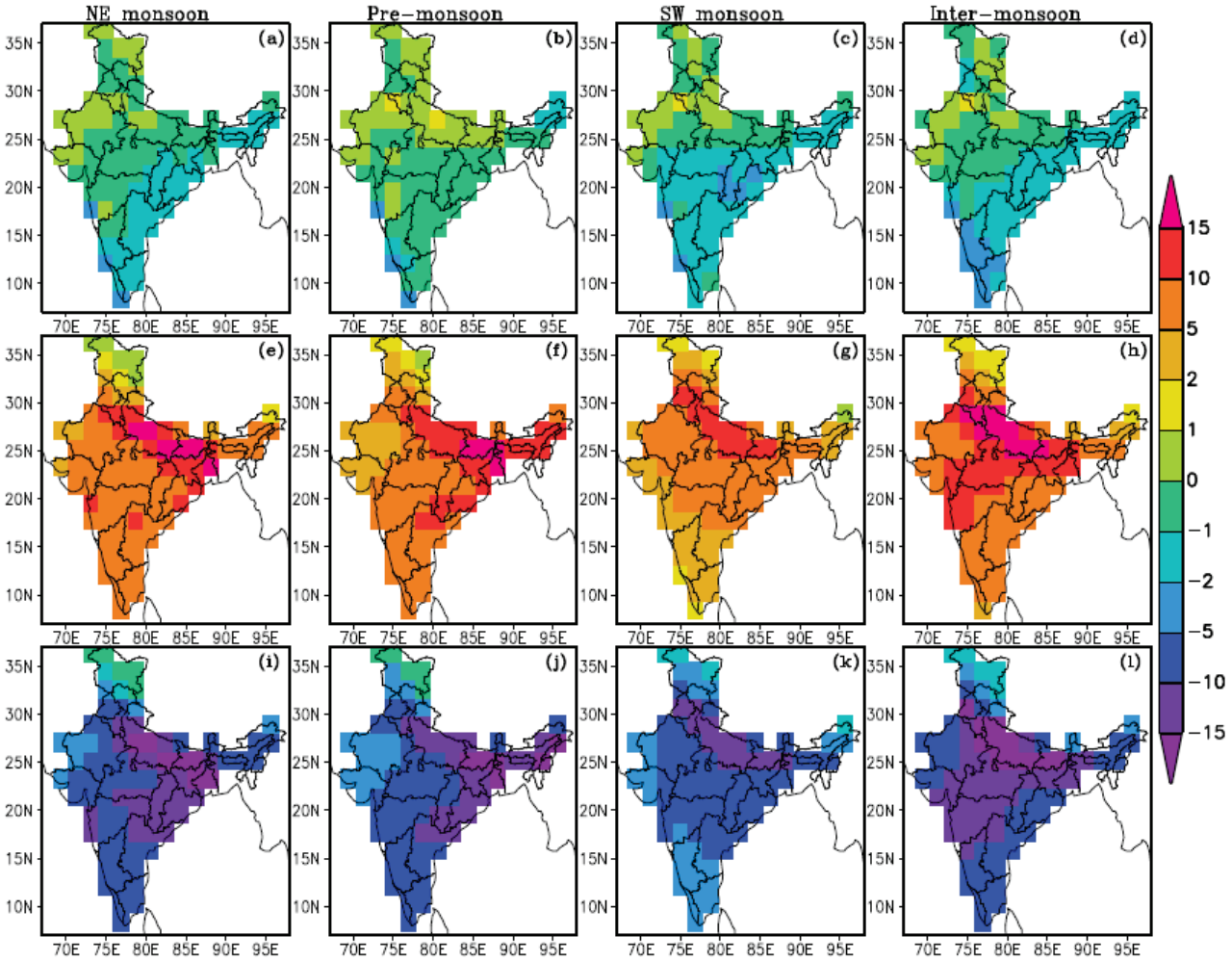

Figure 36: Spatial distribution of the model simulated seasonal mean change in short-wave clear-sky aerosol radiative forcing (ARF, Wm^{-2}) result from the enhanced anthropogenic aerosol over the Indian subcontinent (January 2001 to December 2005), at the Top-of-the-Atmosphere (top row; (a), (b), (c) and (d)), at the Surface (bottom row; (i), (j), (k) and (l)), and due to absorption with in the Atmosphere (middle row; (e), (f), (g), and (h)). The forcing is computed as the difference in mean radiative fluxes between the simulations with present-day (PD) and pre-industrial (PI) anthropogenic aerosol emissions

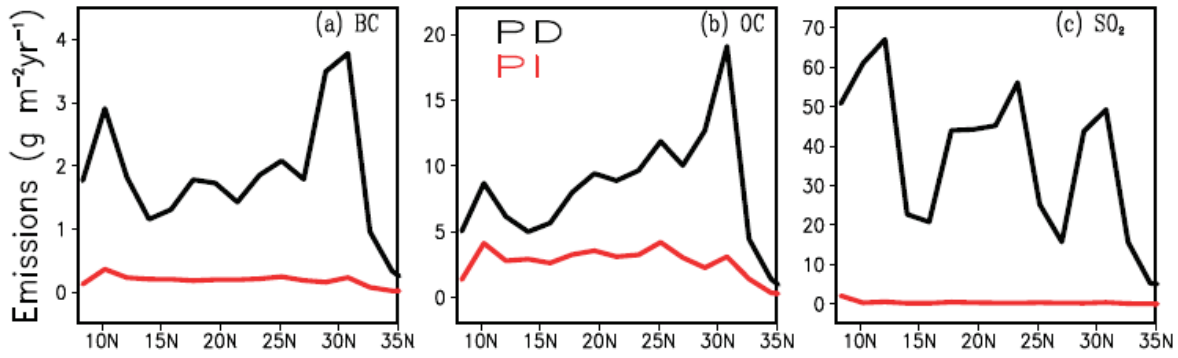

Figure 37: Present-day (PD) and pre-industrial (PI) emissions of (a) BC, (b) OC, and (c) SO_2 over the Indian subcontinent

Table 4: Season mean anthropogenic aerosol induced variability (PD-PI) in aerosol direct radiative forcing (Wm^{-2}) at the Top-of-the-Atmosphere (TOA), Surface (SUR) and the Atmosphere (ATM)

Region	NE Monsoon	Pre-monsoon	SW monsoon	Inter-monsoon
India				
TOA (Wm^{-2})	-0.70	-0.17	-0.88	-0.92
ATM (Wm^{-2})	8.21	8.09	6.07	9.02
SUR (Wm^{-2})	-8.91	-8.26	-6.95	-9.94
Central North India (CNI)				
TOA (Wm^{-2})	-0.98	-0.31	-1.69	-1.05
ATM (Wm^{-2})	10.13	9.17	6.82	10.36
SUR (Wm^{-2})	-11.11	-9.48	-8.52	-11.42
Indo-Gangetic Plain (IGP)				
TOA (Wm^{-2})	-0.18	0.68	-0.23	-0.25
ATM (Wm^{-2})	13.32	11.94	10.99	16.25
SUR (Wm^{-2})	-13.5	-11.26	-11.22	-16.5
North West India (NWI)				
TOA (Wm^{-2})	-0.13	0.17	-0.51	-0.26
ATM (Wm^{-2})	7.18	4.77	5.18	9.15
SUR (Wm^{-2})	-7.31	-4.6	-5.69	-9.41
North East India (NEI)				
TOA (Wm^{-2})	-1.01	-0.69	-1.02	-1.41
ATM (Wm^{-2})	7.48	12.84	5.43	6.61
SUR (Wm^{-2})	-8.49	-13.53	-6.45	-8.02

iii) Variability in Aerosol Indirect Effects

Aerosol radiative effects, defined here as cloudy-sky changes in radiative fluxes, are now examined to understand the indirect aerosol effects on the radiation budget results from the PD anthropogenic aerosol emissions. The short-wave (SW) cloud radiative effect is computed in the model as the difference between all-sky and (assumed) clear-sky radiative fluxes. The aerosol indirect forcing is then defined as the difference in cloud radiative effects between the simulations with PD and PI anthropogenic aerosol emissions. It is found that the indirect forcing both at the TOA and the surface is up to -

8 Wm^{-2} over the CNI regions in both nudged and the ensemble mean of the non-nudged simulations, but much smaller otherwise, and with only negligible absorption within the atmosphere (Figure 38). This reflects the Twomey effect, by which increased concentrations of cloud condensation nuclei (CCN) result in increased concentrations of cloud droplets, and subsequently an enhancement in cloud albedo (*Twomey*, 1977). In contrast, the anomalies (PD-PI) in long-wave (LW) absorption from tropospheric anthropogenic aerosols arising from CCN is found to be very small compared to the SW component and not statistically significant. This is consistent with the findings from previous studies (*Stier et al.*, 2007). The LW cloudy-sky radiative forcing, which was closely connected to high clouds, shows much smaller differences between PI and PD.

iv) Variability in Precipitation

The seasonal mean perturbation (PD-PI) in total precipitation is negative over most of the Indian subcontinent, but generally small. Precipitation changes are found to be statistically significant (95% confidence level based on a student's t-test analysis) only for SW monsoon season, and only over the CNI region (Figure 39). Seasonal mean precipitation changes are not statistically significant in all the other three seasons. The decrease in SW monsoon rainfall (JJAS) over the CNI corresponds well with the trend analysis in the observed rainfall from 1951-2003 by *Ghosh et al.,* (2009). But some of the finer regional features seen in the observed rainfall trends were not captured in the model which may be arising because of low model horizontal resolution (180 km). Also, because of the model set-up, changes near the coasts in the simulation are limited since the prescribed SST boundary conditions remain the same in both, PD and PI simulations. In this pair of simulations, the large-scale meteorology is also prescribed by nudging towards re-analysis data. It is thus interesting to further investigate whether additional changes occur if the dynamics are allowed to respond to the forcing.

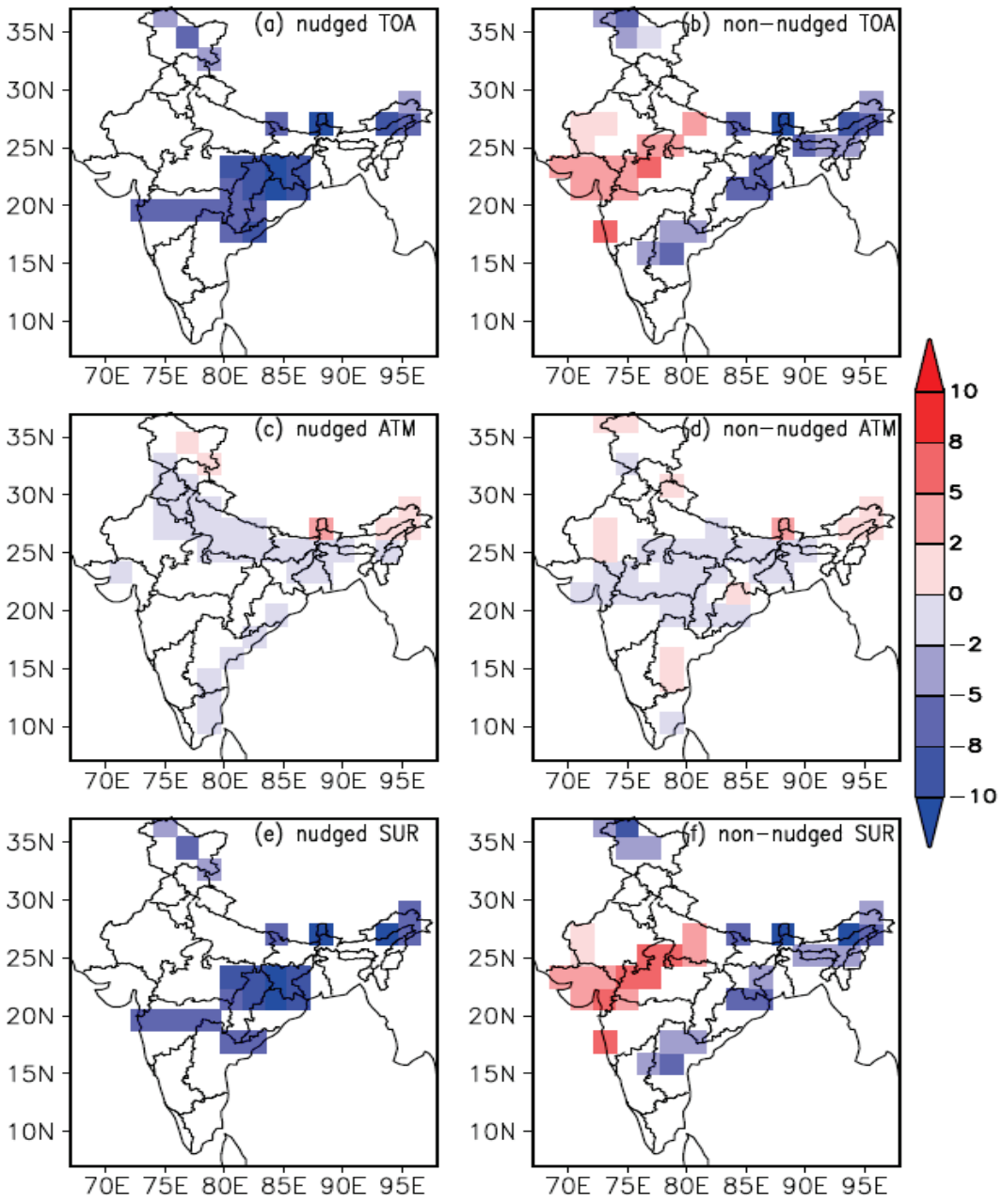

Figure 38: Spatial distribution of model simulated seasonal mean anomalies (PD-PI) in short-wave (SW) cloudy-sky forcing (Wm^{-2}) at the top of the atmosphere, surface and within the atmosphere result from PD anthropogenic aerosol emissions over the Indian subcontinent during the SW monsoon period (January 2001 to December 2005). Only statistically significant differences are shown.

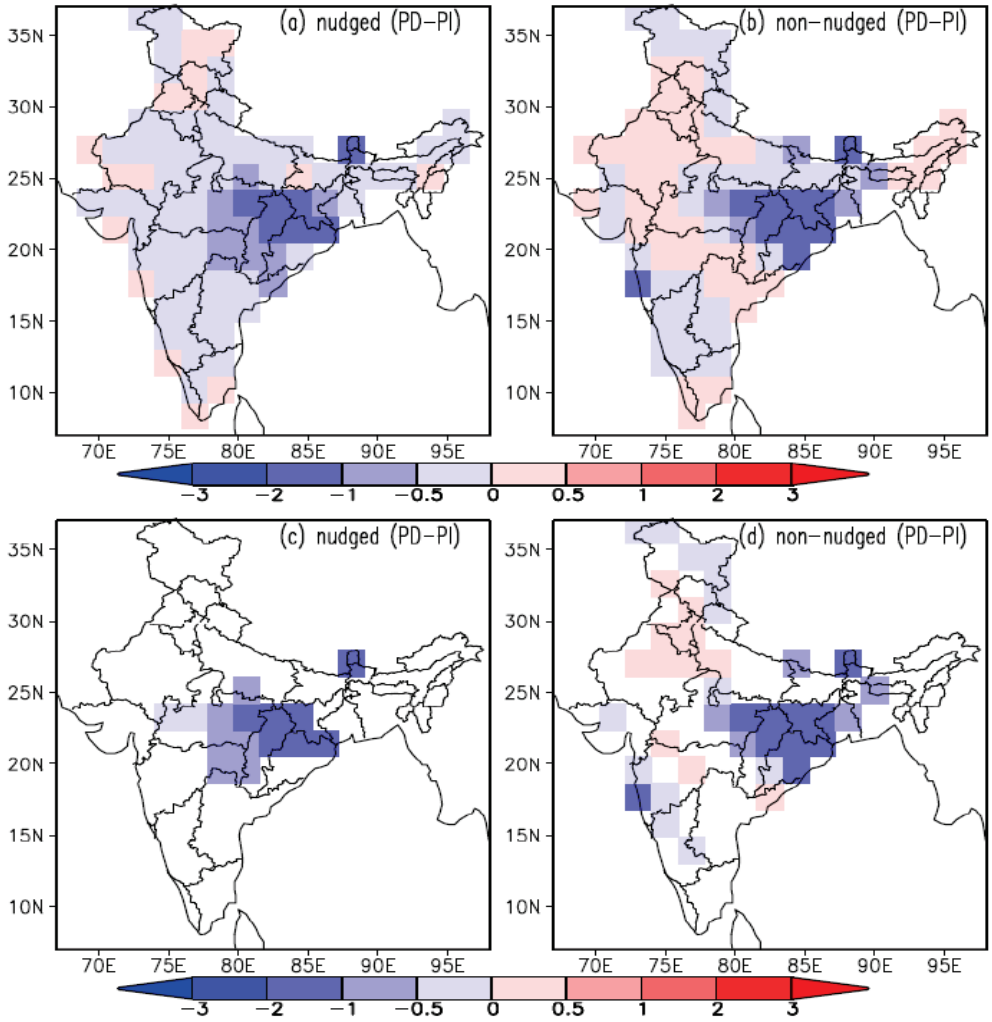

Figure 39: Spatial distribution of model simulated seasonal mean change in total precipitation (mm/day) result from the enhanced anthropogenic aerosol emissions over the Indian subcontinent during the SW monsoon period (January 2001 to December 2005).

The left column shows the nudged simulations as simulated in Figure 2.1-2.6, while the right column shows the ensemble mean of the three non-nudged simulations. Only regions where the differences (PD-PI) are statistically significant at the 95% confidence level were shaded in the bottom panel. Only the SW monsoon season is shown because in the other seasons changes are not found to be statistically significant at the 95% confidence level anywhere on the continent.

For understanding the circulation impacts on anthropogenic aerosol induced precipitation changes, an ensemble of three members of non-nudged simulations are performed for both the PD and PI anthropogenic emissions by slight model parameter perturbations. The ensemble mean of the non-nudged simulations is used for the analysis. These free simulations also show a statistically significant (at the 95% confidence level) decreasing precipitation trend over the CNI region (Figure 39), but of larger intensity, and with a broader geographical extent. Small increasing trends are found over parts of the IGP region. This slight increase in precipitation is consistent with the trends analysis in the observed rainfall from 1951-2003 by *Ghosh et al.*, (2009).

To examine the decreasing trend of total precipitation further, the convective and large scale precipitation anomalies (PD-PI) were analysed separately during the SW monsoon period. The model shows that changes in convective precipitation drive the decreasing trend in total precipitation (Figure 40). It is known that a significant fraction (65%-75%) of total precipitation originates from convective events rather than stratiform events in the Tropics (*Dai*, 2001; *Tost et al.*, 2006). Based on an analysis of satellite data a hypothesis has been formulated that anthropogenic aerosol may invigorate deep convective precipitation by decreasing the cloud droplet size and delaying the onset of freezing (*Albrecht*, 1989; *Rosenfeld and Woodley*, 2000). This is because the activation of a larger number of anthropogenic aerosol particles limits the size to which drops can grow for an available cooling rate. Hence, the number of drops which grow large enough to initiate the collision-coalescence process (the dominant precipitation process in warm clouds) was decreased and precipitation rates are attenuated (or decreased) (*Albrecht*, 1989; *Rosenfeld and Woodley*, 2000).

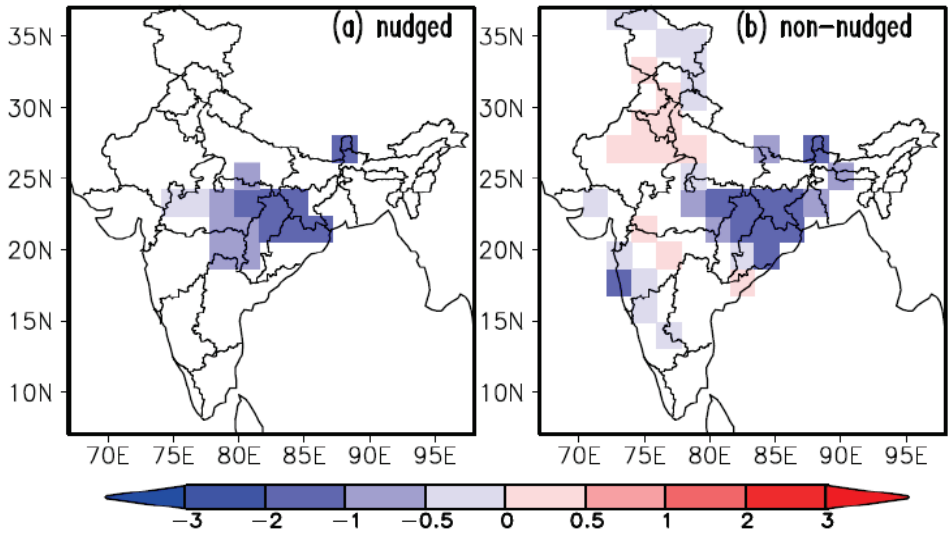

Figure 40: Spatial distribution of model simulated seasonal mean change in convective precipitation (mm/day) result from the enhanced anthropogenic aerosol emissions over the Indian subcontinent during the SW monsoon period (January 2001 to December 2005). Only regions where the differences (PD-PI) are statistically significant at the 95% confidence level were shaded.

This hypothesis was confirmed by a cloud resolving modelling study and showed that aircraft observations of highly supercooled water (>-10^{o}C) in deep convective clouds can only be reproduced if large concentrations of smaller sized cloud droplets exist (*Khain et al.*, 2001). Recent studies also showed that precipitation from single-cell mixed-phase convective clouds was reduced under continental conditions and maritime conditions when aerosol loading is increased (*Yin et al.*, 2000; *Khain et al.*, 2004).

The “cloud lifetime effect” on stratiform clouds, is associated with a higher amount of cloud water from increased anthropogenic aerosol emissions. This is because an increase in anthropogenic aerosol concentration leads to the formation of large amount of smaller sized cloud droplets that reduce the formation of rain drops and enhanced the residence time of cloud water (*Lohmann and Feichter*, 1997). This effect is parameterised in the GCM, and leads to the enhancement of cloud water in the CNI region (Figure 41). It was found that the increase in anthropogenic aerosol emissions since the beginning of the industrialization has caused a reduction in solar radiation at

the surface (solar dimming) and a decrease in precipitation (*Feichter et al.*, 2004; *Roeckner et al.*, 2006).

In the simulations, a strong radiative cooling of the surface is simulated over much of the Indian subcontinent results from the direct aerosol effect. For the indirect effect, in the nudged simulation, the surface cooling is particularly strong where also the precipitation change is found. These surface cooling effects (solar dimming) in the simulation may thus be considered main drivers of the reduction in precipitation. It is worth noting that the "cloud lifetime effect" does not directly reduce precipitation, but rather adds to the effect via radiation. In the simulation, this is manifest by the result that the reduction in total precipitation is mostly from the reduction in convective precipitation which is not directly affected by the cloud lifetime effect.

Evaporation rate anomalies were found to increase during the SW monsoon period from enhanced anthropogenic aerosol emissions (Figure 41). Lower surface evaporation rates are found in regions where solar radiation is reduced from changes in AOD (Figure 41). At the surface, there is a balance between radiation, evaporation (latent heat flux from the surface to the atmosphere), and sensible heat flux. One or all of these components will decrease to compensate for the reduction in surface solar radiation. The absorbed solar radiation at the surface was mainly balanced by evaporation, and it is thus possible that a major fraction of the reduction in surface solar radiation (Figure 36) is balanced by a small (0.01) increase in evaporation and a reduction in rainfall and may effectively spin down the hydrological cycle.

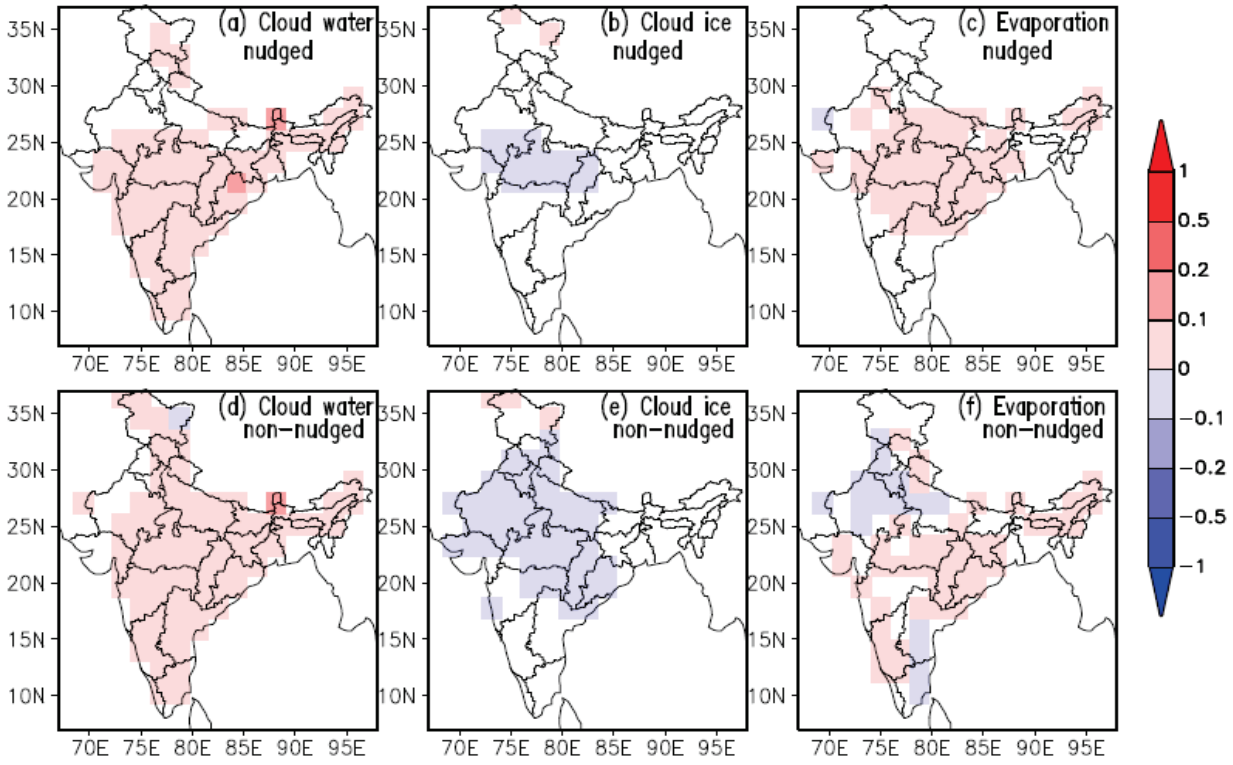

Figure 41: Spatial distribution of model simulated SW monsoon seasonal anomalies (PD-PI) result from the enhanced anthropogenic aerosol emissions for a vertically integrated (a,d) cloud water (g m^{-2}), (b,e) vertically integrated cloud ice (g m^{-2}), and (c,f) evaporation rate (2001 - 2005).

Chapter-5

Important Results of Project 3
Rainfall Extremes based on GCM Simulations

5.1 Low, Medium and Heavy Rainfall Events under RCP2.6, 4.5 and 8.5 Scenarios

The different statistical estimates for the trend analysis are summarized in Tables 5-8 for the low to medium rainfall in historical runs, RCP 2.6 scenario, RCP 4.5 scenario, and RCP 8.5 scenario, respectively. It is clear from the Tables that Mann-Kendall statistics, Z-statistics as well as Sen's slope statistics conform with each other in depicting the trend of the low to medium rainfall.

Table 5: Low to Medium Rainfall in Historical Run

Models	Mann-Kendall Statistics(S)	Kendall's Tau	Z	Sen's Slope
MIROC5	98	0.0800	0.8114	7
HadGEM2-ES	132	0.1078	1.0958	9.3571
CCSM4	27	0.0220	0.2175	2.6296
GFDL	-48	-0.0392	-0.3931	-1.5417

Table 6: Low to Medium Rainfall in RCP2.6 scenario

Models	Mann-Kendall Statistics(S)	Kendall's Tau	Z	Sen's Slope
MIROC5	387	0.0867	1.2410	3.4255
HadGEM2-ES	559	0.1252	1.79400	5.8571
CCSM4	-180	-0.0403	-0.5755	-2.3662
GFDL	339	0.0746	1.0674	1.2500

Table 7: Low to Medium Rainfall in RCP4.5 scenario

Models	Mann-Kendall Statistics(S)	Kendall's Tau	Z	Sen's Slope
MIROC5	1040	0.2329	3.3405	9.9394
HadGEM2-ES	99	0.0222	0.3151	0.8696
CCSM4	-289	-0.0647	-0.9259	-4.3333
GFDL	496	0.1238	1.7252	2.5833

Table 8: Low to Medium Rainfall in RCP8.5 scenario

Models	Mann-Kendall Statistics(S)	Kendall's Tau	Var (S)	Sen's Slope
MIROC5	682	0.1527	9.6742e+04	6.1154
HadGEM2-ES	-552	-0.1236	9.6742e+04	-5.1833
CCSM4	-347	-0.0777	9.6742e+04	-5.4146
GFDL	216	0.0484	9.6742e+04	1.2500

In Figure 42, we show the z-statistics for the heavy rainfall. The estimates of all other trend statistics are summarized in Tables 9-12 for the historical run, RCP2.6 scenario, RCP4.5 scenario, and RCP8.5 scenario, respectively. It is clear from the figure that the CMIP5 models analyzed in the present study predict increasing trend for the heavy rainfall under RCP4.5 and RCP8.5 scenarios. The models, MIROC5 and GFDL-CM3, however, show decreasing trend under RCP2.6 scenario but the values are statistically not very significant. Similar is the case for the CCSM4 model in the historical run. Thus, it may be convincingly argued that the heavy rainfall shall increase under the abrupt climate change.

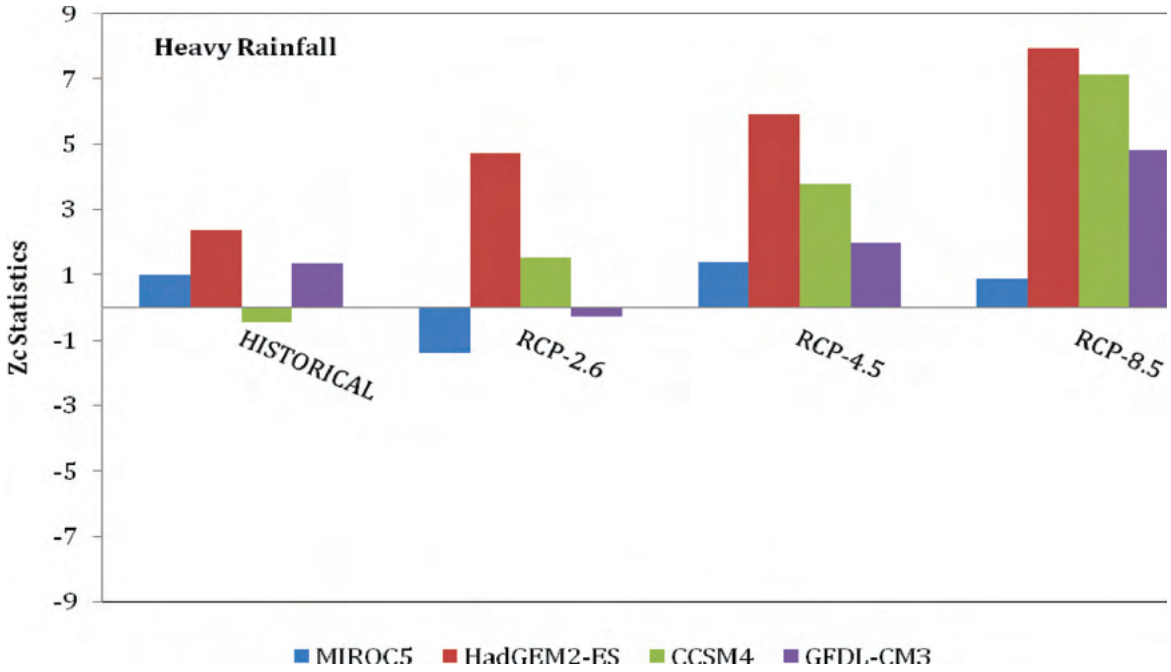

Figure 42: Heavy rainfall events under Historical and RCP2.6, 4.5 and 8.5 scenarios.

Table 9: Heavy Rainfall in Historical run

Models	Mann-Kendall Statistics(S)	Kendall's Tau	Z	Sen's Slope
MIROC5	121	0.0988	1.0038	0.9500
HadGEM2-ES	285	0.2327	2.3756	0.8000
CCSM4	-56	-0.0457	-0.4601	-0.2000
GFDL	165	0.1347	1.3718	0.1071

Table 10: Heavy Rainfall in RCP2.6 scenario

Models	Mann-Kendall Statistics(S)	Kendall's Tau	Z	Sen's Slope
MIROC5	-437	-0.0972	-1.3921	-0.4286
HadGEM2-ES	1473	0.3299	4.7326	0.6404
CCSM4	482	0.1080	1.5465	0.4430

GFDL	-85	-0.0190	-0.2701	0

Table 11: Heavy Rainfall in RCP4.5 scenario

Models	Mann-Kendall Statistics(S)	Kendall's Tau	Z	Sen's Slope
MIROC5	433	0.0970	1.3889	0.4286
HadGEM2-ES	1835	0.4110	5.8965	0.8966
CCSM4	1179	0.2641	3.7874	1.1525
GFDL	571	0.1426	1.9866	0.0714

Table 12: Heavy Rainfall in RCP8.5 scenario

Models	Mann-Kendall Statistics(S)	Kendall's Tau	Z	Sen's Slope
MIROC5	281	0.0629	0.9002	0.2500
HadGEM2-ES	2476	0.5545	7.9573	1.9153
CCSM4	2222	0.4976	7.1407	2.5246
GFDL	1507	0.3375	4.8419	0.2174

5.2 Very Heavy Rainfall Events

In Figure 43, we show the z-statistics for the case of very heavy rainfall. It may be noticed from the figure thatin all the scenarios, the models show increasing trend. Thus, in the context of abrupt climate change, the very heavy rainfall over eastern part of the India is bound to increase. The trends are high positive in the case of RCP 8.5 indicating maximum increase in the frequency of very heavy rainfall under this scenario. The z-values for the RCP 4.5 and RCP 8.5 scenarios are statistically highly significant for all the models confirming robustness of the results obtained among these models. The estimates of other trend analysis values are summarized in Tables 13-16 for the historical run, RCP 2.6 scenario, RCP 4.5 scenario, and RCP 8.5 scenario, respectively. The values are in conformity with each other.

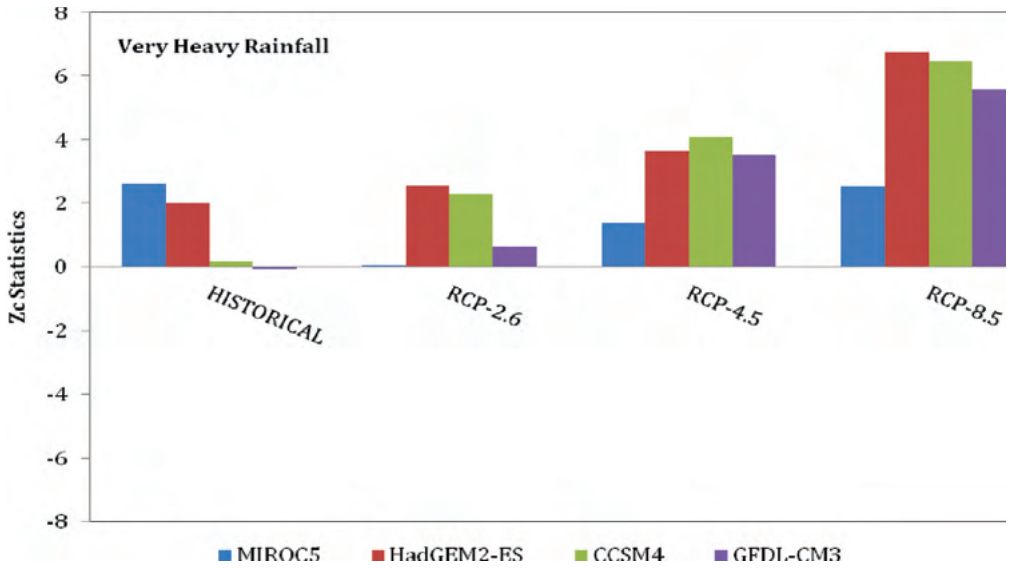

Figure 43: Very Heavy rainfall events under Historical and RCP2.6, 4.5 and 8.5 scenarios.

Table 13: Very Heavy Rainfall in Historical run

Models	Mann-Kendall Statistics(S)	Kendall's Tau	Z	Sen's Slope
MIROC5	315	0.2571	2.6266	0.5000
HadGEM2-ES	241	0.1967	2.0076	0.1667
CCSM4	23	0.0188	0.1840	0.0571
GFDL	-11	-0.0090	-0.0836	0

Table 14: Very Heavy Rainfall in RCP2.6 scenario

Models	Mann-Kendall Statistics(S)	Kendall's Tau	Z	Sen's Slope
MIROC5	11	0.0025	0.0322	0
HadGEM2-ES	797	0.1785	2.5592	0.0822
CCSM4	713	0.1597	2.2891	0.2840
GFDL	23	0.0455	0.6494	0

Table 15: Very Heavy Rainfall in RCP4.5 scenario

Models	Mann-Kendall Statistics(S)	Kendall's Tau	Z	Sen's Slope
MIROC5	428	0.0959	1.3728	0.1351
HadGEM2-ES	1135	0.2542	3.6459	0.1475
CCSM4	1268	0.2840	4.0735	0.5200
GFDL	1011	0.2524	3.5201	0.0164

Table 16: Very Heavy Rainfall in RCP8.5 scenario

Models	Mann-Kendall Statistics(S)	Kendall's Tau	Z	Sen's Slope
MIROC5	785	0.1758	2.5206	0.3261
HadGEM2-ES	2105	0.4714	6.7646	0.4167
CCSM4	2017	0.4517	6.4816	0.9524
GFDL	1852	0.4148	5.9511	0.0606

5.3 Extremely Heavy Rainfall Events

The z-statistics for the case of extremely heavy rainfall are shown in Figure 44. In this case also, the models are showing increasing trend for all the scenarios. It may be concluded that the extremely heavy rainfall events will increase over the eastern part of India in the future climate. It was not possible to find the trend in the MIROC5 model since number of extremely heavy rainfall events were very few in this model. This model may, therefore, be underestimating the rainfall amount over the eastern India. Thus on one hand the frequency of low to medium rainfall will decrease, but on the other hand, the occurrence of heavy, very heavy, and extremely heavy rainfall events will increase. The Mann-Kendall estimate and the Sen's slope are also calculated for estimates the trend of extremely heavy rainfall from these models. The values are summarized in Tables 17-20 for the historical run, RCP2.6, RCP4.5 and RCP8.5 scenarios respectively. The values are in agreement with each other and also with the z-statistics thus confirming robustness of the trend analysis.

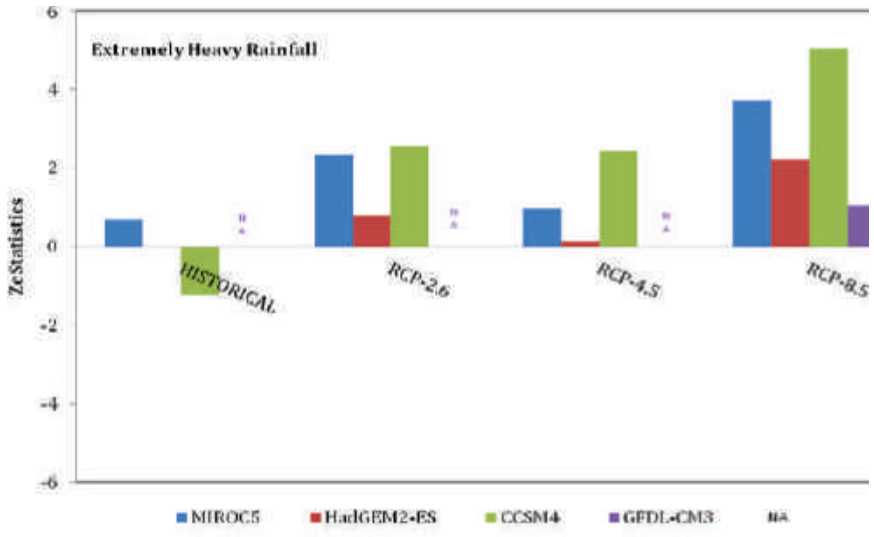

Figure 44: Extremely Heavy rainfall events under Historical and RCP2.6, 4.5 and 8.5 scenarios.

Table 17: Extremely Heavy Rainfall in Historical run

Models	Mann-Kendall Statistics(S)	Kendall's Tau	Z	Sen's Slope
MIROC5	82	0.669	0.6776	0
HadGEM2-ES	nil	nil	nil	Nil
CCSM4	-149	-0.1216	-1.2380	-0.0286
GFDL	nil	nil	nil	Nil

Table 18: Extremely Heavy Rainfall in RCP2.6 scenario

Models	Mann-Kendall Statistics(S)	Kendall's Tau	Z	Sen's Slope
MIROC5	728	0.1630	2.3374	0
HadGEM2-ES	247	0.0553	0.7909	0
CCSM4	803	0.1798	2.5785	0.0423
GFDL	nil	nil	nil	Nil

Table 19: Extremely Heavy Rainfall in RCP4.5 scenario

Models	Mann-Kendall Statistics(S)	Kendall's Tau	Z	Sen's Slope
MIROC5	309	0.0692	0.9902	0
HadGEM2-ES	46	0.0103	0.1447	0
CCSM4	763	0.1709	2.4499	0.0455
GFDL	nil	nil	nil	Nil

Table 20 Extremely Heavy Rainfall in RCP 8.5 scenario

Models	Mann-Kendall Statistics(S)	Kendall's Tau	Z	Sen's Slope
MIROC5	1159	0.2598	3.7231	0.0179
HadGEM2-ES	691	0.1548	2.2184	0
CCSM4	1569	0.3514	5.0413	0.1154
GFDL	328	0.0735	1.0513	0

Chapter-6

SUMMARY AND CONCLUSIONS

For the first time a regional climate model (RegCM) has been successfully integrated under the newly defined climate scenario termed as RCP till the end of the century. Large data set has been obtained for scientific analysis into the future. These data obtained under the CORDEX programme can be utilised for projecting the climate and their extremes into the future. The climate data so projected can be utilised for impact studies especially in the fields of agriculture and health for different regions in India. Attempt has already been made in this regard.

RegCM has also been successfully downscaled to 30km with the output from NCNMRWF T80 model and results show that the downscaled predictions have better skill compared to that of T80 model itself. These results are encouraging from the point of better seasonal prediction over Indian regions by using the dynamical downscaling technique.

Anthropogenic aerosol induced changes in present-day aerosol loading and their climatic effects have been examined with a focus on monsoon precipitation over the Indian subcontinent during January 2001 to December 2005 using the ECHAM5.5-HAM model. In a first step, the model is evaluated using satellite retrievals. The model simulated AOD at 550 nm captures the variability both in time (inter-seasonal variability) and space (distribution patterns) over the Indian subcontinent. However, absolute magnitudes and details of the variability are not well simulated. Similarly, the spatial distribution, and seasonal cycle, of the simulated precipitation (mm/day) was broadly capturing the IMD-observed and TRMM satellite-derived distributions, while in terms of absolute magnitude, the model underestimates precipitation in particular in the SW monsoon season. These findings implied that the characteristics of the variability induced by anthropogenic aerosols may be simulated realistically, while the absolute magnitude of effects may be still questionable.

The model simulates a wide-spread and substantial change in column aerosol concentration results from PD anthropogenic emissions, which leads to a wide-spread and strong surface cooling, consistent with observed trends. This cooling mainly results from aerosol absorption. Significant cloud changes via indirect effects are confined to a smaller region in central India, where a strong surface forcing is exerted in the SW monsoon season. A signal in precipitation is found only over central India, in case of SW monsoon season. This signal is consistent with observed trends. This precipitation reduction is from a reduction in convective precipitation. It is linked mainly to the surface cooling, and further substantially enhanced by the atmospheric stabilisation through aerosol absorption.

In addition to the use of aerosols in GCM, the regional model RegCM has been successfully tested for the impact of aerosols in the Indian region. The impact of aerosols on Indian summer monsoon circulation and rainfall can now be examined in greater detail.

The frequency and occurrence of low to medium, heavy, very heavy, and extremely heavy rainfall over eastern India is quantified in the context of climate change in the IPCC AR5 CMIP5 models. The historical runs and climate change projection scenarios (RCP2.6, RCP4.5, RCP8.5) are used for this purpose. The trend analysis suggests that the frequency of very heavy and extremely heavy rainfall will increase under the abrupt climate change. On the other hand, the occurrence of low to medium rainfall events will decrease.

The learning experience under this project so far will help us to estimate climate uncertainty for different regions of India and then examine their usefulness to the scientific community. The method of quantifying uncertainty in GCM simulations, Projection of climate at regional level by a regional model RegCM, Dynamical downscaling of NCMRWF model output to 30km by RegCM at the time scale of season, statistical downscaling of GCM products to high resolution local climate change information, Simulation of aerosol impact in the Indian region both in GCM and RegCM are the innovative applications under these three projects on climate modelling.

6.1 Strategic knowledge generated

Some of the uncertainties associated with the projections of regional climate change have been addressed to and examined under these projects. Local climate information have been successfully generated by the use of dynamical and statistical downscaling techniques. These information are vital for the study of impact studies in sectors such as agriculture and health.

The regional climate model RegCM of the Abdus Salam ICTP is one of the important regional climate models available to scientists across the world with adequate operational support from time to time. It is widely used in research by a large number of scientists. In this study this model has been extensively used in examining the current and future climate changes at regional level in India. This model has been validated for its use over India. This regional model is the second such model tested and used for India after PRECIS. Further, for the first time a regional climate model such as RegCM has been successfully integrated under the newly defined climate scenarios termed as RCP till the end of the century. Large data set has been obtained for scientific analysis into the future. These data obtained under the CORDEX programme can be utilised for projecting the climatic parameters and their extremes into the future. The climatic parameters so projected can in turn be utilised for impact studies especially in the fields of agriculture and health for different regions in India. Attempt has already been made in this regard.

RegCM has also been successfully downscaled to 30km with the output from NCNMRWF T80 model and results show that the downscaled predictions have better skill compared to that of T80 model itself. These results are encouraging from the point of better seasonal prediction over Indian regions by using the dynamical downscaling technique.

The uncertainties arising out of the treatment of aerosols in the climate models is one of teh major issues in the understanding of impact of aerosols on the climate change. In these projects both GCM and RegCM are successfully tested for the impact of aerosols in the Indian region. Preliminary results indicate the weakening of Indian summer monsoon circulation due to the anthropogenic aerosols. The impact of aerosols on Indian summer monsoon circulation and rainfall need to be examined in greater detail.

Results of these projects further show that very heavy and extreme rainfall events will increase in future. It is a very important finding and is relevant from the point of view of policy making and disaster management. Further, the CMIP5 models are not able to correctly capture the Indian summer monsoon rainfall variability including very heavy rainfall and extremely heavy rainfall events. Extensive study on downscaling of GCM products at high resolution is very essential so as to use the climate products for the benefit of the society.

6.2 Publications/articles emanated from the work

1. Das, S., Dey, S., Dash, S. K. and G. Basil, (2013): Examining mineral dust transport over the Indian subcontinent using the regional climate model, RegCM4.1, *Atmos. Res.*, 134, 64-76.

2. Dash, S.K., Saraswat Vaishali, Panda, S.K., and Neha Sharma, (2013): A study of changes in rainfall and temperature patterns at four cities and corresponding meteorological subdivisions over coastal regions of India, *Global and Planetary Change*, 108, 175–194.

3. Dwivedi, S and F. Kucharski, Quantifying the Change in the Duration of Active and Break Spells of the Indian Summer Monsoon Rainfall during El Niño and La Niña Events, to be communicated to the Geophysical Research Letters, 2014

4. Dwivedi,S, V. Chandra and A. Kundu, Investigating the Occurrence of Very Heavy and Extremely Heavy Rainfall over CentralIndia in the CMIP5 Models, to be communicated to Current Science, 2014.

5. Fernati, R, S. Dwivedi, F. Kucharski, F. Molteni and S. M. Griffies, On Pacific Subtropical Cell Variability over the Second Half of the Twentieth Century, *Journal of Climate*, doi: http://dx.doi.org/10.1175/JCLI-D-13-00707.1, 2014.

6. Kundu, A, and S. Dwivedi, The Analysis of Remote Sensing Satellite Data to Understand Effect of Climate Change on the Vegetation and Health over India, *communicated*, 2014.

7. Mamgain, Ashu, Dash S.K., Mariotti, L., Coppola, E. and Giorgi, F., (2013): Indian winter monsoon circulation and rainfall as simulated by RegCM4 in the CORDEX, *Vayu Mandal*, Vol.39 (3-4), 25-34.

8. Pattnayak, K.C., Panda, S. K. and Dash, S.K., (2013): Annual cycles of circulation and precipitation over India simulated by a Regional Climate Model, *Vayu Mandal*, Vol.39 (3-4), , 35-45.

9. Rai,S, F. Kucharski, F. Molteni, Prediction of South Asian Monsoon from ECMWF System 3 daily forecast, to be communicated to the Geophysical Research Letter, 2014.

10. Sinha, P., Mohanty, U. C., Kar, S. C., Dash, S. K. and S. Kumari (2013): Sensitivity of the GCM driven summer monsoon simulations to cumulus parameterization schemes in nested RegCM3, *Theor Appl Climatol*, 112, 285–306.

11. Tiwari, P.R., Kar, S.C., Mohanty, U.C., Dey, S., Sinha, P. S., Raju, P.V.S., and M.S. Shekhar, (2014), Dynamical downscaling approach for wintertime seasonal scale simulation over the western Himalayas. *Acta Geophysica*., 62(4), 930-952.

6.3 Training/awareness programmes conducted under the project

All the three proposed Training Workshops on "Climate Modelling: Simulations and Analysis" were conducted at CAS, IIT Delhi. The first Training Workshop was held at during Dec 9 – 21 Dec, 2013. The topics included Climate Processes, Basics of Modeling, Model Integration and Climate Data Analysis. Emphasis was given on the Tutorials based on Graphics and Data Visualization, RegCM installation and applications, GCM Simulations and Climate Data Analysis. In total 25 PhD students/early career scientists from institutions such as Andhra University, BHU, JNU, IIT Bombay, IIT Kharagpur, Gujarat University, BIT Mesra, BSIP Lucknow, Calcutta University, NARL, Allahabad University and IIT Delhi participated in the workshop. There were 18 resource persons from premier institutions such as PRL, IISc, NCMRWF, IMD. IITM, IIT Bombay, IIT Bhubaneswar and IIT Delhi. At the end of the first workshop, the participants gave presentations on their current research activities and the future science proposal. Based on their performance and interest in modelling, 15 were selected for their advanced training during the second workshop.

The second Training Workshop was held in CAS, IIT Delhi during June 23 to July 5, 2014. The first week of the workshop was devoted to hands-on training on the regional climate model RegCM. Mr. G. Graziano from the Abdus Salam ICTP, Trieste was kind enough to visit IIT Delhi during that period to impart advanced training on the latest version of RegCM. The second week of the workshop was devoted to practical training on GCM.

The third training workshop was held in CAS, IIT Delhi during 1st June to 12th June 2015. The focus of this workshop was on climate data analysis. Unlike the previous two workshops, hands-on-training started from day 1 with lectures in between on the relevant topics. First the available climate data were introduced to the participants, followed by statistical methods for its analysis. In the first week, tutorial was conducted on 'Phython/CDAT'. Special focus was given on CMIP5 data, its analysis and various diagnostic methods. Participants were given the chance to formulate a project of their own choices using the CMIP5 data at the end of the first week. They applied the methods they learnt in the first week and presented their analysis at the end of the workshop.

6.4 Future Work and Way forward

Surface air temperature and rainfall are the two most important climatic parameters which have great relevance when one thinks about the impact of climate change on the society. There are robust signals of rise in temperature and it extremes over several places in India. Nevertheless, the mapping of the whole country in terms of different categories of temperature extremes is very essential in order to go ahead with the heat stress warning systems as being done in several other parts of the world. Future research in this regard can help in accomplishing this task and broadcast regular heat warning signals.

Climate change does not have certain impact on the increase/decrease in rainfall over India. However, heavy rain events with short duration are showing increasing trends. So

far as the projections of different categories of rain events are there, no clear message emerges from the climate models. Uncertainty analysis of rain events based on output from available important models is of utmost importance. The knowledge obtained from such study will help in water management, agriculture and human health.

More work is in pipeline for understanding the role of natural as well as anthropogenic aerosols on teh Indian summer monsoon with the use of both GCM and RegCM. Today climate modelling efforts are going on in parallel so far as GCM and RegCM are concerned. Getting climate products at high resolution is the most important advantage of RegCM. Understanding the role of aerosols will help in removing uncertainty in climate projections to a large extent.

All the above important activities are achievable in the time scale of 2-3 years. In India, the next step should be to develop a couple of climate models which are India centric. There are several scientific challenges which demand an India centric climate model exclusively for this part of the globe. IITM has taken some steps in this regard. However, one model is not the answer to deal with complexities of the magnitude of climate change. More scientific groups need to be encouraged and nurtured in the country in order to address climate change issues.

The climate projections are not very reliable mainly because of the model biases and also the uncertainties in the emissions and climate projections. It is very much essential to reduce the model biases, especially in the surface temperature and rainfall fields over India before the projections by the same models are used in policy formulation. The most important challenge to the scientific community is to examine the trends in the model errors and correct those at the process level. I other words we need to nurture young scientists in the model development process. Involvement of scientists in the code development is the key. Creations of Centres of Excellence on different aspects of climate science such as model development and validation, downscaling of climate products and their corrections and finally impact studies in the fields of agriculture, ecosystem and human health will help the Indian climate community in the long run.

References

1. Albrecht, B. (1989), Aerosols, Cloud Microphysics, and Fractional Cloudiness, Science, 245, 1227-1230, doi:10.1126/science.245.4923.1227.

2. Andres, R. J., and A. D. Kasgnoc (1998), A time-averaged inventory of subaerial volcanic sulfur emissions, J. Geophys. Res., 103(D19), 25251-25261.

3. Annamalai, H., K. Hamilton, and K. R. Sperber (2007), The South Asian Summer Monsoon and Its Relationship with ENSO in the IPCC AR4 Simulations, J. Climate, 20(1071-1092), doi:10.1175/JCLI4035.1.

4. Bhuiyan, C., Singh, R. P. and Kogan, F. N., 2006, Monitoring drought dynamics in the Aravalli Terrain (India) using different indices based on ground and remote sensing data. International Journal of Applied Earth Observation and Geoinformation, 8: 289–303.

5. Bhuiyan, C. and Kogan, F. N., 2010, Monsoon variation and vegetative drought patterns in the Luni Basin in the rain-shadow zone, International Journal of Remote Sensing, 31: 3223-3242.

6. Bollasina, M. A., Ming, Y., and Ramaswamy, V. (2011), Anthropogenic aerosols and the weakening of the South Asian summer monsoon, Science, 334 (6055), 502-505.

7. Bond, T. C., D. G. Streets, K. F. Yarber, S. M. Nelson, J. H. Woo, and Z. Klimont (2004), A technology-based global inventory of black and organic carbon emissions from combustion, J. Geophys. Res., 109(D14), doi:10.1029/2003JD003697.

8. Boucher, O. and U. Lohmann (1995), The sulfate-CCN-cloud albedo effect: A sensitivity study with two general circulation models, Tellus B, 47, 281–300, 1995.

9. Chaturvedi, R., Joshi, J., Mathangi, J., Bala, G., Ravindranath, N. H.(2012), Multi-model projection of climate change for India under representative concentration pathways. Current Science, 103(7), 1-12.

10. Cherian, R., C. Venkataraman, S. Ramachandran, J. Quaas, and S. Kedia (2011), Examination of aerosol distributions and radiative effects over the Bay of Bengal and the Arabian Sea region during ICARB using satellite data and a general circulation model, Atmos. Chem. Phys. Discuss., 11, 13911-13946, doi:10.5194/acpd-11-13911-2011.

11. Cofala, J., M. Amann, and R. Mechler (2005), Scenarios of world anthropogenic emissions of air pollutants and methane up to 2030, International Institute for Applied Systems Analysis (IIASA)), Laxenburg, Austria.

12. Dabrowska-Zielinska, K., Kogan, F., Ciolkosz, A., Gruszczynska, M. and Kowalik, W., 2002, Modelling of crop growth conditions and crop yield in Poland using AVHRR-based indices. International Journal of Remote Sensing, 23: 1109–1123.

13. Dai, A. (2001), Global precipitation and thunderstorm frequencies. Part I: Seasonal and interannual variations, J. Climate, 14, 1092-1111.

14. Dash, S. K., M. A. Kulkarni, U. C. Mohanty, and K. Prasad (2009), Changes in the characteristics of rain events in India, J. Geophys. Res., 114, D10109, doi:10.1029/2008JD010572.

15. Dash, SK, Ashu Mamgain, Pattnayak, KC, Giorgi, F (2013), Spatial and temporal variations in Indian summer monsoon rainfall and temperature: an analysis based on RegCM3 simulations. Pure Appl. Geophys. 170, 655–674.

16. Dentener, F., et al. (2006), Emissions of primary aerosol and precursor gases in the years 2000 and 1750 prescribed data-sets for AeroCom, Atmos. Chem. Phys., 6, 4321-4344.

17. Dey, S., S. N. Tripathi, R. P. Singh, and B. N. Holben (2004), Influence of dust storms on aerosol optical properties over the Indo-Gangetic basin, J. Geophys. Res., 109, D20211, doi:10.1029/2004JD004924.

18. Dey, S., and L. D. Girolamo (2010), A climatology of aerosol optical and microphysical properties over the Indian subcontinent from 9 years (2000–2008) of Multiangle Imaging spectroradiometer (MISR) data, J. Geophys. Res., 115(D15204), doi:10.1029/ 2009JD013395.

19. Di Girolamo, L., et al. (2004), Analysis of Multi-angle Imaging Spectro Radiometer (MISR) aerosol optical depths over greater India during winter 2001-2004, Geophys. Res. Lett., 31(23), L23115, doi:10.1029/2004GL021273.

20. Dickinson, R., Henderson-Sellers, A., Kennedy, P. (1993), Biosphere atmosphere transfer scheme (BATS) version 1E as coupled to the NCAR community climate model. Technical Report National Center for Atmospheric Research, p. 72.

21. Dutta, D., Kundu, A. and Patel, N. R., 2013, Predicting agricultural drought in eastern Rajasthan of India using NDVI and standardized precipitation index, Geocarto International, 28: 192-209.

22. Eastman, R. and Warren, S. G. 2013: A 39-Yr Survey of Cloud Changes from Land Stations Worldwide 1971-2009: Long-Term Trends, Relation to Aerosols, and Expansion of the Tropical Belt. J. Climate, 26, 1286-1303.

23. Emanuel KA, Zivkovic-Rothman M (1999), Development and evaluation of a convection scheme for use in climate models. J Atmos Sci 56: 1766–1782.

24. Fecan, F., Marticorena, B., Bergametti, G., (1999), Parameterization of the increase of the Aeolian erosion threshold wind friction velocity due to soil moisture for arid and semi-arid areas. Ann. Geophys. 17, 149–157.

25. Feichter, J., E. Roeckner, U. Lohmann, and B. Liepert (2004), Nonlinear aspects of the climate change response to greenhouse gas and aerosol forcing, J. Climate, 17, 2384-2398.

26. Gadgil, S., and S. Sajani (1998), Monsoon precipitation in the AMIP runs, Climate Dynamics, 14 (9), 659-689, doi:10.1007/s003820050248.

27. Ghosh, S., V. Luniya, and A. Gupta (2009), Trend Analysis of Indian Summer Monsoon Rainfall at Different Spatial Scales, Atmos. Sci. Lett., 10(4), 285-290.

28. Giorgi, F., Mearns, L.O. (2002), Calculation of average, uncertainty range, and reliability of regional climate changes from AOGCM simulations via the "reliability ensemble averaging" (REA) method. Journal of Climate, 15, 1141-1158.

29. Giorgi F, Coppola E, Solmon F, Mariotti L, Sylla MB, Bi X, Elguindi N, Diro GT, Nair V, Giuliani G, Turuncoglu UU, Cozzini S, Guttler I, O'Brien TA, Tawfik AB, Shalaby A, Zakey AS, Steiner AL, Stordal F, Sloan LC, Brankovic C (2012) RegCM4: Model description and preliminary tests over multiple CORDEX domains. Clim Res 52:7-29.

30. Giorgi F, Mearns LO (1999), Introduction to special section: Regional climate modeling revisited. Journal of Geophysical Research 104:6335-6352.

31. Grell, G.A., (1993), Prognostic evaluation of assumptions used by cumulus parameterizations. Mon. Weather Rev. 121, 764–787.

32. Gutman, G. G., 1991, Vegetation indices from AVHRR data: an update and future prospects. Remote Sensing of Environment, 35: 121–136.

33. Holtslag A, de Bruijn E, Pan HL (1990), A high resolution air mass transformation model for short-range weather forecasting. Mon Weather Rev 118:1561–1575.

34. Hielkema, J. U., Prince, S. D. and Astle, W. L., 1986, Rainfall and vegetation monitoring in the Savanna zone of Democratic Republic Sudan using NOAA Advanced Very High Resolution Radiometer. International Journal of Remote Sensing, 7: 1499–1514.

35. Huffman, G. J., R. F. Adler, D. T. Bolvin, G. Gu, E. J. Nelkin, K. P. Bowman, Y. Hong, E. F. Stocker, and D. B. Wolff (2007), The TRMM Multi-satellite Precipitation Analysis: Quasi-global, multi-year, combined-sensor precipitation estimates at fine scale, J. Hydrometeor, 8, 38-55.

36. Jethva, H., S. K. Satheesh, and J. Srinivasan (2005), Seasonal variability of aerosols over the Indo-Gangetic basin, J. Geophys. Res., 110, D21204, doi:10.1029/2005JD005938.

37. Justice, C. O., Townshend, J. R. G., Holben, B. N. and Tucker, C. J., 1985, Analysis of the phenology of global vegetation using meteorological satellite data. International Journal of Remote Sensing, 6: 1271–1318.

38. Khain, A., A. Pokrovsky, M. Pinsky, A. Seifert, and V. Phillips (2004), Simulation of Effects of Atmospheric Aerosols on Deep Turbulent Convective Using a Spectral Microphysics Mixed-Phase Cumulus Cloud Model. Part I: Model Description and Possible Applications, J. Aerosol Sci., 61, 2963-2982.

39. Kiehl, J.T., Hack, J.J., Bonan, G.B., Boville, B.A., Breigleb, B.P., Williamson, D., Rasch, P. (1996), Description of the NCAR community climate model (CCM3). Tech. Rep. National Center for Atmospheric Research, NCAR/ TN-420 + STR.

40. Klein, S. A., and D. L. Hartmann (1993), The seasonal cycle of low stratiform clouds, J. Climate., 6, 1587-1606.

41. Kogan, F. N., 1987a, Vegetation index for areal analysis of crop conditions. Proceedings of 18th Conference on Agricultural and Forest Meteorology, AMS, W. Lafayette, Indiana, on 15–18 September 1987 (Indiana, USA), pp. 103–106.

42. Kogan, F. N., 1987b, On using smoothed vegetation time-series for identifying near-optimal climate conditions. Proceedings of the 10th Conference on Probability and Statistics, AMS, Edmonton, Canada (Edmonton, Canada), pp. 81–83.

43. Kogan, F. N., 1990, Remote sensing of weather impacts on vegetation in non-homogeneous areas. International Journal of Remote Sensing, 11: 1405–1419.

44. Kogan, F. N., 1995, Application of vegetation index and brightness temperature for drought detection. Advance in Space Research, 15: 91–100.

45. Kogan, F. N., 2001, Operational space technology for global vegetation assessment. Bulletin of the American Meteorological Society, 82: 1949–1964.

46. Kogan, F. N., 2002, World droughts in the new millennium from AVHRR-based vegetation health indices. EOS Transactions of the American Geophysical Union, 83: 562–563.

47. Kogan, F. N., Gitelson, A., Edige, Z., Spivak, L. and Lebed, L., 2003, AVHRR-based spectral vegetation index for quantitative assessment of vegetation state and productivity: Calibration and validation. Photogrammetric Engineering & Remote Sensing, 69: 899–906.

48. Kripalani, R. H., J. H. Oh, A. Kulkarni, S. S. Sabade, and H. S. Chaudhari (2007), South Asian summer monsoon precipitation variability: Coupled climate model simulations and projections under IPCC AR4, Theor. Appl. Climatol., 90, 133-159, doi:10.1007/s00704-006-0282-0.

49. Lau, K. M., M. K. Kim, and K. M. Kim (2006), Asian summer monsoon anomalies induced by aerosol direct forcing: the role of the Tibetan Plateau, Climate Dynamics 26(7-8), 855-864.

50. Li, J., L. Liu, A. A. Lacis, and B. E. Carlson (2010), An optimal fitting approach to improve the GISS ModelE aerosol optical property parameterization using AERONET data, J. Geophys.Res., 115, D16211, doi:10.1029/2010JD013909.

51. Liu, D., Wang, Z., Liu, Z., Winker, D., Trepte, C. (2008), A height resolved global view of dust aerosols from the first year CALIPSO lidar measurements. J. Geophys. Res. 113, D16214. http://dx.doi.org/10.1029/2007JD009776.

52. Lohmann, U., and E. Roeckner (1996), Design and performance of a new cloud microphysics scheme developed for the ECHAM general circulation model, Climate Dynamics, 12, 557-572.

53. Lohmann, U., and J. Feichter (1997), Impact of sulfate aerosols on albedo and lifetime of clouds: A sensitivity study with the ECHAM GCM, J. Geophys. Res., 102, 13685-13700.

54. Lohmann, U., J. Feichter, C. C. Chuang, and J. E. Penner (1999), Prediction of the number of cloud droplets in the ECHAM GCM, J. Geophys. Res., 104(D8), 9169-9198.

55. Lohmann, U., P. Stier, C. Hoose, S. Ferrachat, S. Kloster, E. Roeckner, and J. Zhang (2007), Cloud microphysics and aerosol indirect effects in the global climate model ECHAM5-HAM, Atmos. Chem. Phys., 7, 3425-3446.

56. Marticorena, B. and Brgametti, G. (1995), Modeling the atmospheric dust cycle: 1. Design of a soil-derived dust emission scheme, J. Geophys. Res., 100 (D8), 16415-16430.

57. Medeiros, B., and B. Stevens (2011), Revealing differences in GCM representations of low clouds, Climate Dynamics, 36, 385-399.

58. Meenu, S., Rajeev, K., Parameswaran, K. (2011), Regional and vertical distribution of semitransparent cirrus clouds over the tropical Indian region derived from CALIPSO data. J. Atmos. Solar-Terr. Phys. 73, 1967–1979.

59. Menon, S., J. Hansen, L. Nazarenko, and Y. F. Luo (2002), Climate effects of black carbon aerosols in China and India, Science, 297(5590), 2250-2253.

60. Misra, A., Tripathi, S.N., Kaul, D., Welton, E. (2012), Study of MPLNET derived aerosol climatology over Kanpur, India, and validation of CALIPSO level 2 version 3 backscatter and extinction products. J. Atmos. Ocean. Technol 29, 1285–1294.

61. Nordeng, T. (1994), Extended versions of the convective parameterization scheme at ECMWF and their impact on the mean and transient activity of the model in the tropics, Tech. Memo. 206, Eur. Cent. for Med. Range Weather Forecast., Reading, UK.

62. O'Neil, N.T., Eck, T.F., Smirnov, A., Holben, B.N., Thulasiraman, S., (2003), Spectral discrimination of coarse and fine mode optical depth. J. Geophys. Res. 108 (D17), 4559.

63. Padma Kumari, B., and B. N. Goswami (2010), Seminal role of clouds on solar dimming over the Indian monsoon region, Geophys. Res. Lett., 37, L06703, doi:10.1029/2009GL042133.

64. Pal JS, Small E, Eltahir E (2000), Simulation of regional-scale water and energy budgets: representation of subgrid cloud and precipitation processes within RegCM. J Geophys Res 105:29579–29594.

65. Prasad, A. K., and R. P. Singh (2007), Changes in aerosol parameters during major storm events (2001-2005) over the Indo-Gangetic Plains using AERONET and MODIS data, J. Geophys. Res., 112, D09208, doi:10.1029/2006JD007778.

66. Rajeevan, M., J. Bhate, J. D. Kale, and B. Lal (2006), High resolution daily gridded rainfall data for the Indian region: Analysis of break and active monsoon spells, Current Science, 91(3), 296-306.

67. Ramachandran, S., and R. Cherian (2008), Regional and seasonal variations in aerosol optical characteristics and their frequency distributions over India during Ramanathan, V., et al. (2001b), Aerosols, Climate, and the Hydrological Cycle, Science, 294, 2119-2124, doi: 10.1126/science.1064034.

68. Ramanathan, V., et al. (2001b), Aerosols, Climate, and the Hydrological Cycle, Science, 294, 2119-2124, doi: 10.1126/science.1064034.

69. Ramanathan V, Chung C, Kim D, Bettge T, Buja L, Kiehl JT, Washington WM, Fu Q, Sikka DR, Wild M (2005) Atmospheric brown clouds: impacts on South Asian climate and hydrological cycle. Proc Natl Acad Sci USA 102:5326–5333

70. Reddy, M. S., and C. Venkataraman (2002), Inventory of aerosol and sulphur dioxide emissions from India: I - Fossil fuel combustion, Atmos. Environ., 36(4), 677-697.

71. Roeckner, E., et al. (2003), The atmospheric general circulation model ECHAM5. PART I: Model description, Report, 1-140 pp, Max Planck Institute for Meteorology, Hamburg, Germany.

72. Roeckner, E., P. Stier, J. Feichter, S. Kloster, M. Esch, and I. Fischer-Bruns (2006), Impact of carbonaceous aerosol emissions on regional climate change, Climate Dynamics, doi:10.1007/s00382-00006-00147-00383.

73. Rosenfeld, D., and W. L. Woodley (2000), Deep convective clouds with sustained supercooled liquid water down to -37.5oC, Nature, 405, 440-442.

74. Rosenfeld, D., U. Lohmann, G. B. Raga, C. D. O'Dowd, M. Kulmala, S. Fuzzi, A. Reissell, and M. O. Andreae (2008), Flood or drought: How do aerosols affect precipitation?, Science, 321(5894), 1309-1313.

75. Shimizu, A. (2004), Continuous observations of Asian dust and other aerosols by polarization lidars in China and Japan during ACE-Asia. J. Geophys. Res. 109 (D19), 1–14. http://dx.doi.org/10.1029/2002JD003253.

76. Singh, R. P., S. Dey, S. N. Tripathi, V. Tare, and B. Holben (2004), Variability of aerosol parameters over Kanpur, northern India, J. Geophys. Res., 109(D23), D23206, doi:10.1029/2004JD004966.

77. Singh, R. P., Roy, S. and Kogan, F., 2003, Vegetation and temperature condition indices from NOAA AVHRR data for drought monitoring over India, International Journal of Remote Sensing, 24: 4393-4402.

78. Solmon F, Giorgi F, Liousse C (2006), Aerosol modeling for regional climate studies: application to anthropogenic particles and evaluation over a European/African domain, Tellus B, 58 (1), 51–72.

79. Stier, P., et al. (2005), The aerosol-climate model ECHAM5-HAM, Atmos. Chem. Phys., 5, 1125-1156.

80. Stier, P., J. H. Seinfeld, S. Kinne, and O. Boucher (2007), Aerosol absorption and radiative forcing, Atmos. Chem. Phys., 7(19), 5237-5261.

81. Tao, J., Zhang, L., Engling, G., Zhang, R., Yang, Y., Cao, J., Zhu, C., Wang, Q., Luo, L. (2013), Chemical composition of PM2.5 in an urban environment in Chengdu, China: importance of springtime dust storms and biomass burning. Atmos. Res. 122, 270–283.

82. Tarpley, J. D., Schnieder, S. R. and Money, R. L., 1984, Global vegetation indices from NOAA-7 meteorological satellite. Journal of Climate and Applied Meteorology, 23:4491–4503.

83. Tebaldi, C. and R. Knutti (2007), The use of the multi-model ensemble in probabilistic climate projections, Phil. Trans. R. Soc. A, 365, 2053–2075.

84. Tegen, I., S. P. Harrison, K. Kohfeld, I. C. Prentice, M. Coe, and M. Heimann (2002), Impact of vegetation and preferential source areas on global dust aerosol: Results from a model study, J. Geophys. Res., 107(D21), 4576, doi:10.1029/2001JD000963.

85. Tiedtke, M. (1989), A comprehensive mass flux scheme for cumulus parameterization in large-scale models, Mon. Weather Rev., 117, 1779–1800.

86. Tompkins, A. M. (2002), A prognostic parameterization for the subgridscale variability of water vapor and clouds in large-scale models and its use to diagnose cloud cover, J. Atmos. Sci., 59, 1917-1942.

87. Tost, H., P. Jockel, and J. Lelieveld (2006), Influence of different convection parameterisations in a GCM, Atmos. Chem. Phys., 6, 5475–5493.

88. Tripathi, S. N., et al. (2006), Measurements of atmospheric parameters during Indian Space Research Organization Geosphere Biosphere Programme Land Campaign II at a typical location in the Ganga basin: 1. Physical and optical properties, J. Geophys. Res., 111, D23209, doi:10.1029/2006JD007278.

89. Tucker, C. J., Gatlin, J., Schnieder, S. R. and Kuchinos, M. A., 1982, Monitoring large scale vegetation dynamics in the Nile delta and river valley from NOAA-AVHRR data. Proceedings of the Conference on Remote Sensing of Arid and Semi-Arid Lands, Cairo, Egypt (Ann Arbor: Environmental Research Institute of Michigan), pp. 973–977.

90. Vadrevu, K. P., E. Ellicott, K. V. S. Badarinath, and E. Vermote (2011), MODIS derived fire characteristics and aerosol optical depth variations during the agricultural residue burning season, north India, Environmental Pollution, 159, 1560-1569.

91. Venkataraman, C., G. Habib, A. Eiguren-Fernandez, A. H. Miguel, and S. K. Friedlander (2005), Residential biofuels in south Asia: Carbonaceous aerosol emissions and climate impacts, Science, 307(5714), 1454-1456, doi:10.1126/science.1104359.

92. Venkataraman, C., G. Habib, D. Kadamba, M. Shrivastava, J. F. Leon, B. Crouzille, O. Boucher, and D. G. Streets (2006), Emissions from open biomass burning in India: Integrating the inventory approach with high-resolution Moderate Resolution Imaging Spectroradiometer (MODIS) active-fire and land cover data, Global Biogeochem. Cy., 20(2), GB2013, doi:10.1029/2005GB002547.

93. Wilhite, D. A., Svoboda, M. D. and Hayes, M. J., 2007, Understanding the complex impacts of drought: A key to enhancing drought mitigation and preparedness, Water Resource Management, 21: 763–774.

94. Yin, Y., A. Levin, T. G. Reisin, and S. Tzivion (2000), The effect of giant cloud condensation nuclei on the development of precipitation in convective clouds - a numerical cloudy, Atmos. Res., 53, 91-116.

95. Ying Xu, Xuejie Gao, Filippo Giorgi (2010), Upgrades to the reliability ensemble averaging method for producing probabilistic climate-change projections. doi: 10.3354/cr00835 Vol. 41: 61-81.

96. Zakey AS, Solmon F, Giorgi F (2006), Development and testing of a desert dust module in a regional climate model, Atmos. Chem. Phys., 6 4687–4704.

97. Zhang, J., U. Lohmann, and P. Stier (2005), A microphysical parameterization for convective clouds in the ECHAM5 climate model: Single-column model results evaluated at the Oklahoma Atmospheric Radiation Measurement Program site, J. Geophys. Res., 110, D15S07, doi:10.1029/2004JD005128